Tomas Bata University in Zlín
Faculty of Technology

Doctoral Thesis

Optimization of processing of powder injection molding feedstocks prone to phase separation

Optimalizace procesu vstřikování práškových materiálů vykazujících fázovou separaci

Author: **Ing. Daniel Sanétrník**

Study programme: P3909 Process Engineering

Field of study: 3909V013 Tools and Processes

Supervisor: Prof. Ing. Berenika Hausnerová, Ph.D.

Reviewers: Prof. Dr. Bernhard Möginger

Prof. Ing. Petr Slobodian, Ph.D.

Zlín, April 2019

The publication was issued in the year 2019

Keywords: *powder injection molding, highly filled polymers, phase separation, wall slip, surface roughness, processing parameters*

Klíčová slova: *vstřikování práškových materiálů, vysoce plněné polymery, fázová separace, skluz na stěně, kvalita povrchu, procesní podmínky*

TABLE OF CONTENTS

ABSTRACT

In the last decades Powder Injection Molding (PIM) became an effective technology for a mass production of precise and shape-complex metal and ceramic items. The main issue of PIM process is phase separation occurring during injection molding step. The phase separation causes defects which are detected mostly after final sintering, and thus leading to significant economic and ecological losses.

The aim of the thesis is optimization of PIM process and detection of powder/binder separation during/after injection molding step, when the process is still reversible - materials can be regranulated and used again. Direct testing of molded samples, without any additional treatments or knowing an exact composition of used binders, is provided for a broad cast of PIM feedstocks including commercially available ones. The proposed testing method combines scanning electron microscopy with energy dispersive X-ray to detect changes in powder or binder concentrations due to a phase separation, which are then analyzed with a mathematical approach to provide the single variability parameter to quantify the tendency of the particular feedstocks towards phase separation.

Further, rheological properties of PIM feedstocks were investigated with the special regard to wall slip effect, which serves as a parameter indicating phase separation during shear deformation. The results reveal the importance of the surface roughness and geometry of the processing tools for the wall slip development; therefore, these parameters should be considered for reliable testing to optimize the molding step of PIM.

Finally, the influence of processing parameters such as injection molding temperature and debinding route on the sintered surface structure of PIM parts revealing signs of phase separation was investigated by contactless scanning. The obtained qualitative data were then treated with suitable statistical approaches to quantify the quality of the resulting PIM parts.

This thesis provides the contribution to predict and reduce the phase separation of PIM feedstocks, thus positively influencing the effectivity of the PIM process.

ABSTRAKT

Technologie vstřikování práškových materiálů (tzv. PIM) patří v posledních letech mezi rychle se rozvíjející postupy pro velkoobjemovou výrobu přesných a tvarově komplexních produktů z kovu a keramiky. Defekty finálních výrobků jsou zpravidla způsobeny fázovou separací materiálu (polymerní pojivo a kovový/keramický prášek) během fáze vstřikování. Tyto vady jsou detekovány až v poslední fázi výroby (sintrace), kde je proces nevratný, což působí značné ekonomické a ekologické ztráty.

Dizertační práce se zabývá optimalizací procesu vstřikování práškových materiálů a detekcí fázové separace kovového/keramického prášku a polymerního pojiva během vstřikování, kdy je proces ještě vratný. V rámci dizertační práce byla vyvinuta nová testovací metoda za použití elektronové mikroskopie v kombinaci s prvkovou analýzou EDX. Výhoda této metody spočívá v přímém testování vstřikovaných tělísek bez nutnosti dalších úprav, a je možné ji použít i pro komerčně dostupné materiály bez znalosti složení použitého polymerního systému. Tato nová metoda byla otestována na komerčně dostupných materiálech a také na materiálech připravených na UTB ve Zlíně. EDX data byla analyticky zpracována s cílem poskytnout kvantifikaci náchylnosti jednotlivých PIM materiálů k fázové separaci prostřednictvím jednoduchého parametru, tzv. koeficientu separace.

Materiály používané v PIM technologii byly také testovány z reologického hlediska, a to se zaměřením na skluz na stěně, který při toku kanálem mění hodnoty gradientů smykových rychlostí, a tím ovlivňuje míru fázové separace. Pro testování bylo zvoleno několik typů kapilár s rozdílnou geometrií a povrchovou drsností. Výsledky ukazují na citlivost reologických dat vysoce plněných materiálů vzhledem ke zvoleným charakteristikám tokového kanálu.

Kvantifikace vlivu procesních parametrů na kvalitu povrchu finálních sintrovaných produktů byla provedena pomocí bezkontaktní profilometrie. Optimalizace vstřikovací teploty a způsobu odstranění polymerního pojiva za účelem dosažení lepší finální povrchové struktury sintrovaného výrobku se jeví jako perspektivní nástroj pro potlačení projevů fázové separace.

Tato disertační práce představuje přínos k porozumění a potlačení jevu fázové separace vysoce plněných materiálů, a tím přispívá ke zvýšení efektivity procesu vstřikování práškových materiálů.

INTRODUCTION

Metal and ceramic products bring many advantages in comparison to polymeric materials. They have usually high strength, stiffness, higher temperature resistance, and also better electric and magnetic properties in case of metals. On the other hand, they exhibit inferior processability in comparison to plastics [1-3].
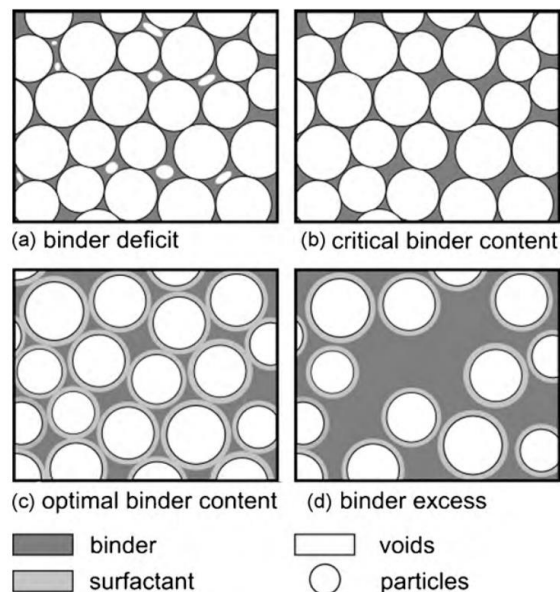
Powder injection molding technology (PIM) combines advantages of metals/ceramics with processability of polymers [4]. Polymeric binders are used for shaping of metal/ceramic powders by injection molding, holding them until bonding in a sintering furnace close to a theoretical density. PIM includes four basic steps consisting of mixing, injection molding, debinding and sintering. All these steps contribute to precise final product without defects. Nowadays, the main problem of the process is a detection of defects resulting from so called phase separation in final products after sintering, when process is irreversible. Thus, current research is focused on methods capable to determine and reduce issues and defects prior sintering [1,5-7].

THEORETICAL BACKGROUND

1. Compounds for powder injection molding

Highly filled polymers used in PIM technology contain typical binder volume of 35 – 60 vol. % to form a homogeneous feedstock. Four parameters determine performance of feedstocks – binder composition, powder characteristics, powder/binder ratio, and mixing method [1,8].

The ratio between powder and binder determines quality of whole process. Three possibilities are described in Figure 1. Binder deficit causes formation of voids in a material and defects during sintering; also processability is limited by high viscosity of a compound. On the other hand, an excess of binder leads to a binder separation from a powder during injection molding. The critical solid loading corresponds to the particles in the close contact. The powder/binder ratio slightly less than critical solid loading is an optimal state for processing (Figure 1c) [1,5].

(a) binder deficit   (b) critical binder content

(c) optimal binder content   (d) binder excess

binder   voids

surfactant   particles

Figure 1 – Feedstocks according to various powder/binder ratio [5]

The role of binder system is to provide suitable flow properties to a feedstock during injection molding step, and holding powder particles into the required shape prior sintering. The binder system usually consists three main parts. First one is main component (low molecular polymer – paraffin, PEG, etc.) which ensures flow properties of a bulk feedstock; polar waxes improve also an adhesion between powder and binder system [1,6]. The backbone polymer that provides strength to the initial of sintering is the next ingredient (e.g. PE, PP,

PS, PMMA). Binder systems also contain a small amount (less than 5 vol. %) of additives (dispersants, stabilizers, plasticizers and intermolecular lubricants) to enhance suitable rheological behavior [1,9].

Second component of a PIM feedstock is powder. Typical powders used in PIM technology are based on iron (alloy steels, high speed steels, stainless steels, etc.), reactive titanium powders or ceramics (Al_2O_3, ZrO_2) [1,10]. The typical size of particles is usually between 0.1 to 45 μm with round shape, but there are many variations in particle size and shape [11]. The size and shape of particles affect not only flow properties of the feedstock, but whole PIM process - dimensional control in debinding (interparticle friction), sintering (particle microstructure, packing density), debinding rate (size, shape, packing density). Requirements on an ideal powder representing a balance among all these factors are summarized bellow [1,6,9]:

- particle size smaller than 20 μm
- tap density over 50 % of theoretical
- round shape
- no agglomeration and clean surface
- low explosion and toxicity hazard
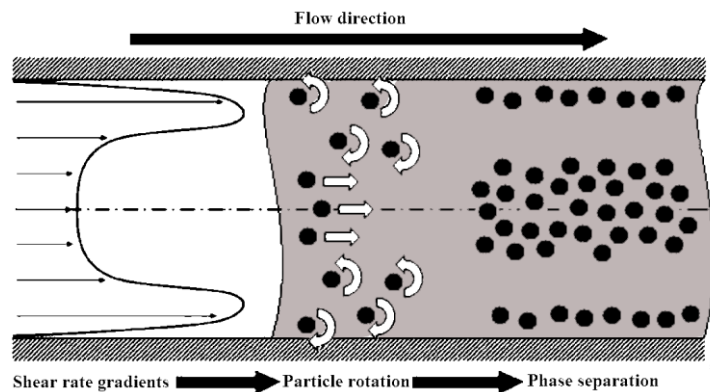
2. Phase separation

Nowadays, the main issue of the PIM technology is the powder/binder separation during injection molding step. The phase separation causes up to 25 % imperfections such as surface defects, porosity or cracks on the final products due to non-optimized molding/flow properties [12]. These defects are usually non visible after injection molding, neither during debinding. Furthermore, these defects cannot be removed from the final products. Thus, for an efficient production it is very important to analyze and prevent phase separation during injection molding step, because after molding the process is still reversible.

2.1. Mechanism of phase separation

The role of local shear rate gradients in a phase separation of highly filled PIM feedstocks (assuming no slip conditions) was proposed by Thornagel [13]. There is a significant shear rate gradient near the wall, and a plateau of a lower shear rate in the middle of the channel (Figure 2). The shear rate gradients cause

rotation of the particles near the wall. Naturally, the rotating particles try to move to the area in the middle of the channel, where the values of the shear rate are lower. The result is the area near the wall showing a high concentration of separated binder, and powder particles are concentrated in the middle of the channel. This axial solids concentration gradient was also studied by Segre and Silberberg decades ago [14]; they observed an equilibrium position of rigid spheres located at $0.6R$ (R –pipe radius) during laminar flow.

Figure 2 – Shear rate gradients as a cause of phase separation [13]

Local shear rate gradients are the cause of phase separation, but the location of shear rate peaks does not always lead to the location of phase separation because the feedstock flow transports the separation pattern and changes the pattern continuously, therefore the phase separation depending also on the travelling history (Figure 3).

Thornagel [13] furthermore provides a flow simulation to predict phase separation. The influence of the history of the feedstock travelling through the barrel, nozzle, runner system and cavity is considered in his model.
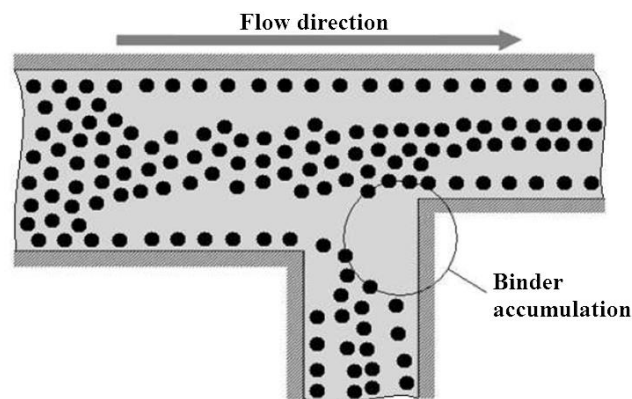
Figure 3 – Phase separation as a result of mold cavity pattern [13]

9

2.2. Testing of phase separation

The phase separation is commonly tested by moldability test, i.e. filling of a spiral mold [1]. The moldability is expressed with the length of the filled spiral. During flow, a frozen layer is continuously created along a cold wall of a mold, therefore channel is gradually closed and flow stops. This effect is called a fountain flow, Figure 4 [15].
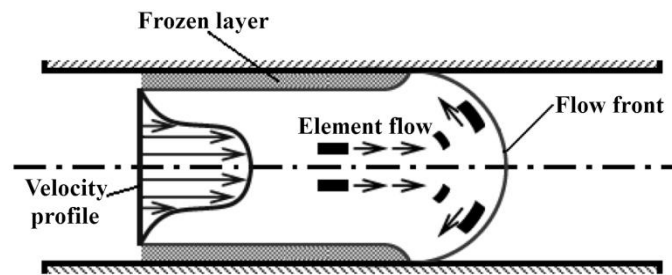

Figure 4 – Fountain flow effect during injection molding [15]

The pioneer investigation on moldability of particle filled (glass spheres) polymers was done by Kubat and Szalanczi [16]. They investigated the influence of different size of glass particles and length of spiral testing mold on a phase separation. The glass concentration after molding was determined gravimetrically on incinerated samples.

From their study it can be concluded that phase separation increases with a spiral length. The particles with large diameter (50-100 μm) were more prone to the phase separation than smaller particles (4-40 μm), because larger particles travel faster along a spiral mold (Figure 5).
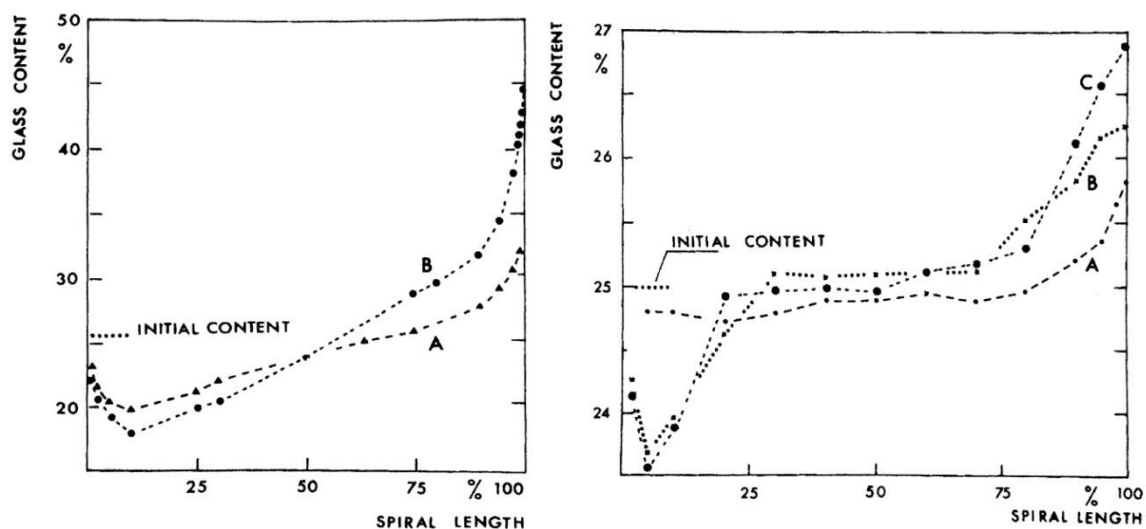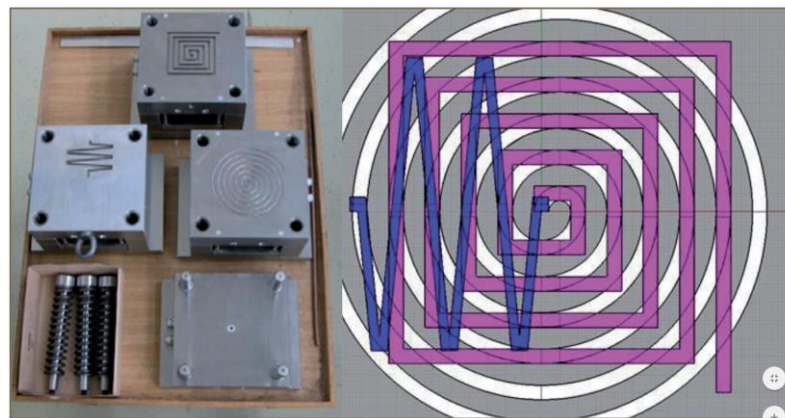

Figure 5 – Influence of spiral length on glass spheres concentration [16]
Left – small spheres, Right – large spheres; length of spiral rises from A to C

Another approach was proposed by Jenni et al. [17], which compared spiral, square spiral and zig-zag molds (Figure 6) for testing of moldability and associated phase separation.


Figure 6 – Design of testing molds proposed by Jenni [17]

Jenni et al. [17] compared the balance model, representing a flow of solid, spherical particles in a Newtonian fluid, with the experimental data.

More sophisticated mold design to test phase separation (Figure 7) was developed at the Polymer Center, TBU Zlin in cooperation with Fraunhofer IFAM, Bremen (Utility Design 001704974-0001). The testing mold contains all critical elements, such as inner and outer corners, radical thickness changes, weld lines, thin gates, films and flashes.

The testing mold is composed of four square elements connected by gates 1 mm long and 0.5 mm wide. Size of the inner wall of the first three elements is 10 mm. The length of the outer sides of square elements is gradually decreasing from 3.0 mm to 2.5 mm and 2 mm. The fourth 0.3 mm high element serves as an outlet of third element. Each square element contains 16 notches for easy position determination.
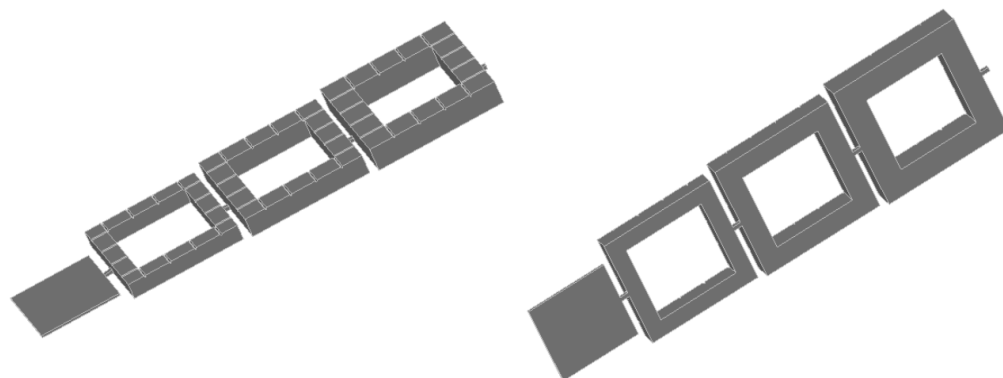
Figure 7 – New design of testing mold; top and bottom side [15]

11

Highly separated areas (Figure 8) were found near the gate of each element by initial testing, but more precise testing and quantification of separation was needed, thus the topic of the thesis presented was proposed.
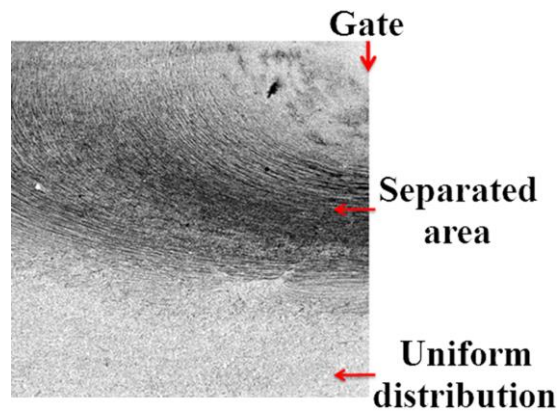

Figure 8 – SEM of powder/binder separation

2.2.1. Quantification of phase separation

Differential scanning calorimeter (DSC) was used by Jenni et al. [17,18] for local powder content monitoring from the differences in glass transition temperatures. The experiments run under various moldability conditions – flow length, nozzle and mold temperature or injection speed. Experiments obtained by DSC, radiography and tomography showed lower powder content in the corners of the mold cavity (Figure 9). This was confirmed by a balance model (solid particles in Newtonian fluid), however the instabilities of the feedstock such as wall slip or fountain flow were not predicted by this model [17,18].
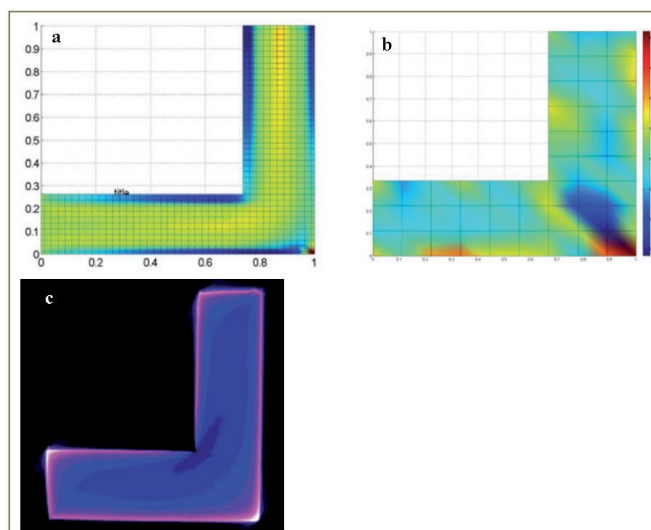

Figure 9 – Distribution of powder in square spiral mold [17]
a – balanced model, b – DSC, c – tomography

Currently, the research of phase separation phenomenon is carried out mainly using X-ray tomography [19-21]. Yang et al. [19] presented a new method of detailed quantification analysis of the different powder–binder separation characteristics of the SiC molded samples with different initial solid loadings. In their study the linear fitting equation between gray value of X-ray and actual density of sample was used (the output from an X-ray scanner is a gray-scale image where the variations in gray darkness correspond to variations in density) [22]. According to this assumption, the actual density at a specific area of molded sample can be calculated, when we know density of pure binder system and powder particles. Furthermore, the powder content in the feedstock is calculated from this actual density [19]. In their studies [20,21] the method is tested on L-shape mold (Figure 10) with different processing parameters. As in the previous researches [13,18,19], binder rich areas were formed near gates and mold walls.
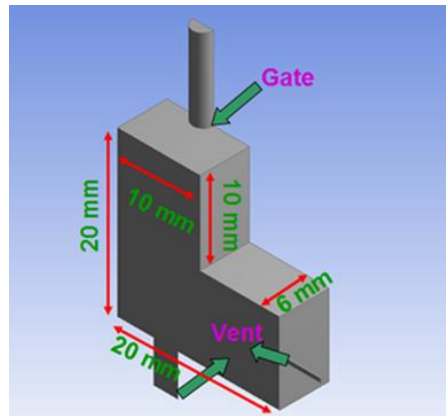
Figure 10 – Design of testing mold proposed by Yang et al. [20]

However, the analyses are complicated by several factors, the separation is accompanied by a non-homogeneity of a material caused by flow instabilities or a movement of particles from a solid wall to a center of a channel during flow. Currently, the mechanism of phase separation occurrence has still not been fully understood [23].

2.3. Flow behavior of highly filled compounds

As mentioned before, the important parameter preventing the phase separation is homogeneity of feedstock, which affects whole PIM process. The inhomogeneity of the feedstock can be detected by pressure instabilities obtained from a capillary rheometer (Figure 11) [24].
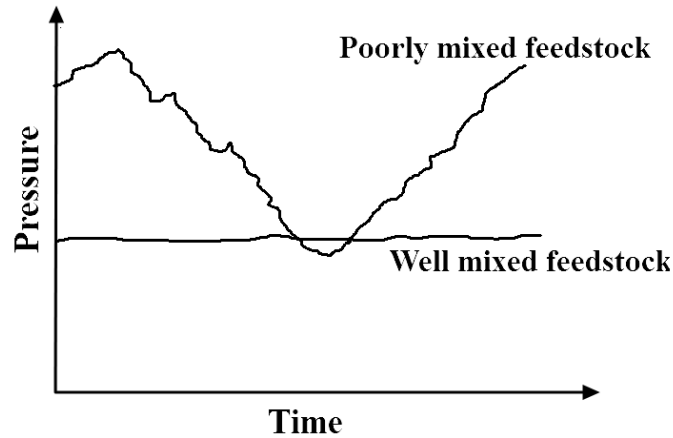
Figure 11 – Capillary rheometer – pressure output of mixed feedstocks [24]

The other problems are resulting from processing conditions during injection molding. This step usually needs an expensive, time consuming, trial and error testing to design desired process conditions [17]. In addition, as thermoplastics, highly filled materials also exhibit moldability defects such as jetting, air traps, dead zones, flash or welding lines. Figure 12 shows entire injection molding process with possible defects caused by poorly set-up process conditions of injection speed and pressure [1].
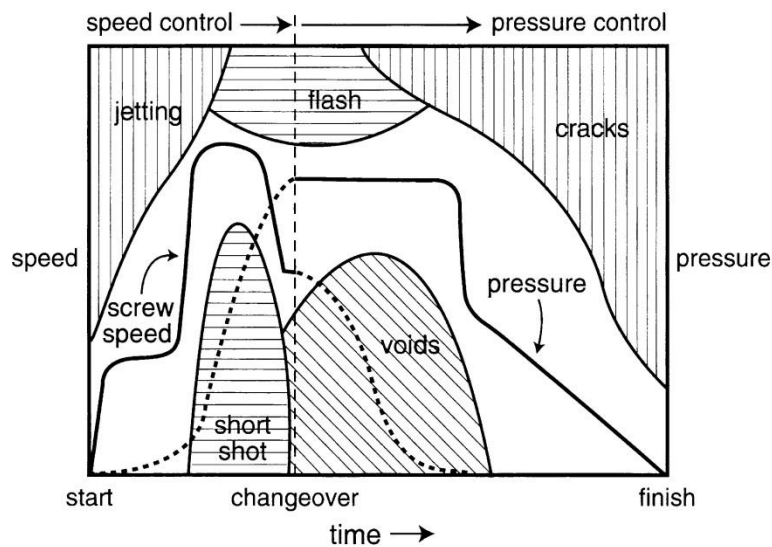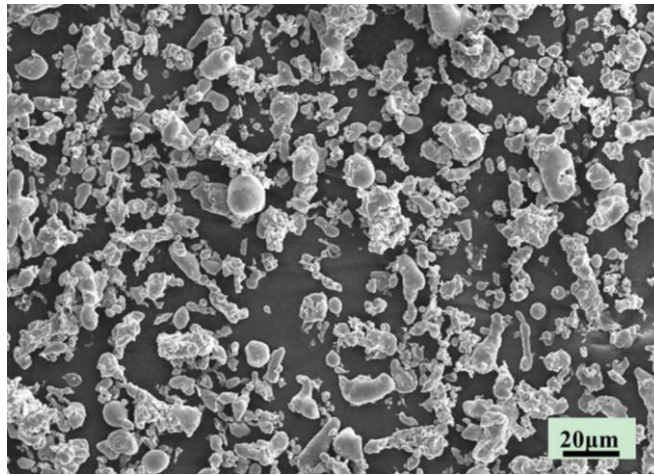

Figure 12 – Diagram of injection molding defects [1]

PIM compounds introduce also many obstacles and limitations because of a multi-component character of polymer binder and complex powder characteristics, mainly irregular shape and broad particle size distribution (Figure 13) [1,6,25].

Figure 13 – SEM of 316L stainless steel powder [26]

First problem during shearing of highly filled systems is agglomeration of solid particles in non-Newtonian fluid. This phenomenon has been already studied in seventies by Michele et al. [27]. They found that - upon shearing - glass solid particles can create chains or agglomerate groups in non-Newtonian fluids (Figure 14).
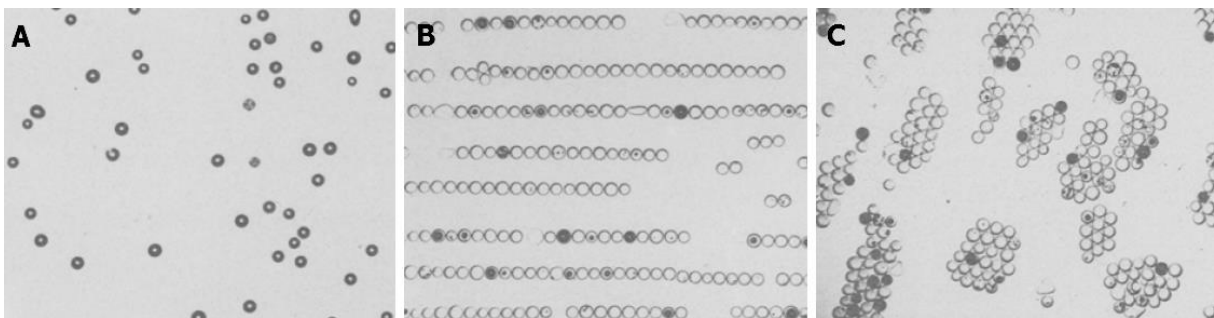
Figure 14 – Glass particles in non-Newtonian fluid
a – before shearing, b –one dimension shearing, c –circular shearing [27]

This effect has a significant relevance for rheological testing. Measurement of flow curves can derive different viscosity data if an experiment is started from low shear rates towards higher or vice versa, because agglomerated structure created at higher shear rates will not be destroyed at lower shear speeds.

Complexity of rheological behavior and thermal properties of the PIM feedstocks which affect injection molding step was tested by Ahn et al. [28]. They concluded that non-Newtonian index is more sensitive to a binder selection than to a powder. Both, powder and binder composition has the same effect on thermal conductivity and heat capacitance of the feedstocks. The injection pressure and clamping force can be minimalized better by binder systems, but controlling of the maximum shear rate is affected by both powder and binder systems.

Unstable flow behavior of highly filled polymers was also studied by Isayev et al. [29] and Hausnerova et al. [4]. Their studies demonstrate change of shear thinning behavior into a dilatant flow (Figure 15). The viscosity is decreasing due to the orientation of particles with the flow at the low shear rates, but at higher shear rates the particles cannot form layers and slide over each other, thus viscosity is increasing [4,29]. These findings bring many obstacles for rheological modeling. Herschel – Bulkley or Casson models cannot describe flow curves in a whole range of shear rates, and more complicated eight parameter model has to be applied [4,30].
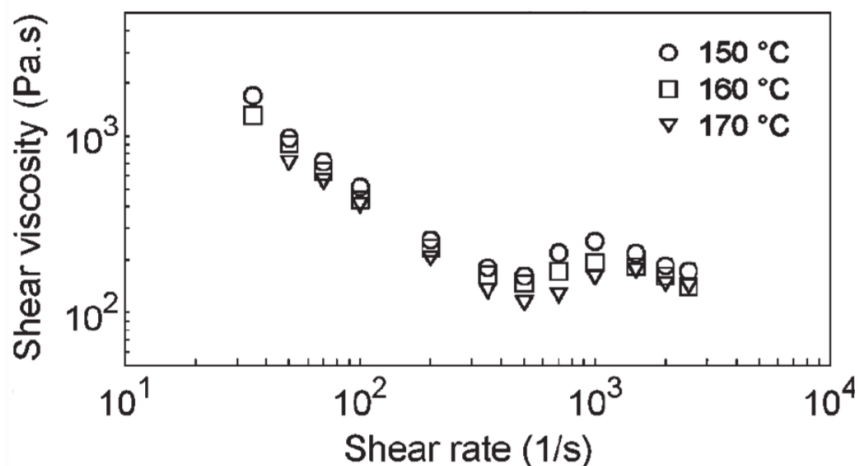
Figure 15 – Flow curves of 60 % alumina feedstock [4]

Shivashankar et al. [31] studied the relation between a phase separation and a rheological behavior of filled compounds. They assumed that a suspension system consists three volume parts (Figure 16) – solid volume fraction (ϕ), interstitial space liquid binder (ϕ_{L1}) and liquid spherical shells of particles (ϕ_{L2}). The total volume of system is given as:

$$\phi + \phi_{L1} + \phi_{L2} = 1 \tag{1}$$

Figure 16 – Volume fractions of highly filled system [31]

The volume of liquid spherical shells (ϕ_{L2}) is decreasing to zero when the critical solid loading (ϕ_m) is reached:

$$\phi_{L2} = 1 - \phi - \phi_{L1} = 1 - \frac{\phi}{\phi_m} \qquad (2)$$

According to Krieger-Dougherty relationship [1], a volume of liquid spherical shells can be also expressed using relative viscosity η_r:

$$\eta_r = \left(1 - \frac{\phi}{\phi_m}\right)^{-2} \qquad (3)$$

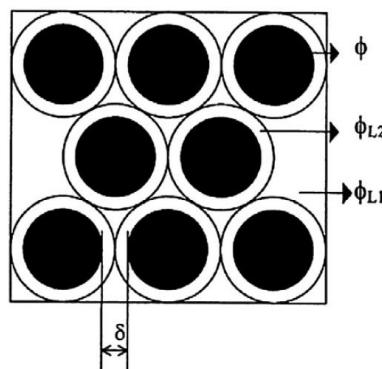From these empirical equations it is obvious that a higher amount of solid particles causes decreasing of liquid shells of solid particles (ϕ_{L2}), and increasing of a relative viscosity due to an enhanced inter-particle friction. Shivashankar et al. [31] in his study observed the pronounced phase separation for the systems with high relative viscosity (Figure 17). Thus, he concluded that the tendency to a phase separation is related not only to the viscosity, but also to the inter-particle particle spacing parameter δ that is given by solid volume fraction (ϕ) and particle diameter D_P:

$$\delta = \frac{2}{3} D_P \left[\frac{1 - \phi}{\phi}\right] \qquad (4)$$
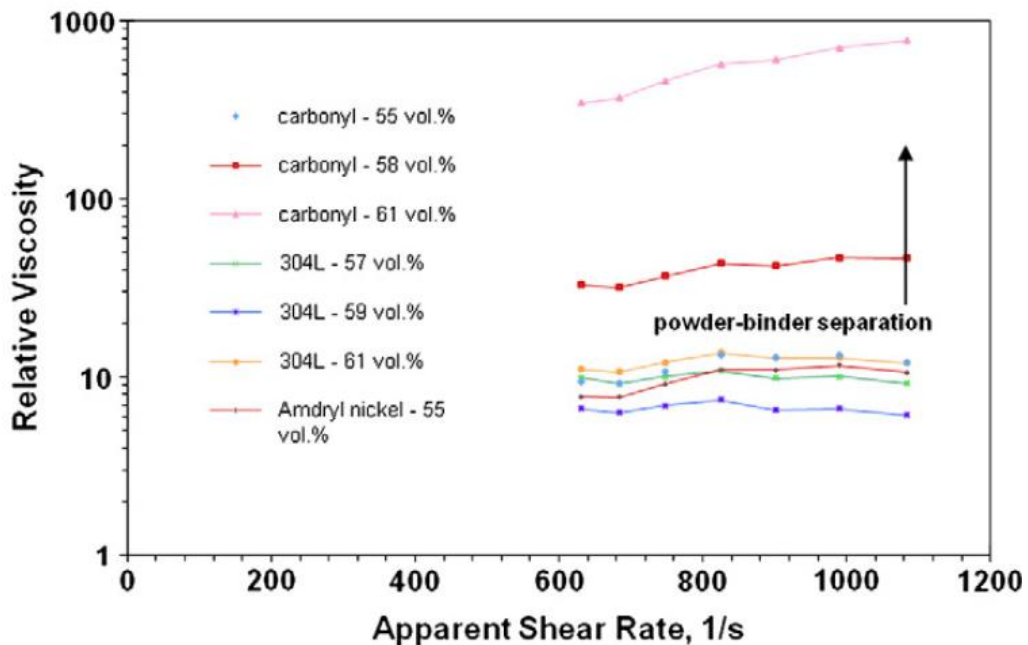

Figure 17 –Relation between relative viscosity and phase separation of PIM compounds [31]

All feedstocks characteristics (DSC, viscosity, thermal behavior) as well as pressure-volume-temperature (PVT) data are important to modeling of flow behavior of material during the flow into the mold cavity. Nowadays only few simulation approaches contain the characteristics for highly filled materials, one of these is PIMSolver [28] developed at CetaTech Inc., South Korea which uses a hybrid method of a finite element method (FEM) and a finite difference method (FDM) for calculating flow and temperature fields in PIM applications.

2.3.1. Wall slip as rheological parameter related to phase separation

The mechanism of separation proposed by Thornagel [13] supposed no slip condition during flow, however the wall slip may cause instabilities during injection molding and understanding of this phenomenon is important.

While Newtonian fluids exhibit no-slip conditions during the flow [1,31,32] through the tubes, and the solid-liquid boundaries have exactly the same velocity (Figure 18a), highly filled suspensions exhibit flow instabilities at high stresses [33]. These instabilities usually start by shark skin (visibly rough surface) followed by slip-stick or spurt flow. Some authors [34] consider onset of shark skin as an indication of evolving wall slip. Nowadays there are three theories on the wall slip effect.

The first one assigns wall slip to an adhesive failure of polymer chains at the solid wall. The second one is a cohesive failure resulting from disentanglement chains between bulk and chains absorbed at the solid wall, thus polymer is slipping along these absorbed chains (Figure 18b) [34-36]. These two situations are called a true slip.
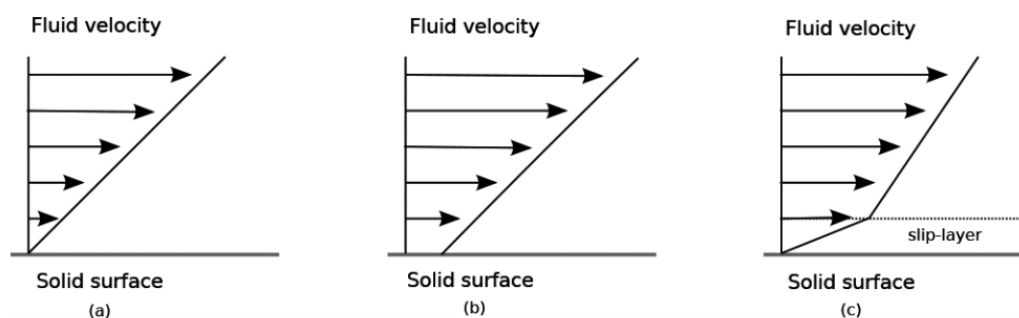

Figure 18 – Schematic presentation of no-slip and wall slip conditions [36]

Nevertheless, these adhesive and cohesive failure theories seem to be an inappropriate for multi-phase systems. The third theory, known as an apparent slip [37], assumes that upon shearing a narrow polymer layer of low viscosity

with typical thickness of 0.1 – 10 µm is created near the wall and solid particles are migrating away from walls (Figure 18c) [34,38,39]. Theory of this migration was proposed by Delime and Moan [40]. They expected that the migration of solid particles is initiated by the failure of Brownian movement near the walls, which is supported by shear rate gradients which promote particles collision [38,40]. Other experiments confirm this theory especially for particles in range 20 – 100 µm [41].

2.3.2. Evaluation of slip velocity

Mooney [42,43] proposed a method for wall-slip evaluation from capillary and couette flow data to determine the slip velocity from the slope of the apparent shear rate versus reciprocal radius or gap data collected at constant apparent wall shear stress. Mooney method is based on measurement with three different capillaries having the same length-to-diameter ratio (*L/D*), but different diameter of the dies.

The presence of slip can be also detected from single geometry measurement such as unexpected low Newtonian plateau, sometimes with an apparent-yield stress at even lower stresses, as well as sudden breaks in the flow curve at higher shear stresses or rates [34]. Further, the flow curves of material should be independent on capillary dimensions or surface roughness when wall slip does not occur. Some studies [38,44] reports increasing slip velocity with higher temperature, and proportionally increasing low molecular layer with increasing size of the particles. Figure 19 demonstrates the role of surface roughness to prevent wall slip effect. In case of a rough wall, solid particles can move into the groove, therefore the whole material flow as a continuum [45].
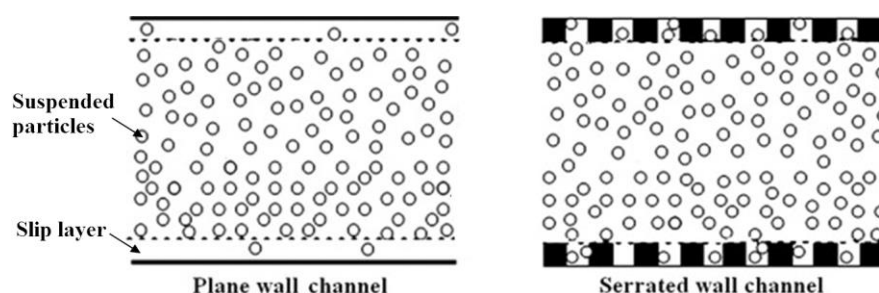
Figure 19 – Influence of surface roughness to wall slip effect [45]

Chen et al. [46] tested the effect of roughness of a capillary wall on a wall slip of LLDPE. A copper capillary (*L/D* – 57.6) with different roughness parameter was used for evaluation of wall slip velocity (Figure 20).
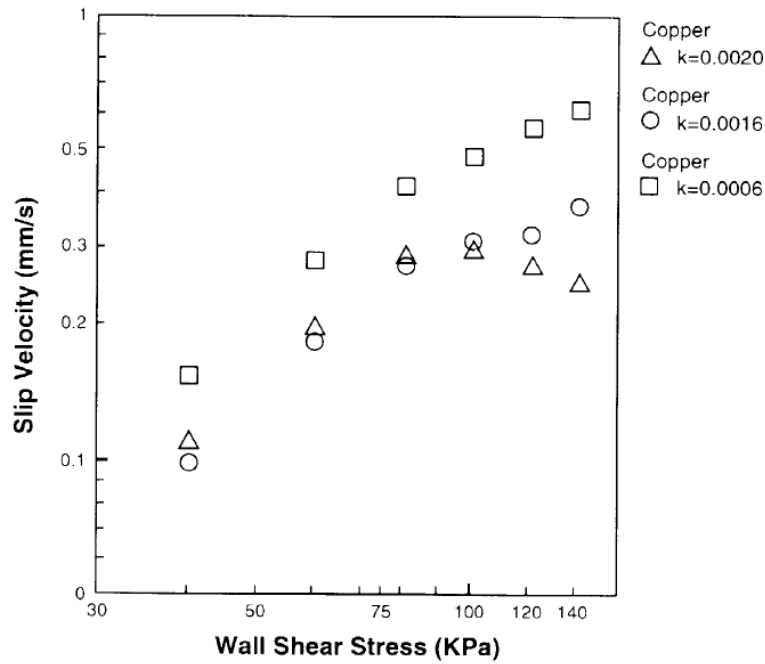
Figure 20 – Effect of surface roughness on wall slip velocity [46]

The experiment confirmed the theoretical findings - for the smooth capillary the wall slip velocities are about 50 – 150 % higher than for roughened capillary. Furthermore, the effect of various capillary materials was considered in this study (Figure 21). Stainless steel resulted in considerably higher wall slip velocities in comparison with alumina.
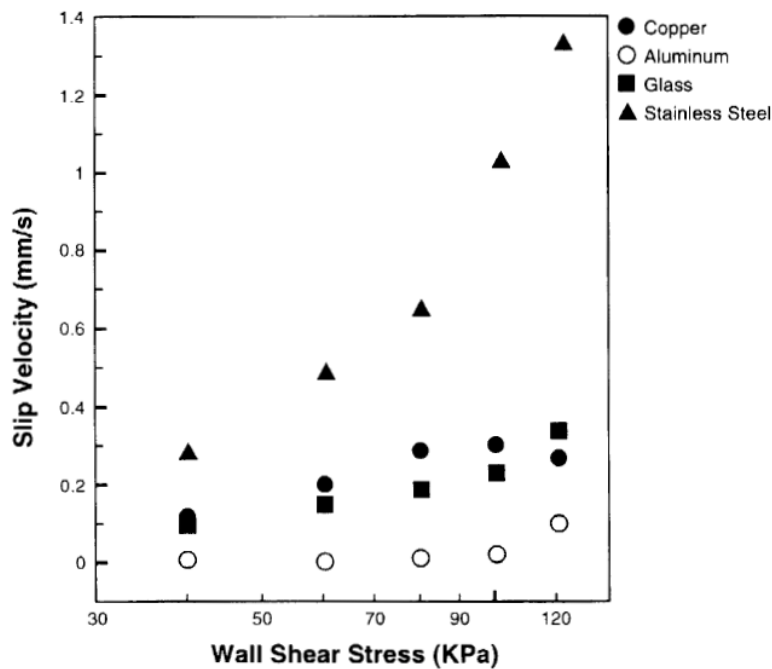
Figure 21– Effect of capillary die material to wall slip velocity [46]

20

From the previous studies it can be observed that the most significant conditions causing a slip effect are [35,36,45,47-49]:

- strong dependence of viscosity on a filler concentration
- large particles as a dispersed phase
- smooth flow channel walls
- small flow geometry size
- low speed rates
- electrostatic charges of wall or particles.

Very recently, slip of PIM compounds was considered by Liu et al. [50] for a micro-PIM of zirconia feedstocks with the clear conclusion that wall slip cannot be ignored in numerical simulations, because it leads to unrealistic low viscosity values, and as a consequence to a failure of flow simulation approaches applied. In the following work, Liu et al. [51] supported this finding when compared the simulations of temperature, viscosity and pressure gradient distributions during mold filling including/excluding wall slip. Therefore, the slip is the crucial flow phenomenon influencing the most severe issue of injection molding step of PIM [23].

DISCUSSION OF RESULTS

The discussion of the work performed within this thesis is divided into three sections describing different approaches to optimization of Powder Injection Molding (PIM) process in order to achieve a final structure of PIM parts without defects resulting from phase separation.

First, the development of the new non-destructive method for the quantification of the phase separation of highly filled polymers is proposed. Second, the wall slip as a rheological phenomenon affecting shear rate gradients causing phase separation during a flow of PIM feedstocks is investigated with the regard to an appropriate choice of testing methods and tools as a type of rheometer, surface roughness of dies, capillary dimensions and capillary entrance angles. Third, the surface structure of the final sintered parts as a function of processing parameters of injection molding and debinding steps of PIM is quantified via contactless surface scanning following with a statistical analysis of the results obtained.

3. Quantification of phase separation

This chapter summarizes findings published in the Paper I

As shown in the theoretical background, currently used testing methods detecting a phase separation on molded parts employ simple mold geometries such as square spiral or L-shape [17,20]. These mold shapes are not entirely suitable for the testing of highly filled polymers as they do not contain most severe critical areas causing a phase separation as rapid thickness changes, thin films or weld lines. In addition, the methods to quantify the separation presented so far are inaccurate (DSC) and time consuming (X-ray computed tomography) [17-21]. Both methods have not proved to be a suitable approach to detect the changes in powder concentrations for feedstocks containing multi-component binders (typical for PIM feedstocks) [17-21].

Therefore, a development of a new testing approach should be focused on a simple and precise method testing molded samples from a broad cast of feedstock types. In this respect, the scanning electron microscopy (SEM) seems to be useful method for the qualitative analysis of the development of the phase separation prior to debinding and sintering, where the whole process is still reversible (material still can be re-granulated and re-used). Especially, backscattered electrons detector (BSE) can be used to detect materials with

22

different atomic numbers [52]. Therefore, the samples prepared on a testing mold developed at TBU and IFAM were analyzed by a BSE detector to confirm its suitability. From the results, the signs of the powder/binder separation was detected at the entrance to each square element (Figure 22: dark points – carbon, bright points – iron) which complies with theoretical assumptions [13].
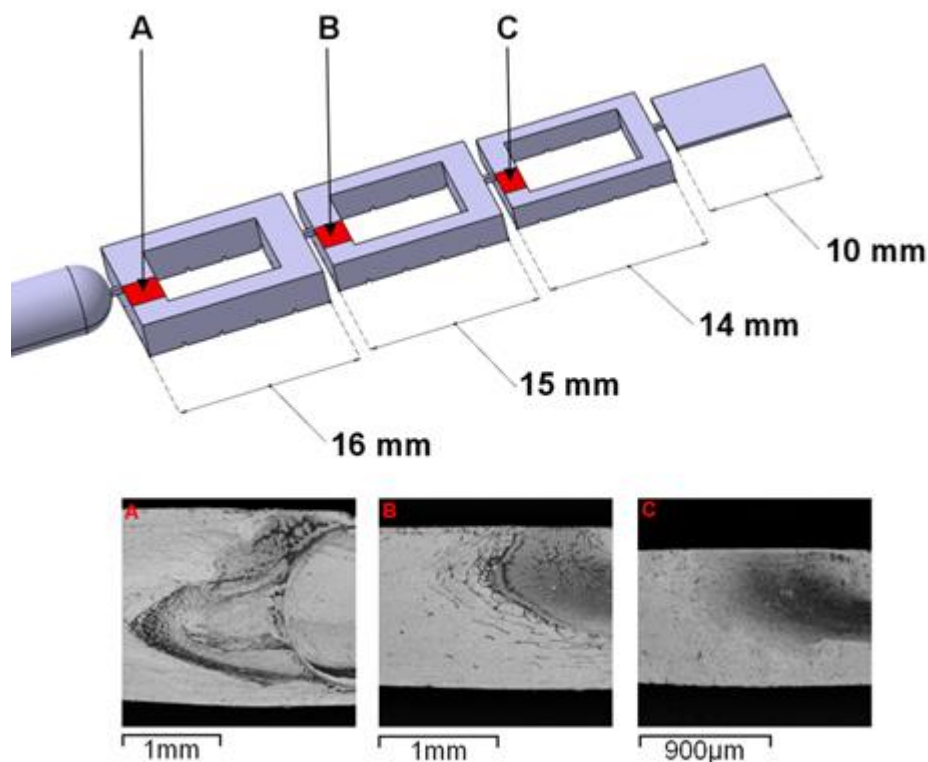
Figure 22 – Development of a flow front obtained at the positions A to C of the testing mold in separated areas

However, a qualitative analysis is not sufficient for the purpose, because it does not provide information about the degree of a phase separation which would help PIM producers to predict the structure defects as unacceptable porosity and cracks of their products. For this reason, combination of SEM with EDX analysis (Energy-dispersive X-ray spectroscopy) of the distribution of elements typical for binder (carbon) and powder (iron/oxide ceramics) was performed in order to quantify phase separation.

SEM/EDX is a semi-empirical method, which allows for a major and minor element concentration determination – in our case carbon and iron/oxide ceramics. It is capable to detect elements appearing in concentrations higher than 0.1 % with analytical accuracy commonly ± 2% [53]. This is acceptable for PIM feedstocks as they contain tens of percent of carbon and iron/oxide

ceramics [1,6]. In comparison to the DSC or X-ray methods [18,20], where the results have to be compared to the standard samples of a known composition and a powder concentration, the SEM/EDX analysis offers quantitatively significant results. This can be seen from the examples of EDX spectrum derived from unseparated and separated areas depicted in Figure 23. As can be seen in Table 1, the occurrence of elements typical for the binder (carbon) rises more than two times in the area of separation, while the occurrence of the iron as well as other alloying elements of the powder considerably decreases.
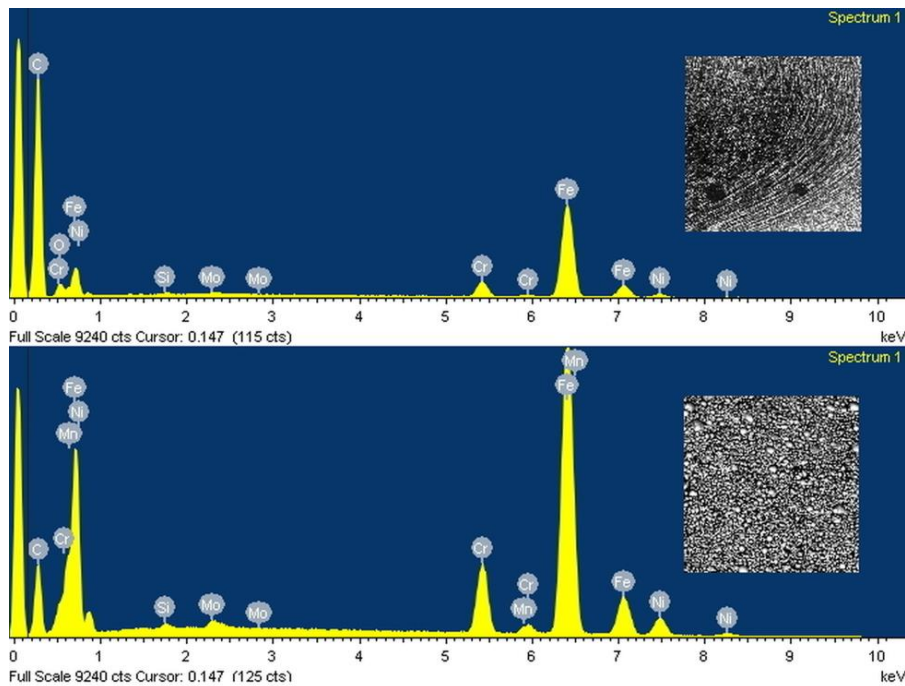
Figure 23 – EDX spectra of separated and unseparated areas in PIM feedstocks

Table 1 – Concentration of elements in separated and unseparated areas displayed in Figure 23.

Separated area		Unseparated area	
Element	Weight (%)	Element	Weight (%)
C	**62.61**	**C**	**24.98**
Si	0.09	Si	0.24
Cr	2.71	Cr	8.35
Mn	-	Mn	0.15
Fe	**27.43**	**Fe**	**59.73**
Ni	1.51	Ni	5.52
Mo	0.36	Mo	1.03

SEM/EDX arises a possibility to provide a quantitative EDX mapping of testing areas A to C representing individually a distribution (in weight percentage) of an element typical for powder or binder. The concentration of iron or ceramic oxide has been selected as a measure of the separation or the uniformity of the distribution of the powder particles within the binder. In the following, the EDX maps were converted to a black/white scale for a better data processing. Figure 24 demonstrates such distribution map of iron from 0 % (black color) to 100 % (white color) in positions A to C of the tested stainless steel sample. Clearly, there is an evidence of the separation, which is more pronounced with the flow front.
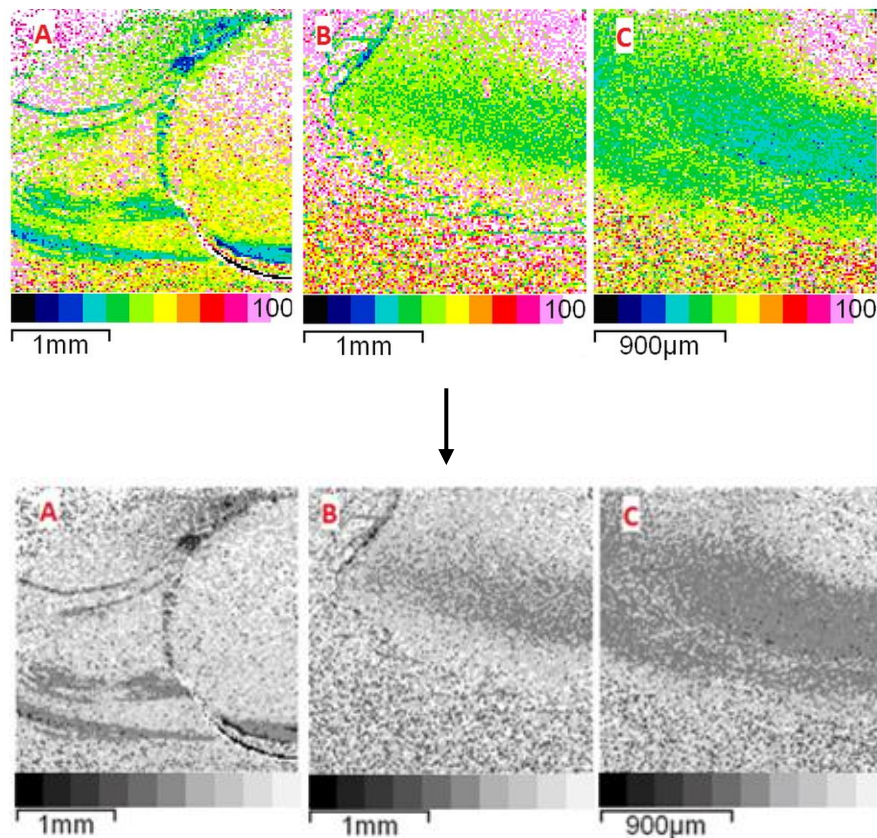
Figure 24 – EDX quantification maps of iron distribution; black/white conversion

For a purpose of a simple comparison among different feedstocks, the distributions of the elements were analyzed mathematically in order to provide a single parameter (so called variability coefficient of separation) characterizing a tendency of tested feedstocks to separation.

The rate of the phase separation represents the non-uniformity of powder and binder distribution, i.e. non-uniformity of bright and dark points on EDX maps. First, the data smoothing by averaging the value of the neighboring pixels was provided (due to tests artifacts resulting from processing). Then, if a completely

bright area is assigned with 100 % and purely dark picture to 0 %, it is possible to convert an image into a matrix. For the determination of the variability coefficients, the compute of standard deviations (σ) of pixels in averaged images was used. The phase separation expressed the deviation from the original content of powder in the feedstocks, therefore the $\bar{x}$ (mean value) in the Equation 5 is replaced by the parameter B representing the original content of the powder in a feedstock (measured by EDX for an exact comparison).

$$\sigma = \sqrt{\frac{1}{N} \sum_{i=1}^{N} (x_i - B)^2} \tag{5}$$

Thus, the variability is calculated relatively to the initial (unseparated, unmolded) state of a powder concentration. Schema of a calculation of variability coefficients is depicted in Figure 25.
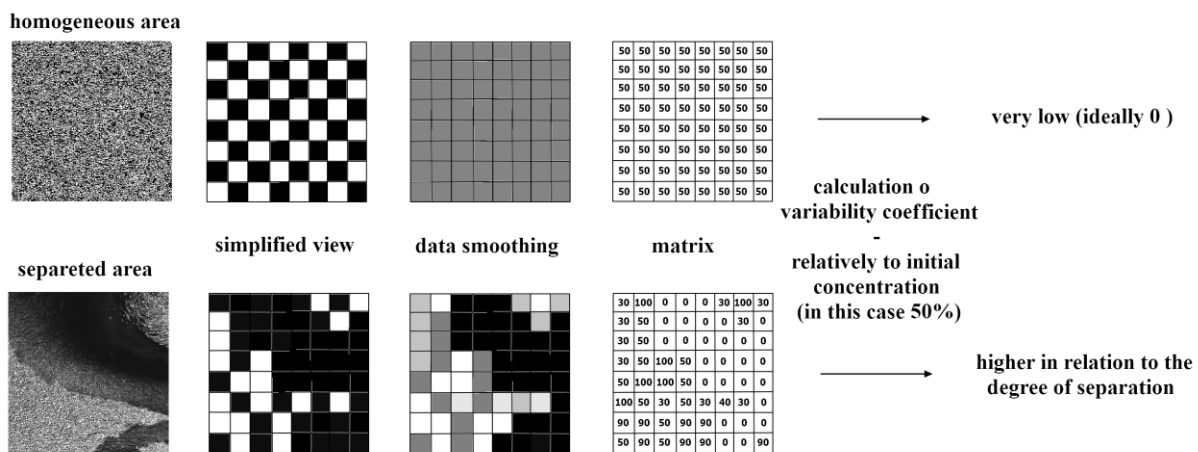
Figure 25 – Schematic demonstration of variability coefficient calculation

The testing of the developed method covered both in-house prepared and commercially available PIM feedstocks; their composition can be seen in Table 2. Commercial feedstocks C316L, P316L and E316L were based on gas atomized pre-alloyed stainless steel 316L and varied in polymer binders (abbreviated C, P and E for catalytic, partly water soluble and partly ethanol soluble binder systems, respectively). All these feedstocks had powder volumetric concentration higher than 60 %. On the other hand, ceramic powders – zirconium oxide (ZrO_2) and aluminum oxide (Al_2O_3) – were admixed to commercially available binder system Licomont EK 583 at the loading level of 50 vol.%.

Table 2 – Overview of tested feedstocks

Abbreviation of feedstock	Type of powder	Type of binder	Commercial name	Producer
C316L	Stainless steel 316L	Catalytic (Poly-acetal based)	Catamold 316LG	BASF
P316L	Stainless steel 316L	Partly water soluble (PEG based)	PolyMIM 316L D 110 E	PolyMIM GmbH
E316L	Stainless steel 316L	Partly ethanol soluble	Embemould 316L S16	eMBe GmbH
ZrO_2	Ceramic ZrO_2	LDPE+EVA+PW	-	in-house
Al_2O_3	Ceramic Al_2O_3	LDPE+EVA+PW	-	in-house

Results of the analysis (Figure 26) for Fe, Al and Zr as typical elements of tested feedstocks provide the quantification of the development of the separation at the tested positions (A, B, C) of the mold. Low and uniform variability anticipates the PIM process without defects arising from the separation. Each feedstock was also inspected in the area without separation (sample prepared by pressing; dotted lines in Figure 26). As can be seen, the samples without separation reached low and constant variability ranging from 2 to 5 % for E316L and other feedstocks, respectively.
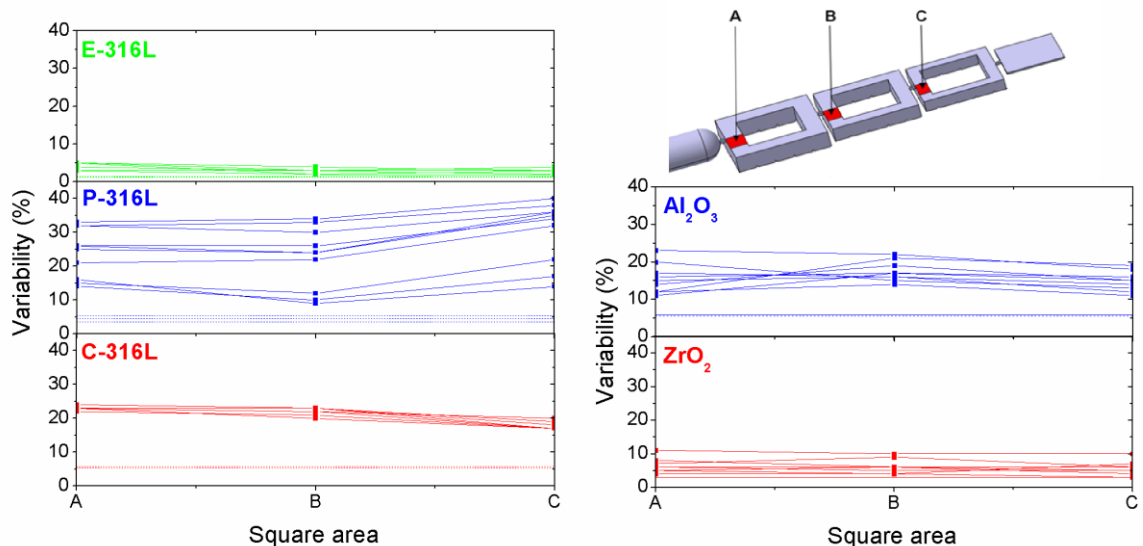

Figure 26 – Variability coefficients of tested feedstocks

at positions A to C of testing mold (each representing a set of 10 samples)

From the results obtained on the separated samples the different mechanism of the separation for tested materials is evident. The variability of the tested materials shows that C316L is faster prone to the separation, but it has a certain ability to reverse it back, while the continuous progress is attained for P316L. The reproducibility is very good for C316L (±2) in comparison to about ±10 in case of P316L feedstock. The feedstock E316L exhibited the lowest variability (with reproducibility ±2), even the values of separated E316L could be compared with values of unseparated C316L and P316L. This means very low tendency of E316L to a phase separation affected by critical geometric elements of injection molds, which is advantageous for PIM production.

In case of ceramic feedstocks, zirconia oxide feedstock exhibited a better reproducibility (4 %) in comparison with alumina oxide feedstock (7 %). In addition, the uniform and lower variability of zirconia feedstock reduced defects of PIM process.

The group of metal based feedstocks contained the same type of powder with the different binders, on the other hand, the group of ceramic feedstocks was composed of the same type of binder with two different powders. Therefore, the different tendency of PIM materials to the phase separation can be concluded. Both – powder and binder – are important for optimization of PIM feedstocks to ensure efficient manufacturing process.

The new approach to detect the phase separation of highly filled polymers prior debinding/sintering provides some advantages in comparison with exiting methods. The analysis can be done without the need for standard sample preparation of defined powder concentration. In addition, it is not necessary to know a composition of a binder, and therefore, commercially available feedstocks can be tested. Finally, the molded samples can be analyzed directly without any additional treatment.

4. Wall slip effect during the flow of PIM materials

This chapter summarizes findings published in Papers II and III

Phase separation is closely related to a wall slip effect; shear rate gradients located close to flow channel walls cause a displacement of powder particles during shearing. Nevertheless, the wall slip affects not only a phase separation, but also an overall rheological performance of PIM materials. Mooney [54] proposed rheological approach to determine the wall slip velocities already in 1931. This analysis is based on changing the surface-to-volume ratio of the

capillary dies via changing length L and radius R of the dies, but keeping their ratio constant.

For a capillary rheometer, apparent values of shear rate $\dot{\gamma}_a$ and shear stress τ_a are determined as

$$\dot{\gamma}_a = \frac{4\dot{Q}}{\pi R^3}; \; \tau_a = \frac{\Delta p R}{2L} \tag{6}$$

where $\dot{Q}$ is the volumetric flow rate and Δp is the measured pressure drop.

Consequently, a true average velocity (v_{true}) is given by the difference of an average v_{av} $\left(= \dot{Q}/\pi R^2\right)$ and slip v_{slip} velocities

$$v_{true} = v_{av} - v_{slip} \tag{7}$$

Multiplying this relation by $4/R$ and using Eq. (6) we obtain the dependence of a slip-corrected shear rate on apparent shear rate and wall slip velocity

$$\dot{\gamma}_{a,slip-corrected} = \dot{\gamma}_a - \frac{4v_{slip}}{R} \tag{8}$$

or in other form

$$(intercept) = \frac{4\dot{Q}}{\pi R^3} - (slope)\frac{4}{R} \tag{9}$$

Geometrical interpretation of the last two relations is illustrated in Figure 27.
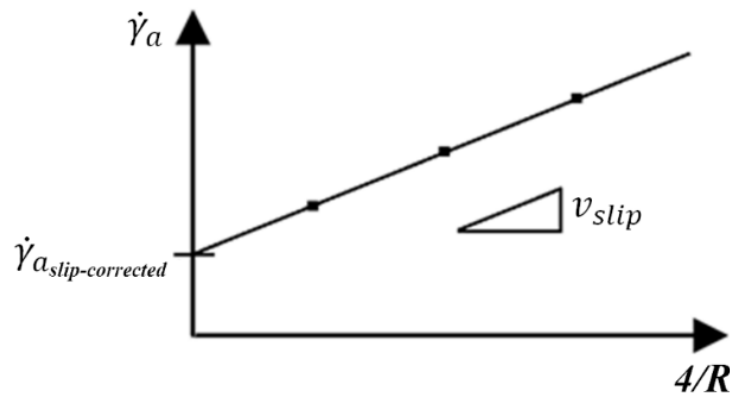

Figure 27 – Calculation of wall slip velocity using Mooney approach

As can be seen from Eq. 8 and/or Eq. 9, the viscosity of a compound exhibiting a wall slip must be corrected; otherwise, obtained shear rate values are unrealistic.

From the previous studies (described in the theoretical part of the Thesis) it can be concluded that the wall slip velocity of highly filled compounds is affected above all by:

- binder system and testing temperature through variations in a thickness of a polymer layer formatted close to walls [44,55]

- size of powder particles; small particles can approach close to a wall, and thus reduce a polymer layer thickness [56]

- mold design, material and surface roughness [46,57,58].

Therefore, first part of a wall slip analysis focused on online rheometer testing with adjustable die gap and different surface roughness (Table 3) in order to obtain experimental data at the conditions close to processing ones.

Table 3 – Characteristics of slit dies used

Metal powder feedstocks			Ceramic powder feedstocks		
Geometry (mm)	Surface	Roughness S_a (μm)	Geometry (mm)	Surface	Roughness S_a (μm)
10x0.5x100	smooth	0.25 ± 0.03	10x1x100	smooth	0.81 ± 0.03
	roughened	0.95 ± 0.02		roughened	9.65 ± 0.18
15x1x100	smooth	0.07 ± 0.00	10x2x100	smooth	0.82 ± 0.04
	roughened	0.77 ± 0.03		roughened	7.87 ± 0.70

At first, the purpose was to point out that wall slip is a typical rheological effect for PIM compounds, occurring for the most often employed PIM feedstocks, and thus it should be always examined when performing rheological characterization of these highly filled polymers. Therefore, both commercially available and in-house metal and ceramic feedstocks (Table 4) were tested.

Table 4 – Wall slip tested PIM feedstocks

Abbreviation of feedstock	Type of powder	Type of binder	Commercial name	Producer
P316L	Stainless steel 316L	Partly water soluble (PEG based)	PolyMIM 316L D 110 E	PolyMIM GmbH
P17-4PH	Stainless steel 17-4PH	Partly water soluble (PEG based)	PolyMIM 17-4PH D 110 E	PolyMIM GmbH
C316L	Stainless steel 316L	Catalytic (Poly-acetal based)	Catamold 316 L G	BASF
C17-4PH	Stainless steel 17-4PH	Catalytic (Poly-acetal based)	Catamold 17-4PH G	BASF
ZrO_2	Ceramic ZrO_2	LDPE+EVA+PW	-	in-house
Al_2O_3	Ceramic Al_2O_3	LDPE+EVA+PW	-	in-house

Concerning the effect of processing tools (roughness and chemical nature of materials), stainless steel was found more prone to a wall slip than aluminum [46] and the rough surface, where solid particles can move into a groove, suppresses the formation of a low molecular layer on channel walls [45]. In case of PIM compounds, we obtained the same trend during testing metal powders (316L and 17-4PH) in a catalytic binder and ZrO2 feedstocks, where the effect of surface roughness was evident – a lower viscosity is obtained for the smooth surfaces. The observed trend is also in an agreement with the simulations performed by Papanikolaou et al.[59], where parallel liquid layers formed near a smooth wall surface were disturbed in case of a roughened surface (leading to a higher viscosity).

On the other hand, there are some unexpected results, such as imperceptible influence of a surface roughness for the water soluble binder. In that case the thickness of the polymer layer formed at the channel wall, must be higher than the surface irregularities of the tested slit dies [45,60]. Figure 28 demonstrates that the values of slip velocities obtained for Al_2O_3 powder in the smooth slit die are comparable with the slip velocities of ZrO_2 feedstock in the roughened slit die. However, Al_2O_3 feedstock could not be tested at the roughened slit die due to the pressure fluctuations occurring during the flow.
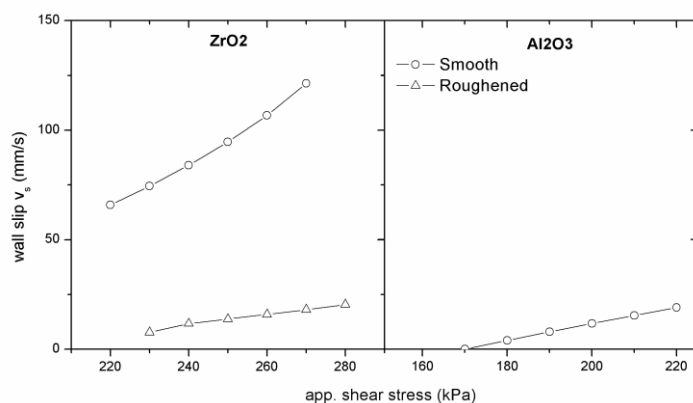
Figure 28 – Effect of surface roughness on wall slip velocity of zirconium oxide (ZrO$_2$) and aluminium oxide (Al$_2$O$_3$) powders in LDPE+EVA+PW binder

Another factor influencing wall slip might be a die geometry. The feedstocks based on stainless steel powders as well as ZrO$_2$ feedstock showed the same trend in the slip dependence on die dimension regardless of surface roughness – the smaller gap height (1 mm) supported the wall slip effect, while this was substantially reduced for 2 mm gap. However, the feedstocks with partly water-soluble binder (P316L and P17-4PH) show a stronger influence of the flow channels geometry on viscosities than that with the catalytic binder, indicating an enhanced tendency to slip. In addition, the tendency of Al$_2$O$_3$ feedstock to wall slip as a function of the die geometry and surface roughness is generally less pronounced than for ZrO$_2$ compound, although as it was showed recently by Hausnerova et al. [61], their surface characteristics (surface energies) were fairly similar - 44 and 47 J/m2 for ZrO$_2$ and Al$_2$O$_3$, respectively.

The results obtained correspond to findings on pure linear low density polyethylene in capillaries with different surface roughness [46] as well as on suspensions containing polymer matrix poly(butadiene-acrylonitrile-acrylic acid) filled with glass spheres (particles mean size 35.3 μm and 85.4 μm) [57] and poly(methyl methacrylate) solid spheres (121.2 μm) in hydroxyl-terminated polybutadiene [56], where smooth flow channels wall and small channels geometry [38,62] were found to be the most significant factors causing wall slip.

Finally, the influence of an entrance angle of a capillary die was investigated. Application of flat or conical dies (Figure 29) might change both – slip layer thickness and slip velocity.
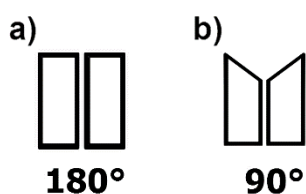
32

Figure 29 – Schematic representation of testing dies: a – flat, b – conical

The literature comparing flat and conical dies in connection with a wall slip is rather scarce. Liang [63] and Ardakani et al. [64] tested changes in a pressure drop with different capillary entrance angles during extrusion. They found that under a constant pressure, the shear rate increased with the capillary entrance angle. In our experiment, the dies tested are flat (180°) and conical (90°). Suitability of each die was evaluated by Mooney method with respect to compatibility of the obtained results with the general findings on a wall slip issue stated in literature.

The same metal-based feedstocks as in previous on-line rheomery testing were used, see Table 4. From the results of wall slip velocities, the strong effect of the entrance angle of the capillary is obvious (Figure 30).
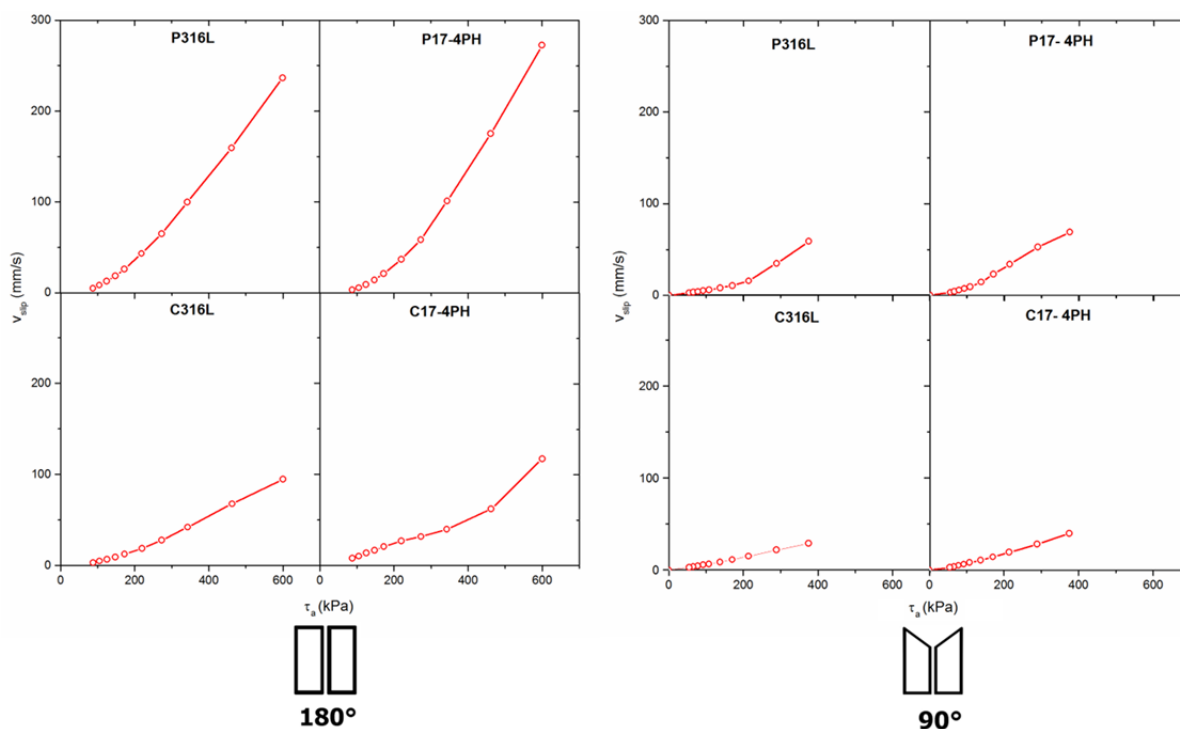

Figure 30 – Wall slip velocity as a function of apparent shear stress based on using of flat 180°and conical 90° entrance dies

According to Figure 30 both metal feedstocks (316L and 17-4PH) based on the partly water soluble binder system (P) exhibited the substantially higher slip velocity at the wall than those containing the catalytic binder system (C).

33

Further, the slip velocities of both binder systems with 17-4PH powder are slightly higher than those with 316L compounds. When considering rounded shape of all types of powders (gas atomized), and also their similar particle distribution, the interactions between binder and powder plays a significant role in a wall slip evaluation. This applies also for an overall improvement of the processing of PIM feedstocks, where the interactions between binder system components are critical as we recently showed in the studies dealing with the interactions among parafin, acrawax, carnauba wax and polyethylene glycol binders [65,66].

The same procedure was carried out with a conical 90° entrance die, see Figure 30. The lower (conical) entrance angle decreases the wall slip velocity. Similar observations have been done for viscoelastic materials; Liang [63] founded that the minimum pressure drop occurred about 75° entrance angle, during testing of unvulcanised rubber compound (natural rubber, styrene-butadiene rubber, sulphur, stearic acid, carbon black, etc.) on Monsanto processability tester. This result was confirmed by Ardakani et al. [64] for an extrusion of toothpaste compounds, where almost negligible pressure drop in a conical zone was obtained.

Nevertheless, the main finding of this experiment is the better linear proportionality between wall slip velocity v_{slip} and shear stress τ_a obtained with 90° entrance dies. The relation has been proposed by Yilmazer and Kalyon [55] and Soltani and Yilmazer [44] for concentrated suspensions

$$v_{slip} = a(T)\tau_a \qquad (10)$$

where $a(T)$ is a temperature dependent coefficient.

As it can be seen from Figure 30, only results obtained for 90° entrance dies comply with the above linear relation (especially for the catalytic binder system). No such relation can be derived in Figure 30 for a flat 180° die. This justifies the applicability of the conical entrance dies in simulations of PIM feedstock flows. The flat 180° entrance die enhances the tendency of the feedstocks to the separation of polymer binder and powder, which is then accumulated in the dead zones (edges) above the dies. In addition, the sharp edges cause rapid changes in a shear rate, which further support separation of feedstocks (binder and powder) components [13,67,68] resulting in higher wall slip velocities.

# 5. Surface properties of PIM parts related to processing conditions

This chapter summarizes findings published in Papers IV and V

Nowadays, optimization of powder injection molding step is done largely by a trial and an error approach; therefore, there is a strong need for investigation of the relation between the processing conditions and the final surface properties evaluated with the help of appropriate mathematical/statistical methods.

Mixing and injection molding parameters are selected usually according to viscosity data (Figure 31), while conditions for debinding and sintering are set up based on thermal analyses of PIM feedstocks (Figure 32). It has been generally accepted that the rheological performance of PIM feedstocks is also important parameter affecting the surface quality of final PIM items.
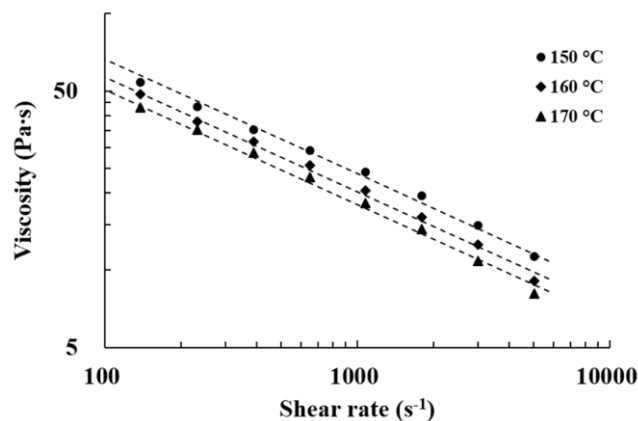
Figure 31 – Temperature dependent viscosity data of PIM feedstock (67 vol.% titanium powder)
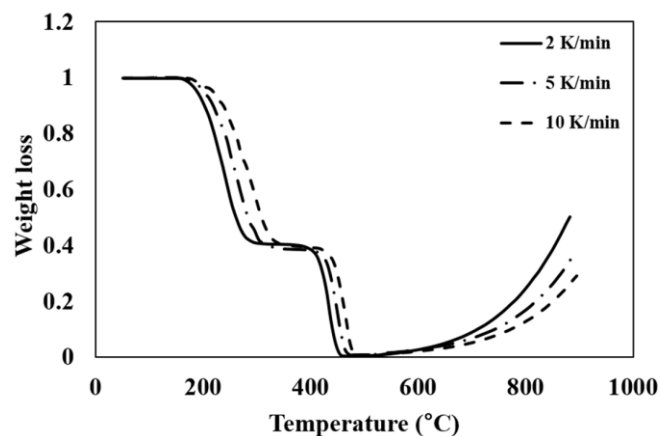
Figure 32 – Thermogravimetric analysis of PIM feedstock (67 vol.% titanium powder)

Last part of the thesis deals with optimization of processing conditions of PIM process to achieve an acceptable surface quality of final sintered parts. PIM items with high surface quality requirements as those depicted in Figure 33 were tested. They are made of aluminium oxide and contain complicated rotational areas. The internal sections of the spirals exhibited the surface cracks and defects after sintering resulting from the phase separation during the injection molding step of PIM (Figure 34).

Figure 33 – Design of tested Al₂O₃ PIM part
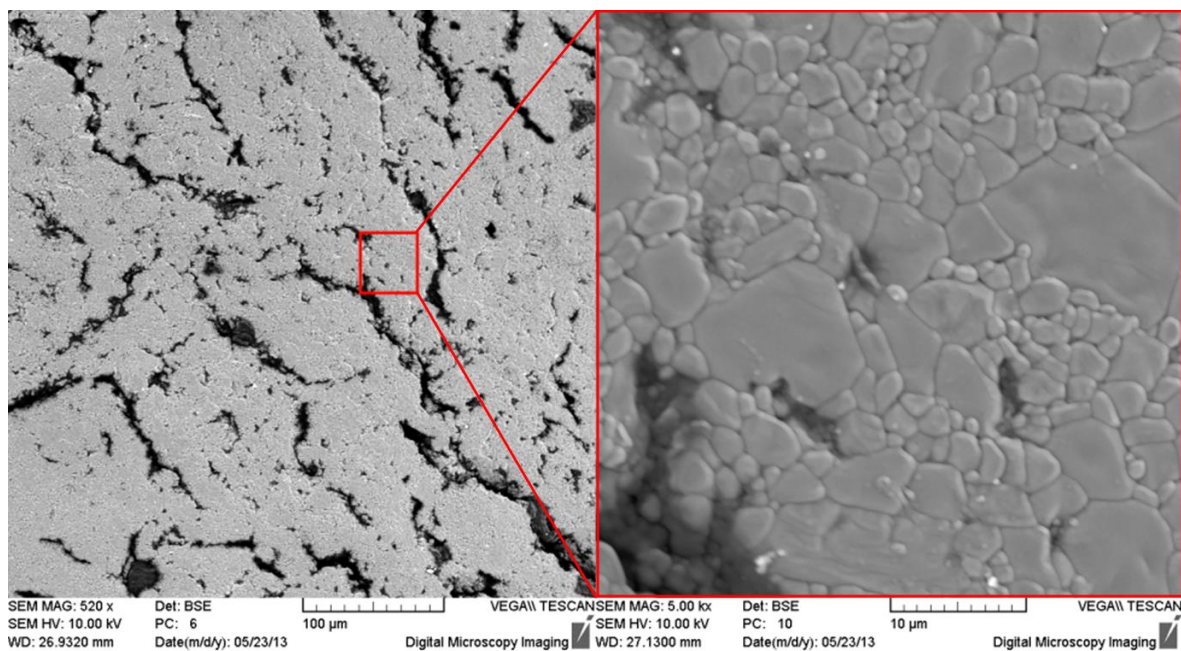
Figure 34 – Surface defects of sintered alumina oxide PIM part

The testing samples were prepared by injection molding of 60 vol.% of Al_2O_3 powder compounded with a commercial multi-component binder Licomont EK 583-G and surfactant (1 wt.% oleic acid) at various conditions. Two series of samples were selected differing in molding (nozzle) temperatures – 150 °C and 160 °C, and debinding routes, where T in the abbreviation means that the sample were debound thermally and ST stands for combined solvent/thermal debinding. In order to obtain a quantitative analysis, a contactless 3D Chromatic Length Aberration (CLA) scanner (Talysurf 300, Taylor and Hobson, UK) was used for roughness measurement. Tested surfaces were subjected to a height measurement over a rectangular area (1 x 1) mm with the scanning rate of 100 μm/s and spacing 5 μm.

Firstly, the Box-Plot diagrams of R_p, R_v and R_a showing the considerable scatter of measured data were created for samples molded at 150 and 160 °C, and then debound thermally or solvent/thermally (Figure 35).

Therefore, Kruskal-Wallis statistical approach has been employed further as it enables simple analysis of a median scatter of differently processed samples (differing in temperature and debinding route). A Zero-hypothesis expects that the particular surface roughness parameters (R_p, R_v, R_a) have the same median values in the sample groups. In the following, the Zero-hypothesis for R_a parameter of the samples molded at two different temperatures and debound thermally (150T and 160T) in the longitudinal direction is:

$$H_0: \tilde{X}_{Ra}150T_1 = \tilde{X}_{Ra}150T_2 = \tilde{X}_{Ra}150T_3 = \tilde{X}_{Ra}160T_1 = \tilde{X}_{Ra}160T_2 = \tilde{X}_{Ra}160T_3$$

The alternative hypothesis expects not equal of median:

$$H_A: NON$$

$$p = 0$$

According to this result, Zero-hypothesis H_0 is denied on the confidential level 0.95 %, i.e. we suppose that the differences in the investigated surfaces are due to the changes in the processing conditions (in this case – temperature).

The same procedure has been made for the samples molded at two different temperatures and debound by a combined solvent/thermal route (150ST and 160ST) in the longitudinal direction as well for the sample groups in transverse direction (Table 5).
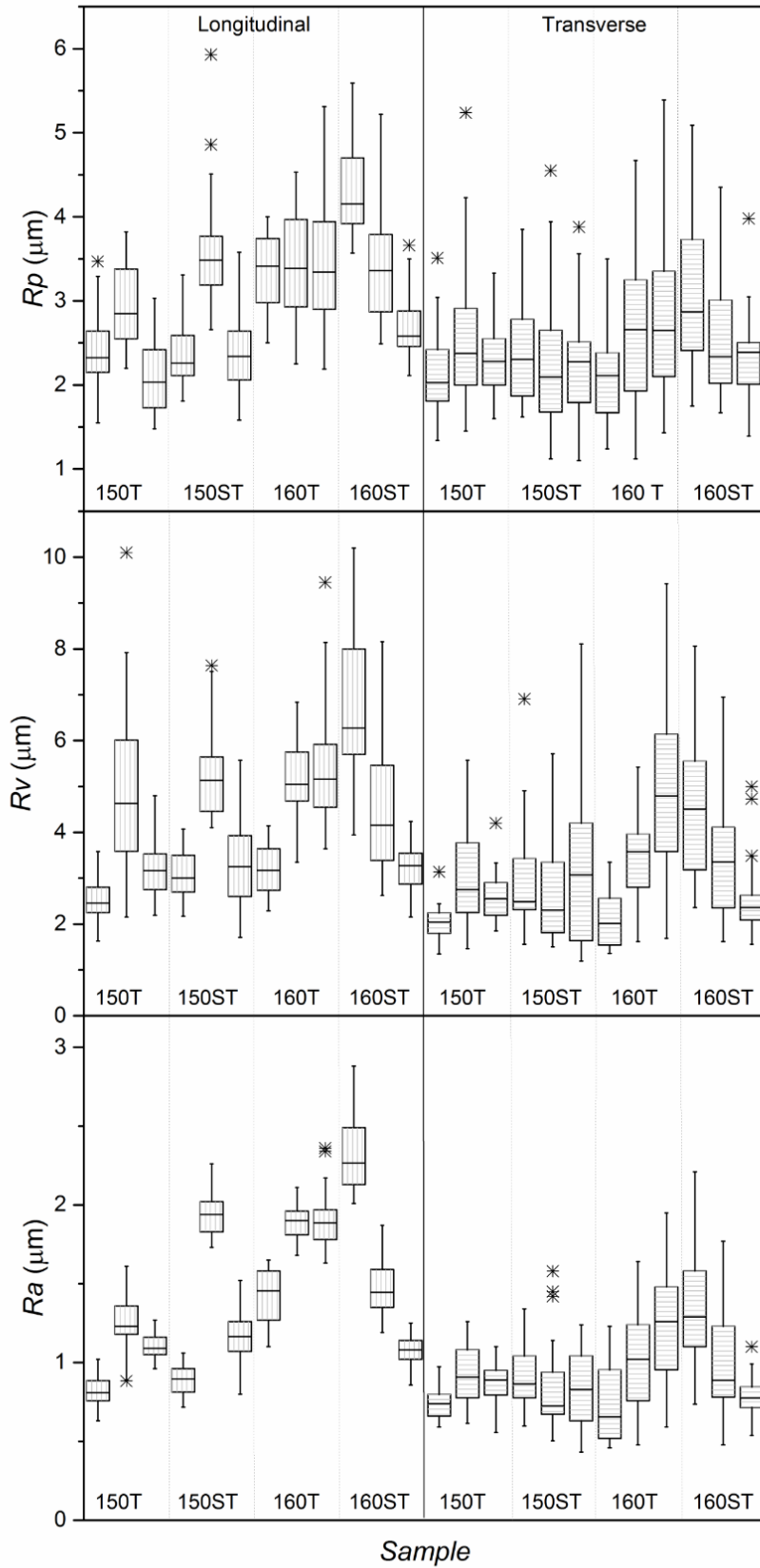
Figure 35 – Box-Plot diagrams of Rp, Rv and Ra for measured samples

Table 5 – Results of Kruskal-Wallis analysis

Testing group	P value	H_0
150T/160T – Longitudinal	$0 < 0.05$	denied
150ST/160ST – Transverse	$0 < 0.05$	denied
150T/160T – Longitudinal	$0 < 0.05$	denied
150ST/160ST – Transverse	$0 < 0.05$	denied

Zero-hypothesis for all sample groups was denied. It means, Kruskal-Wallis method confirmed on the confidential level 0.95 (i.e. 5 % error) that the medians of selected samples do not vary at random, and surfaces of samples were affected by molding temperature (150 °C or 160 °C) as well by debinding route. Therefore, the surface structure of sintered parts depended on these processing conditions and according this knowledge process can be optimized in relation to surface properties.

Unfortunately, parameters R_p, R_v or R_a cannot intercept a profile shape of a surface. Thus, Abbott-Firestone curves, which describe a surface texture of an object and detect a flatness or pointedness of surface, were also derived. All measured surface profiles were quantified by a cumulative probability of values of Abbott-Firestone curves (Figure 36).
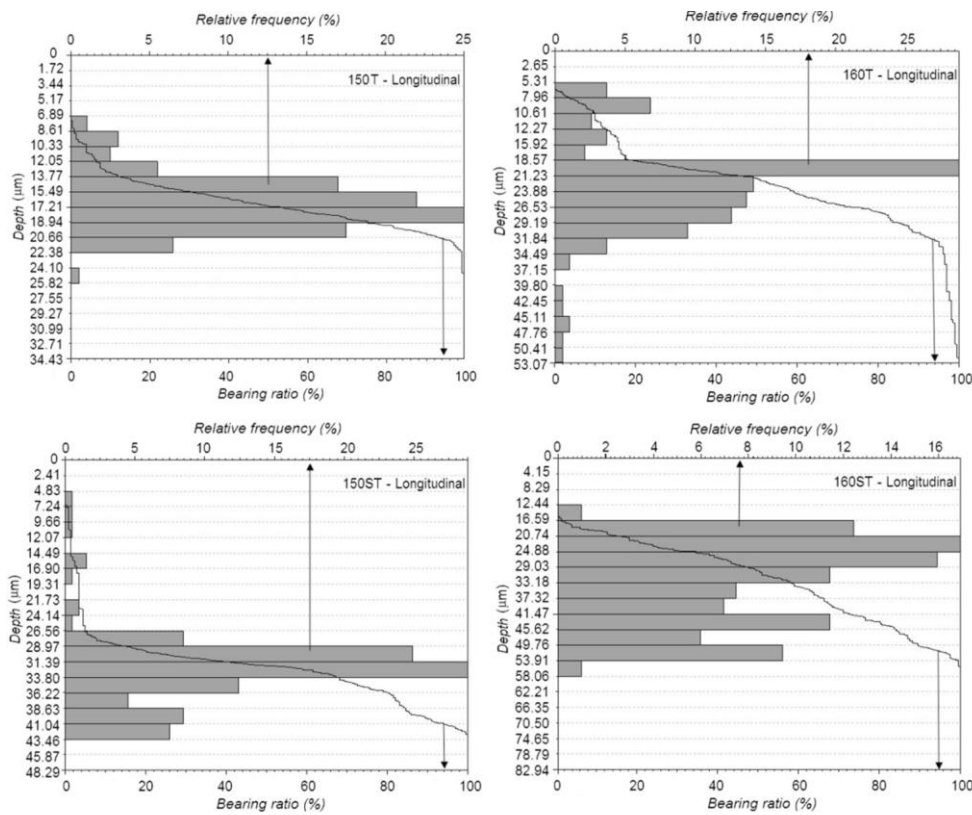

Figure 36 – Abbott-Firstone curves of tested surfaces

This analysis shows that the Abbott-Firstone curves of the surfaces molded at 150 °C decline faster than those obtained at 160 °C (for both debinding routes). A steeper curve means a low accumulation and a sharp surface profile, which should be avoided whenever a smooth surface of parts is desired. In this respect, the conclusion is that the higher temperature of injection molding results in the more suitable surface structure of the alumina sintered items.

Overall, the obtained surface roughness data treated with suitable statistical analytical methods reveals the effect of the processing conditions during the PIM process on the final parts. Relating the surface properties of the final sintered parts to the processing parameters might provide a powerful tool to control the particular steps of PIM process.

CONCLUSION

The thesis is devoted to phase separation of highly filled materials employed in Powder Injection Molding (PIM) causing defects on final sintered parts. These defects cannot be removed from sintered parts with a post-processing treatment, and thus the separation is a source of considerable economic and environment losses. The detection of the phase separation prior debinding/sintering is an important step in optimization of PIM process.

In this regard, the non-destructive method for the quantification of the phase separation was developed by combination scanning electron microscopy and energy-dispersive X-ray spectroscopy in order to intercept inhomogeneities in distribution of chemical elements contained in PIM feedstocks. These inhomogeneities (resulting from separated binder and powder) were quantified with the help of a mathematical approach based on standard deviations of analyzed element concentrations. Then, the tendency to the phase separation is expressed as a single parameter, so called variability coefficient of separation.

From rheological point of view, the phase separation is connected to a wall slip phenomenon. Commercially available as well as in-house PIM materials were tested to a wall slip, and it was found that at certain flow conditions they all are slip-prone. Thus, a slip correction cannot be neglected when reliable rheological data are derived, especially for flow simulations of injection molding step of PIM. The research results reveal also an importance of a surface roughness of flow channels to wall slip development if surface irregularities are higher than polymer layers formed at flow channel walls. Wall slip velocities decrease with increasing surface roughness. In addition, higher tendency of PIM materials to wall slip was observed in smaller flow dies. Finally, wall slip velocities are affected not only by surface roughness and dimension of dies, but also by entrance angle of a die. In this respect, lower entrance angle of capillaries was proposed for testing of PIM materials as it provides more accurate rheological data.

Finally, final sintered structures resulting from a phase separation might be affected by process conditions. The relation of the final surface roughness to the molding and debinding conditions might provide a powerful tool to optimize PIM process. Surface properties of sintered PIM items were evaluated and treated by carefully selected statistical methods (Kruscall-Wallis and Abbot-Firstone) and it was observed that the surface profiles of the tested samples do not vary at random with the processing conditions as mold temperature or debinding route. Therefore, PIM process can be optimized to reduce and/or

eliminate phase separation by tailoring not only feedstocks compositions, but also by controlled set-up of processing conditions during injection molding and debinding step.

CONTRIBUTION TO SCIENCE AND PRACTICE

Nowadays, the phase separation of feedstock components during Powder Injection Molding (PIM) causes up to 25 % defects [12] of final sintered parts. The PhD thesis represents the contribution to eliminate this issue. In this respect, the new approach to quantify the phase separation prior sintering, when the products can be still re-granulated and employed again, was developed. In addition, the research focused on an investigation of phase separation via rheological approaches, where a wall slip phenomenon is a parameter to be tested. Concerning PIM compounds, there are - to our best knowledge - no studies considering the dimensions and surface roughness of the processing dies for the wall slip measurements of PIM materials. Also, there are no wall-slip studies performed on commercial feedstocks available. Finally, the method to relate and quantify PIM processing conditions to surface structure of final products resulting from phase separation was proposed.

The following findings can be considered as important contributions of the PhD thesis to science and practice:

- non-destructive method for quantification of phase separation enabling direct testing of molded samples developed
- integrating of wall slip to rheological characterization of PIM feedstocks - requirements for the proper rheological testing set up investigated and proposed
- processing conditions related to resulting surface quality of PIM items supported with the reliable and suitable statistical analysis.

In summary, this work conduced understanding of PIM process aimed to eliminate its most severe issue - phase separation of feedstock components occurring during injection molding step. The results presented in the thesis were published in highly respected scientific journals.

REFERENCES

[1] German R. M., Bose A., *Injection Molding of Metals and Ceramics, Metal Powder Industry*, 1997, ISBN 978-1878954619

[2] German R. M., *Metal Injection Molding*, 2011, ISBN 978-0-9819496-6-6

[3] Bilovol V. V., Kowalski L., Duszczyk J., Modeling of transient temperature fields during filling stage of powder injection moulding, *Powder Metallurgy*, 2000, 43, 228-232

[4] Hausnerova B., Marcanikova L., Filip P., Saha P., Optimization of Powder Injection Molding of Feedstock Based on Aluminum Oxide and Multicomponent Water-Soluble Polymer Binder, *Polymer engineering and science*, 2011, 51, 1376-1382

[5] Mannschatz A., Hohn S., Moritz T., Powder-binder separation in injection moulded green parts, *Journal of European Ceramic Society*, 2010, 30, 2827-2832

[6] Heaney D. F., *Handbook of metal injection molding*, 2012, ISBN 978-0-85709-066-9

[7] Huang B., Liang S., Qu X., The rheology of metal injection molding, *Journal of Materials Processing Technology*, 2003, 137, 132-137

[8] Liu Z. Y., Loh N. H., Tor S. B., Khor K. A., Characterization of powder injection molding feedstock, *Materials Characterization*, 2003, 49, 313-320

[9] Moritz T., Lenk R., Current status of ceramic injection moulding, *Fraunhofer Institute for Ceramic Technologies and Systems*, 2010

[10] Zauner R., Micro powder injection moulding, *Microelectronic Engineering*, 2006, 83, 1442-1444

[11] Hartwing T., Veltl G., Petzoldt F., Kunze H., Scholl R., Kieback B., Powders for Metal Injection Molding, *Journal of the European Ceramic Society*, 1998, 18, 1211-1216

[12] Williams N., Fraunhofer IFAM: A Commitment to industry oriented research helps drive MIM product development, *PIM International*, 2009, 3, 51-56

[13] Thornagel M., MIM-Simulation: A Virtual Study on Phase Separation, *Euro PM 2009*, 2009, 135-140

[14] Matas J., P., Morris J. F., Guazzelli E. S., Inertial migration of rigid spherical particles in Poiseuille flow, *Journal of Fluid Mechanic*, 2004, 515, 171-195

[15] Jiranek L., Testing mold design for investigation of powder-binder separation during powder injection molding, *Master Thesis*, Tomas Bata University in Zlin, Faculty of Technology, 2010

[16] Kubat J., Szalanczi A., Polymer-Glass Separation in the Spiral Mold Test, *Polymer Engineering and Science*, 1974, 14, 873-877

[17] Jenni M., Schimmer L., Zauner R., Stampfl J., Morris J., Quantitative study of powder binder separation of feedstocks, *Powder Injection Moulding International*, 2008, 2, 50-55

[18] Jenni M., Zauner R., Stampfl J., Measurement Methods for Powder Binder Separation in PIM Components, *Euro PM2009*, 2009, 141-146

[19] Yang S., Zhang R., Qu X., X-ray tomographic analysis of powder-binder separation in SiC green body, *Journal of the European Ceramic Society*, 2013, 33, 2935-2941

[20] Yang S., Zhang R., Qu X., X-ray analysis of powder-binder separation during SiC injection process in L-shaped mould, *Journal of the European Ceramic Society*, 2015, 35, 61-67

[21] Yang S., Zhang R., Qu X., Optimization and evalution of metal injection molding by using X-ray tomography, *Materials Characterization*, 2015, 104, 107-115

[22] Busignies V., Leclerc B., Porion P., Evesque P., Couarraze G., Tchoreloff P., Quantitative measurement of localized density variations in cylindrical tables using X-ray microtomography, *European Journal of Pharmaceutics and Biopharmaceutics*, 2006, 64, 38-50

[23] Hausnerova B., Marcanikova L., Filip P., Saha P., Wall-slip Velocity as A Quantitative Measure Of Powder-Binder Separation During Powder Injection Moulding, *World Congress PM2010*, 2010, 557-562

[24] Adames, J.M., Characterization of polymeric binder for metal injection molding (MIM) process, *Doctoral Thesis*, Arkon, Ohio, 2007

[25] Hausnerova B., Rheological characterization of powder injection molding compounds, *Polimery-W*, 2010, 55, 3-11

[26] Wei F., Xinbo H., Ruijie Z., Shidi Y., Xuanhui Q., The effects of filling patterns on the powder-binder separation in powder injection molding, *Powder Technology*, 2014, 256, 367-376

[27] Michele J., Patzold R., Donis R., Alignment and aggregation effects in suspension of spheres in non-Newtonian media, *Rheologica Acta,* 1977, 16, 317-321

[28] Ahn S., Park S. J., Lee S., Atre S. V., German R. M., Effect of powder and binder on material properties and molding parameters in iron and stainless

steel powder injection molding process, *Powder Technology*, 2009, 193, 162-169

[29] Isayev A. I., Xiyun F., Steady and oscillatory flows of silicon-polypropylene ceramic compounds, *Journal of Materials Science*, 1994, 29, 2931-2938

[30] Filip P., David J., Pivokonsky R., Modelling of non-monotonous flow curves using empirical constitutive equations, *Acta Technica CSAV*, 2006, 51, 349-362

[31] Shivashankar T. S., Enneti R. S., Park S. J., German R. M., Atre S. V., The effects of material attributes on powder-binder separation phenomena in powder injection molding, *Powder Technology*, 2013, 243, 79-84

[32] Mohseni M. M., Rashidi F., Axial annual flow of a Giesekus fluid with wall slip above critical shear stress, *Journal on Non-Newtonian Fluid Mechanics*, 2015, 223, 20-27

[33] Laun M. H., Capillary rheometry for polymers melts revisited, *Rheologica Acta*, 2004, 43, 509-528

[34] Denn M. M., Extrusion Instabilities and Wall Slip, *Annual Review of Fluid Mechanics*, 2001, 33, 265-287

[35] Kwon T. H., Ahn S. Y., Slip characterization of powder/binder mixtures and its significance in the filling process analysis of powder injection molding, *Powder Technology*, 1995, 85, 45-55

[36] Korhonem M., Mohlaschemi M., Puisto A., Illa X., Alava M. J., Apparent wall slip in non-Brownian hard-sphere suspensions, *European Physical Journal E*, 2015, 38

[37] Lam Y. C., Wang Z. Y., Chen X., Joshi S. C., Wall slip of concentrated suspension melts in capillary flows, *Powder Technology*, 2007, 177, 162-169

[38] Barnes H. A., A review of the slip (wall depletion) of polymer solutions, emulsions and particle suspensions in viscometers: its cause, character, and cure, *Journal of Non-Newtonian Fluid Mechanics*, 2005, 56, 221-251

[39] Bryan M. P., Rough S. L., Wilson D. I., Investigation of static zone and wall slip through sequential ram extrusion of contrasting micro-crystalline cellulose-based pastes, *Journal of Non-Newtonian Fluid Mechanics*, 2015, 220, 57-68

[40] Delime A., Moan M., Lateral migrations of solid spheres in tube flow, *Rheologica Acta*, 1991, 30, 131-139

[41] Lam Y. C., Chen X., Tan K. W., Chai J. C., Yu S. C. M., Numerical investigation of particle migration in poiseuille flow of composite system, *Composites Science and Technology*, 2004, 64, 1001-1010

[42] Kalyon D. M., Review of factors affecting the continuous processing and manufacturability of highly filled suspensions, *Journal of Materials Processing and Manufacturing Science*, 1993, 2, 159-187

[43] Martin P. J., Wilson D. I., A critical assessment of the Jastrzebski interface conditions for capillary flow of pastes, foams and polymers, *Chemical Engineering Science*, 2005, 60, 493-502

[44] Soltani F., Yilmazer U., Slip Velocity and Slip Layer Thickness in flow of Concentrated Suspensions, *Journal of Applied Polymer Science*, 1998, 70, 515-522

[45] Medhi B. J., Kumar A. A., Singh A., Apparent wall slip velocity measurement in free surface flow of concentrated suspensions, *International Journal of Multiphase Flow*, 2011, 37, 609-619

[46] Chen Y., Kalyon M., Bayramli E., Effects of Surface Roughness and the Chemical Structure of Material of Construction on Wall Slip Behavior of Linear Low Density Polyethylene in Capillary Flow, *Journal of Applied Polymer Science*, 1993, 50, 1169-1177

[47] Ghosh S., Ende D., Mugele F., Duits M. H. G., Apparent wall-slip of colloidal hard suspensions in microchannel flow, *Colloids and Surfaces A: Physicochemical and Engineering Aspects*, 2016, 491, 50-56

[48] Yoshimura A., Prud'homme R. K., Wall slip corrections for Couette and parallel disk viscometers, *Journal of Rheology*, 1988, 32, 53-67

[49] Nickerson C. S., Kornfield J. A., A "cleat" geometry for suppressing wall slip, *Journal of Rheology*, 2005, 49, 865-874

[50] Liu L., Ma Y.H., He Z.Y., Rheological behavior of zirconia feedstock flowing through various channels considering wall-slip, *Ceramics International*, 2018, 44, 22387-22392

[51] Liu L., Gao Y.Y., Qi X.T., Qi M.X., Effect of wall slip on ZrO2 rheological behavior in micro powder injection molding, *Ceramics International*, 2018, 44, 16282-16294

[52] Postek M.T., Critical Issues in Scanning Electron Microscope Metrology, *Journal of Research of the National Institute of Standards and Technology*, 1994, 99, 641-671

[53] Hobbs A.L., Almirall J.R., Trace elemental analysis of automotive paints by laser ablation–inductively coupled plasma–mass spectrometry (LA–ICP–MS), *Analytical and Bioanalytical Chemistry*, 2003, 376, 1265-1271

[54] Mooney M., Explicit formulas for slip and fluidity, *Journal of Rheology*, 1931, 2, 210–222

[55] Yilmazer U., Kalyon D.M., Slip effects in capillary and parallel disk torsional flows of highly filled suspensions, *Journal of Rheology*, 1989, 33, 1197-1212

[56] Gulmus S.A., Yilmazer U., Effect of volume fraction and particle size on wall slip in flow of polymeric suspension, *Journal of Applied Polymer Science*, 2005, 98, 439-448

[57] Aral B.K., Kalyon D.M., Effects of temperature and surface roughness on time-dependent development of wall slip in steady torsional flow of concentrated suspension, *Journal of Rheology*, 1994, 38, 957-972

[58] Gulmus S.A., Yilmazer U., Effect of the surface roughness and construction material on wall slip in the flow of concentrated suspensions, *Journal of Applied Polymer Science*, 2006, 103, 3341-3347

[59] Papanikolaou M., Frank M., Drikakis D., Effects of surface roughness on shear viscosity, *Physical Review E*, 2017, 95, 1-12

[60] Lam Y.C., Wang Z.Y., Chen X., Joshi S.C., Wall slip of concentrated suspension melts in capillary flows, *Powder Technology*, 2007, 77, 162–169

[61] Hausnerova B., Bleyan D., Kasparkova V., Pata V., Surface adhesion between ceramic injection molding feedstocks and processing tools, *Ceramics International*, 2016, 42, 460–465

[62] Jeong M., Kim Y., Zhou W., Tao W.Q., Ha M.Y., Effects of surface wettability, roughness and moving wall velocity on the Couette flow in nano-channel using multi-scale hybrid method, *Computers & Fluids*, 2017, 147, 1–11

[63] Liang J.Z., Influence of Die Angles on Pressure Drop during Extrusion of Rubber Compound, *Journal of Applied Polymer Science*, 1999, 80, 1150-1154

[64] Ardakani H.A., Mitsoulis E., Hatzikiriakos S.G., Thixotropic flow of toothpaste through extrusion dies, *Journal of Non-Newtonian Fluid Mechanics*, 2011, 166, 1262-1271

[65] Bleyan D., Svoboda P., Hausnerova B., Specific interaction of low molecular weight analogues of carnauba wax and polyethylene glycol binder of ceramic injection moulding feedstocks, *Ceramics International*, 2015, 41, 3975-3982

[66] Bleyan D., Hausnerova B., Svoboda P., The development of powder injection moulding binders: A quantification of individual components` interactions, *Powder technology*, 2015, 286, 84-89

[67] He H., Li Y., Lou J., Li D., Liu Ch., Prediction of density variation on powder injection moulding-filling process by using granular modelling with interstitial power-law fluid, *Powder Technology*, 2016, 291, 52-59

[68] Liang J.Z., Chan J.S.F., Wong E.T.T., Effects of operation conditions and die angles on the pressure losses in capillary flow of polystyrene melt, *Journal of Materials Processing Technology*, 2001, 114, 118-121.

LIST OF FIGURES AND TABLES

Figures

Tables

LIST OF SYMBOLS AND ACRONYMS

Abbreviations

BSE – Backscattered electrons
C – Catalytic binder system
DSC – Differential scanning calorimetry
E – Partly ethanol soluble binder system
EDX – Energy-dispersive X-ray spectroscopy
FEM – Finite element method
FDM – Finite difference method
IFAM – Fraunhofer Institute for Manufacturing Technology and Advanced Materials
LLDPE – Linear low-density polyethylene
P – Partly water soluble binder system
PE – Polyethylene
PEG – Polyethylene glycol
PIM – Powder injection molding
PP – Polypropylene
PMMA – Polymethyl methacrylate
PS – Polystyrene
PVT – Pressure-Volume-Temperature
SEM – Scanning electron microscopy
TBU – Tomas Bata University

Symbols

$a(T)$ – Temperature dependent coefficient
B – Original content of the powder in a feedstock
D – Capillary diameter
D_P – Particle diameter
L – Capillary length
ΔP – Pressure drop
$\dot{Q}$ – Volumetric flow rate
R – Pipe/Capillary radius
R_p, R_v, R_a – Roughness parameters
$\bar{x}$ – Mean value
$\tilde{x}$ – Median value
$\dot{\gamma}$ – Apparent shear rate

δ – Inter particle spacing parameter

η_r – Relative viscosity

v_{av} – Average velocity

v_{Slip} – Slip velocity

v_{True} – Average true velocity

σ – Standard deviation

τ – Shear stress

τ_a – Apparent shear stress

Φ – Solid volume fraction

Φ_{L1} – Interstitial space liquid binder volume

Φ_{L2} – Liquid sphere shell volume

ACKNOWLEDGMENTS

LIST OF PAPERS

I **Surface Structure Analysis of Injection Molded Highly Filled Polymer Melts**
Hausnerova B., Sanetrnik D., Ponizil P.
Polymer Composites 2013, 34, 1553-1558

II **Influence of capillary die geometry on wall slip of highly filled powder injection molding compounds**
Sanetrnik D., Hausnerova B., Filip P., Hnatkova E.
Powder Technology 2018, 325, 615-619

III **Online Rheometry Investigation of Flow/Slip Behavior of Powder Injection Molding Feedstocks**
Sanetrnik D., Hausnerova B., Pata V.
Polymers 2019, 11, 432

IV **Rheological and thermal debinding properties of blended elemental Ti-6Al-4V powder injection molding feedstock**
Lin D., Sanetrnik D., Cho H., Chung S.T, Kwon Y.S., Kate K.H., Hausnerova B., Atre S.V., Park S.J.
Powder Technology, 2017, 311, 357-363

V **Surface Properties of Powder Injection Moulded Parts Related to Processing Conditions**
Hausnerova B., Sanetrnik D., Pata V.
Manufacturing Technology 2018, 18, 895-899

Paper I

Surface Structure Analysis of Injection Molded Highly Filled Polymer Melts

Berenika Hausnerova,[1,2] **Daniel Sanetrnik,**[1,2] **Petr Ponizil**[2,3]

[1]*Department of Production Engineering, Faculty of Technology, Tomas Bata University in Zlín, nám. T.G. Masaryka 5555, 760 01 Zlín, Czech Republic*

[2]*Centre of Polymer Systems, University Institute, Tomas Bata University in Zlín, Nad Ovcirnou 3685, 760 01 Zlín, Czech Republic*

[3]*Department of Physics and Material Engineering, Faculty of Technology, Tomas Bata University in Zlín, nám. T.G. Masaryka 5555, 760 01 Zlín, Czech Republic*

Material components' separation limits to a great extent the efficiency of injection molding of highly filled polymer melts. An uneven redistribution of particle filler within a polymer melt is evaluated with the specially developed testing mold allowing observing the progress of separation during injection molding. Then, scanning electron microscopy of the particular areas derived from the testing mold combined with energy dispersive X-ray analysis of the distribution of elements typical for filler and analytical approach are employed to derive a quantitative parameter describing the tendency of highly filled feedstocks to the separation. POLYM. COMPOS., 34:1553–1558, 2013. © 2013 Society of Plastics Engineers

INTRODUCTION

Injection molding of highly filled (about 60 vol%) polymer melts brings several specific rheological issues limiting processing efficiency [1–4]. This is stressed especially for powder injection molding (PIM), where a considerable number of parts (in some instances up to 25% of the production [5]) are rejected due to a failure in quality requirements resulting from separation of polymer matrix (binder) and powder during mold filling.

On the other hand, due to the integration of polymer processing and metallurgical tools, PIM products have advantages of both—material flexibility of powder metallurgy and design flexibility of plastics molding, and thus the technology serves as a solution for designs hardly attainable by other techniques, e.g. recent construction of an articulating laparoscopic instrument (awarded the 2008 Medical Design Excellence Award for technology) enabling scarless surgery [6].

Currently, the separation is detected when the final stage of the process is reached. Its origin, mechanism, and cause are neither fully understood, nor its onset/extent is satisfactorily quantified. Thornagel [7] has demonstrated (assuming no slip, i.e. good adhesion of feedstock to the channel wall) that the phase separation might arise as a consequence of local shear rate gradients occurring close to the wall of the flow channel. The description is complicated by the fact that the separation pattern changes continuously, demanding a multi-phase simulation, i.e. taking into account individual feedstock components.

Jenni et al. [8,9] employed differential scanning calorimetry (DSC) to quantify local changes in powder concentration through the differences in glass transition temperatures. For evaluation of the tendency of compounds to separation they used three testing molds—spiral, square spiral, and zig–zag, and experimental findings (obtained through radiography, computer tomography, and DSC) compared with a software simulation based on the balance model. A lot of effort has been spent to relate the onset of separation to moldability parameters (flow length and mold geometry) as well as input variables (nozzle and mold temperatures and injection speed). Moldability was found to be strongly dependent on these

factors. Further, on comparing 60 and 50 vol% solid loadings, the difference of the filled length attained was about 68%. The binder flowed more easily due to low viscosity, leaving the remaining powder particles behind. Thus, lowering both temperature and injection speed reduced phase separation.

Previous experimental studies of separation [8,9] employed various testing molds and compared the results with a balance model. Nevertheless, the balance model represents the flow of spherical particles in a Newtonian fluid, and portrays the migration of particles only for simple geometries, disregarding typical feedstock flow phenomena such as slip at the wall.

Thus, the prediction of separation onset and its development during mold filling requires consideration of relevant processing factors and conditions, and their relation to the separation phenomenon, but first, a reliable approach to quantify the separation at the critical geometrical conditions has to be proposed. Therefore, the aim of this study is to develop a method of quantification of the separation resulting in a single characteristic parameter, which would help to predict the structure defects as unacceptable porosity and/or cracks resulting from injection molding affected by separation.

EXPERIMENTAL

Commercially available highly filled feedstocks for PIM applications (abbreviated C-316L and P-316L) based on stainless steel powder 316L with sintered densities 7.96 and 7.75 g/cm^3, respectively, were tested. Powder is composed of Fe (balance), C (0.03), Ni (10.0–14.0), Cr (16.0–18.5), Mo (2.0–3.0), Mn (2.0), Si (1.0). The feedstocks varied in polymer binders as can be seen from the transition temperatures obtained from the second heating scan (Mettler Toledo DSC1 Star, temperature range from 0 to 250°C in nitrogen, 10°C/min) depicted in Fig. 1.

The injection molding machine ARBURG Allrounder 370S (EUROMAP size 700-100) was used to prepare the testing samples. The processing parameters were optimized as displayed in Table 1.

Scanning electron microscopy (SEM) images of molded parts (VEGA II LMU, TESCAN) were taken at the magnifications 78, 94, and 115 times according to the size of the particular square element of the testing mold, and accelerating voltage of 30 kV with BSE detector. Data collection time for energy dispersive X-ray (EDX) was 1,800 s. The size of EDX maps were (2.8 × 2.8) mm on the first element and then gradually decreased to (2.4 × 2.4) mm and (1.9 × 1.9) mm on the second and third elements, respectively. EDX quantification maps were derived with a resolution (128 × 128) pixels, representation of elements is expressed as weight % (wt%).

RESULTS AND DISCUSSION

During the PIM process, metal or ceramic powder is mixed with a suitable polymer-based binder into a homo-
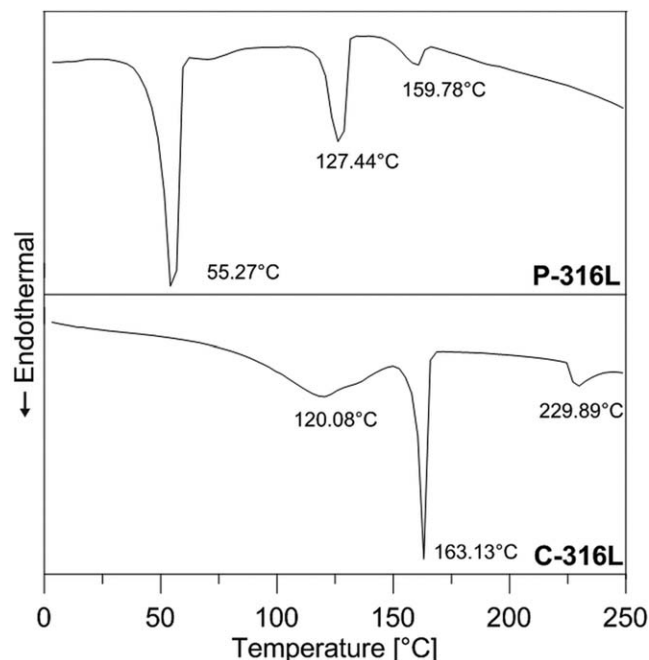
FIG. 1. DSC of P-316L and C-316L feedstocks (10°C/min, second heating scan).

geneous compound. In the next step, the compound is formed by injection molding into desired shape. This stage is followed by debinding, where the binder is extracted (in our case by combination of both thermal and chemical route), and remaining product is sintered to a density close to the theoretical. Currently, the separation is detected on the final parts as cracks and pores (Fig. 2), and an earlier recognition, i.e. prior to debinding and sintering steps, remains a challenge.

In order to quantify the separation during injection molding (prior to debinding and sintering, where the process is still reversible), new design of the testing mold (Fig. 3) has been developed (TBU in Zlín in cooperation with Fraunhofer IFAM, Bremen) to depict the main critical geometrical issues appearing on the molded parts in practice. In comparison to zig–zag, spiral, or square spiral cavities it includes not only inner and outer corners but

TABLE 1. Optimized injection molding parameters of P-316L and C-316L feedstocks.

Material	P-316L	C-316L
Zone 1 temperature (°C)	160	160
Zone 2 temperature (°C)	185	170
Zone 3 temperature (°C)	190	180
Zone 4 temperature (°C)	195	190
Nozzle temperature (°C)	200	200
Mold temperature (°C)	85	85
Injection speed (mm/s)	220	188
Injection pressure (bar)	2,000	2,000
Injection time (s)	0.19	0.19
Hold pressure (bar)	2100	2100
Hold pressure time (s)	4.0	4.0
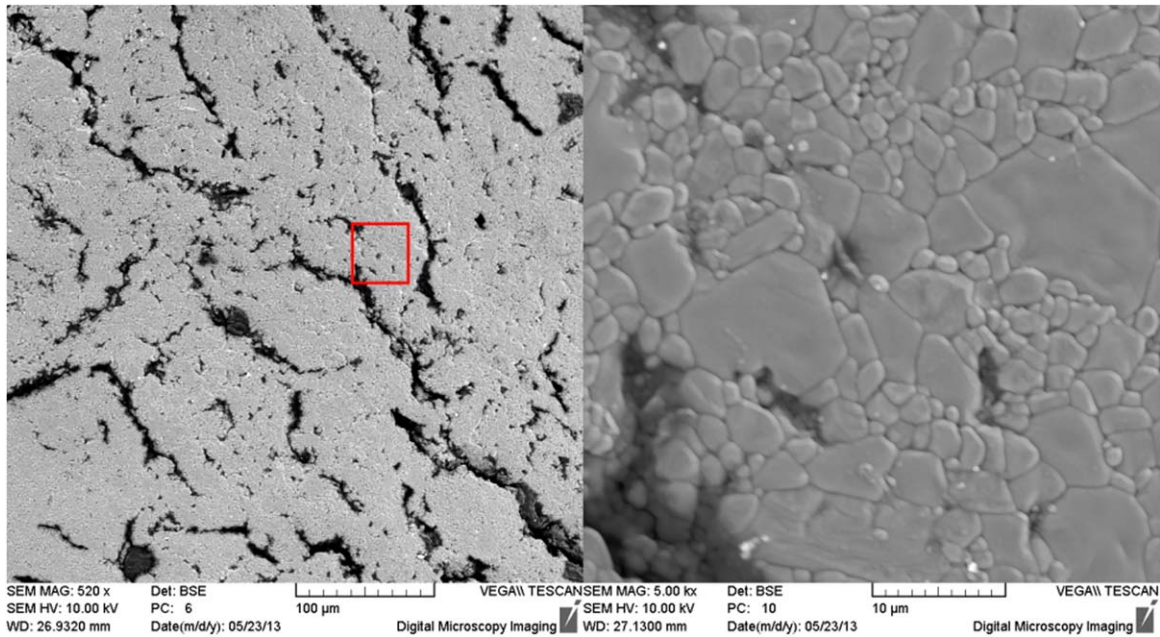
FIG. 2. SEM micrographs of the final structure of sintered parts with voids resulting from the separated polymer binder areas (a detail of zoomed area on the right). [Color figure can be viewed in the online issue, which is available at wileyonlinelibrary.com.]

also radical thickness changes, weld-lines, and very thin parts [10].

The mold is composed of four elements connected by gates. The first three elements contain the external and internal corners. Size of the inner wall of the first three elements is 10 mm, length of the sides of square cross-section is then gradually decreased from 3 mm to 2.5 mm and 2 mm. Each element contains 16 slots for easy position determination.

The separation was the most evident at the areas close to the entrance of the particular element of the testing mold (positions A–C depicted in Fig. 3). The development of the phase separation with the flow front at the indicated positions (red color) can be seen in Fig. 4. Bright points reveal the powder particles and dark areas account for separated polymer binder in comparison to the surface without evidence of separation (obtained at
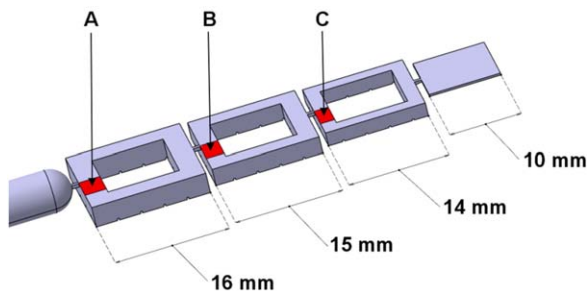
FIG. 3. Design of testing mold with highlighted areas prone to powder/binder separation. [Color figure can be viewed in the online issue, which is available at wileyonlinelibrary.com.]

the positions indicated on the tested mold with blue color) characterized with uniform distribution of powder particles within polymer binders. Although, to some extent the separation is detectable also on the core, the figure shows top views, where the separation is the most evident.

SEM analysis of particular critical areas derived from the proposed testing mold was combined with EDX analysis of the distribution of elements typical for powder and binder in order to quantify powder and binder separation. In comparison to the DSC employed by Jenni et al. [8,9], which has not proved to be a suitable approach to detect the changes in powder concentrations for feedstocks containing multi-component binders (typical for PIM feedstocks), the SEM/EDX analysis offers quantitatively significant results. This can be seen from the examples of EDX spectra derived from unseparated and separated areas depicted in Fig. 5. As it can be seen in Table 2, the occurrence of elements typical for the binder (carbon) rises more than two times in the area of separation, while the occurrence of iron as well as other alloying elements considerably decreases.

SEM/EDX is a semi-empirical method, which allows for major and minor element concentration determination, lacking the sensitivity for trace analysis [11]. The discrepancy in the concentration decay for iron and chromium, silicon, or nickel is due to the fact that the accuracy of SEM/EDX lowers as the concentration of a particular element in the sample diminishes. It is capable to detect elements appearing in concentrations greater than 0.1%, thus manganese decreasing to negligible values was not
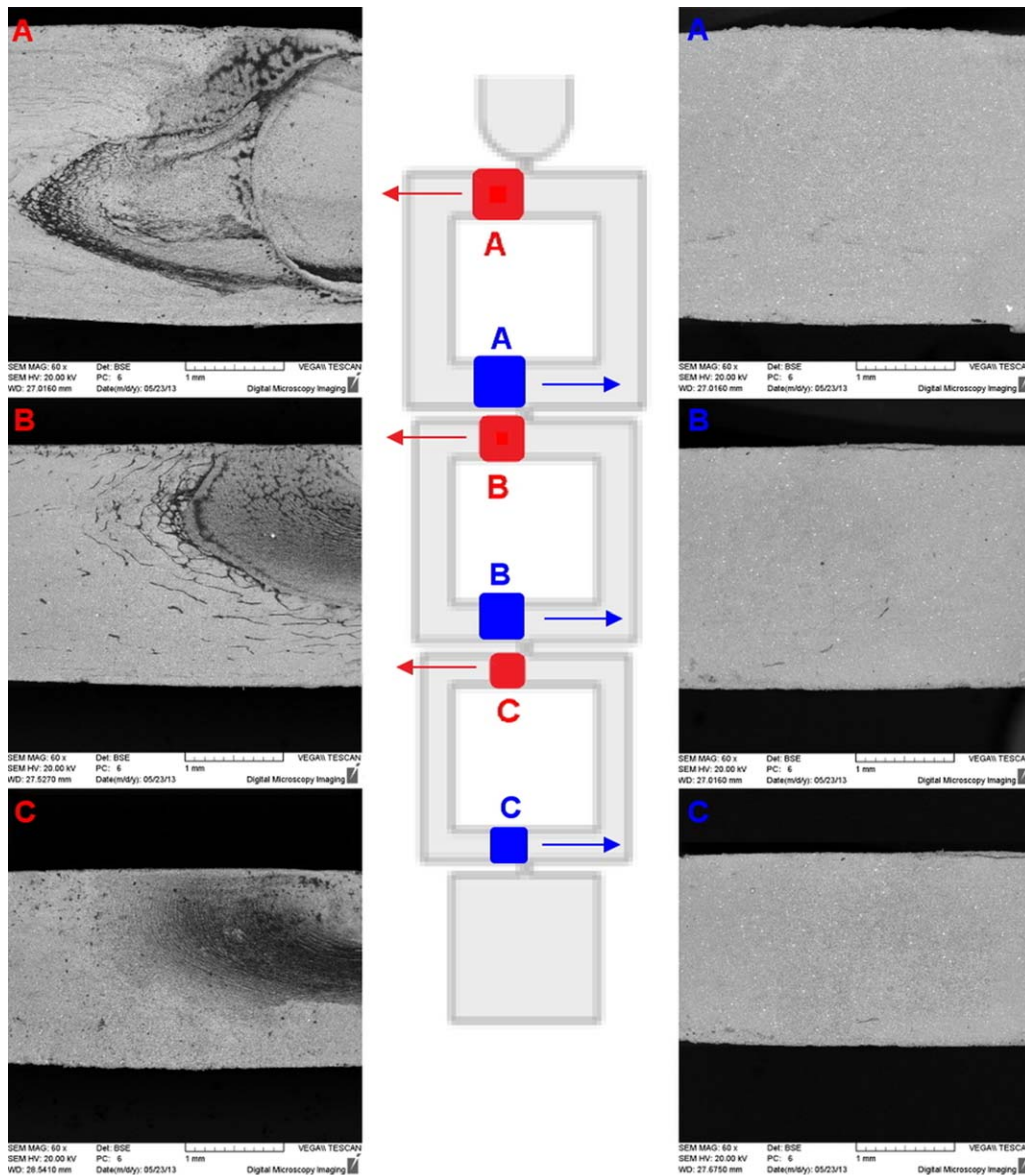
FIG. 4. Development of the flow front obtained at the positions A to C of the testing mold in separated (red) and unseparated (blue) areas. [Color figure can be viewed in the online issue, which is available at wileyonlinelibrary.com.]

detected in the separated area. Another disadvantage of the method is peak overlap of barium and titanium lines and sulfur and lead lines, making interpretation difficult when both members are present [11], but this was not the case of materials employed in this study.

Therefore, quantitative EDX mapping was created representing individually the distribution of the element typical for powder—iron—whose concentration has been selected as a measure of separation or uniformity of distribution of powder particles within binder. The discrepancies between the separations of the two materials tested are clearly visible in Fig. 6. Large phase separation seems to occur especially for C-316L as its X-ray maps portray large areas without evidence of iron (black areas in Fig. 6).

Further, the distributions are analyzed mathematically in order to provide a single parameter (so called variability) characterizing the tendency of the tested feedstocks to separation. The rate of the phase separation represents non-uniformity of powder and binder distribution, i.e. non-uniformity of bright and dark points on EDX maps. If a completely bright area is assigned with 100% and purely dark picture to 0% it is possible to convert the image into a matrix. Then, the data smoothing (Fig. 7)— by averaging the value of the element concentration where each pixel is considered as an average of (5×5) neighboring pixels—is provided in order to eliminate local inhomogeneities.

For determination of the variability coefficient, two methods with similar results are proposed. The first relies
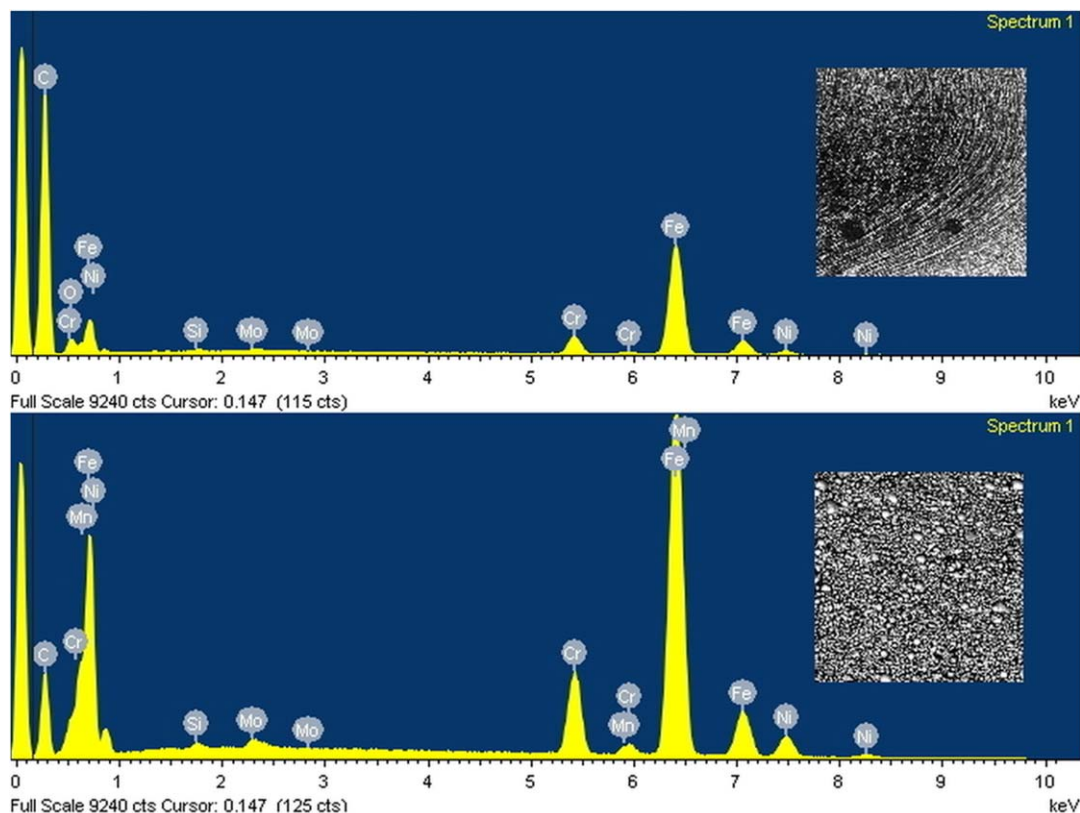
FIG. 5. EDX spectra of separated and unseparated areas (P-316L). [Color figure can be viewed in the online issue, which is available at wileyonlinelibrary.com.]

on an approximation of element presence in the pixel neighborhood by plane, and determination of its gradient as a measure of the particle distribution variability. The second method (which was selected in this study) is to compute standard deviations/coefficients of variance of element content in the same pixel neighborhood.

Results of the analysis in Fig. 8 (for Fe as a typical element of powder) provide the quantification of the development of the separation at the tested positions (A, B, C). The low and uniform variability anticipates an efficient PIM process without defects arising from the separation. It should be stressed that the variability is calculated relatively to the initial (unseparated, unmolded) state, where the concentration of iron in the samples is

TABLE 2. EDX concentration of elements typical of binder (C) and powder (Fe, Ni, Cr, Mo, Mn, Si) in separated and unseparated areas displayed in Figure 5.

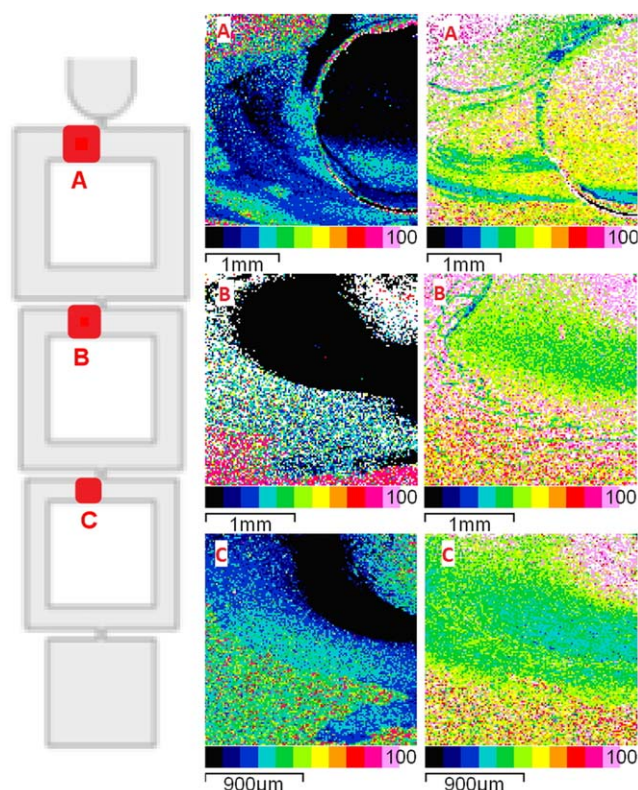| Separated area		Unseparated area	
Element	Weight (%)	Element	Weight (%)
C K	62.61	C K	24.98
Si K	0.09	Si K	0.24
Cr K	2.71	Cr K	8.35
Mn K	–	Mn K	0.15
Fe K	27.43	Fe K	59.73
Ni K	1.51	Ni K	5.52
Mo L	0.36	Mo L	1.03

FIG. 6. EDX quantification maps of iron distribution for C-316L (left) and P-316L (right). [Color figure can be viewed in the online issue, which is available at wileyonlinelibrary.com.]

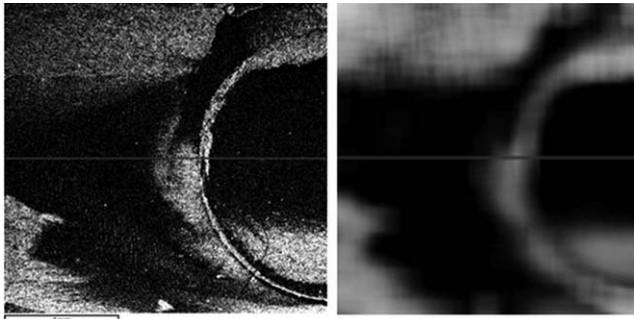FIG. 7. Analytical procedure applied on distribution maps: original (left) and smoothed (right) scan.

TABLE 3. Average values of concentration and variability of Fe element in C-316L and P-316L samples at the positions A to C of the testing mold.

Element	Fe concentration (wt%)	Fe variability (−)
C-316L—molded samples		
A	16 ± 7	24 ± 2
B	19 ± 6	23 ± 2
C	24 ± 5	19 ± 2
P-316L—molded samples		
A	65 ± 11	23 ± 8
B	66 ± 12	20 ± 10
C	57 ± 11	29 ± 10

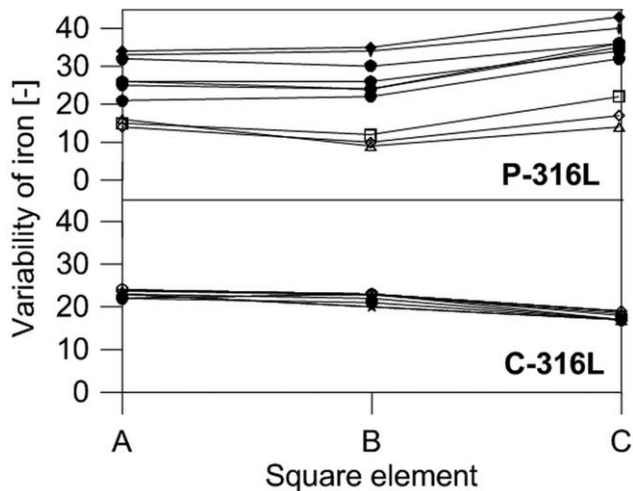

FIG. 8. Variability coefficients of P-316L and C-316L iron distributions at positions A to C of the testing mold (a set of 10 samples).

(36 ± 1) wt% for C-316L and (80 ± 1) wt% for P-316L with the corresponding variabilities 6 ± 1 and 5 ± 1, respectively. As it can be seen from Table 3, summarizing variability coefficients as well as the concentrations of iron in the tested separated areas, the different mechanism of separation for the two materials is obtained. In case of C-316L the concentration decay is the most visible (about 55%) at the first position entered by flow front (position A), and then it is partly balanced back (about 30% at position C), while for P-316L it is similar for the first two positions (about 20% at A and B) and then it drops down (about 30% at C position). On the other hand, the reproducibility for C-316L by means of the standard deviations is better than that of P-316L.

The initial variabilities of two feedstocks are similar with the values 6 ± 1 (C-316L) and 5 ± 1 (P-316L). In agreement to the decay in concentration, the variability of the tested materials shows that C-316L is faster prone to the separation, but it has a certain ability to reverse it back, while the continuous progress is attained for P-316L. Again, the reproducibility (see also Fig. 8) is very

good for C-316L (± 2) in comparison to about ± 10 in case of P-316L feedstock.

SUMMARY

Flow-induced separation occurring during processing of highly filled polymer melts evaluated on the specially designed testing mold was quantified via analytical computation approach applied to SEM/EDX distribution maps. The method was tested on two commercially available feedstocks. According to the obtained findings, the so called variability coefficient resulting from the employed approach might serve as a single parameter quantifying the separation, and consequently reduction/ elimination of the issue and production of defect-free items.

REFERENCES

1. B. Hausnerova, L. Marcanikova, P. Filip, and P. Saha, *Polym. Eng. Sci.*, **119**, 2925 (2011).
2. T. Honek, B. Hausnerova, and P. Saha, *Appl. Rheol.*, **12**(2), 72 (2002).
3. B. Hausnerova, *Polimery*, **55**(1), 3 (2010).
4. B. Hausnerova, P. Saha, and J. Kubat, *Int. Polym. Process.*, **14**(3), 254 (1999).
5. N. Williams, *PIM Int.*, **3**(3), 51 (2009).
6. D. Danitz, "Scarless Surgery," In *Proceedings of International Conference on Powder Injection Molding*, Metal Powder Industries Federation, Orlando (2009).
7. M. Thornagel, *Eur. Powder Metallurgy Assoc.*, **2**, 135 (2009).
8. M. Jenni, L. Schimmer, R. Zauner, J. Stampfl, and J. Morris, *PIM Int.* **2**(4), 50 (2008).
9. M. Jenni, R. Zauner, and J. Stampfl, *Eur. Powder Metallurgy Assoc.*, **2**, 141 (2009).
10. L. Jiranek, B. Hausnerova, and T. Hartwig, *Community Design 001704974*, Office for Harmonization in the Internal Market, Alicante (2010).
11. A.L. Hobbs, and J.R. Almirall, *Anal. Bioanal. Chem.*, **376**, 1265 (2003).

Paper II

Influence of capillary die geometry on wall slip of highly filled powder injection molding compounds

Daniel Sanetrnik [a,b], Berenika Hausnerova [a,b,*], Petr Filip [c], Eva Hnatkova [a,b]

[a] Dept. of Production Engineering, Faculty of Technology, Tomas Bata University in Zlin, nam. T.G.Masaryka 5555, 760 01 Zlin, Czech Republic
[b] Centre of Polymer Systems, University Institute, Tomas Bata University in Zlin, Trida T. Bati 5678, 760 01 Zlin, Czech Republic
[c] Institute of Hydrodynamics, Academy of Sciences of the Czech Republic, Pod Patankou 5, 166 12 Prague, Czech Republic

A B S T R A C T

Uneven distribution of solid particles contained in the feedstocks used in the process of powder injection molding (PIM) is observed in the close vicinity of the walls. A particle-free thin layer adjacent to the walls is formed by the binder only and is characterized by so-called wall slip. Wall slip is a key to successful modeling of injection molding step of PIM. For its determination we used capillary rheometers equipped with the dies of different entrance angles applied to four PIM feedstocks. The entrance angle has been found to be a crucial parameter to intercept wall slip. Conical dies are more suitable to obtain reliable slip velocity values of highly filled compounds than capillaries having plane entrance, which are used in the majority of studies.

© 2017 Elsevier B.V. All rights reserved.

1. Introduction

The process of powder injection molding (PIM) introduces the material flexibility of powder metallurgy to the traditional plastic injection molding. The process involves four consecutive steps: incorporation of the metal (nano-, micro-) powder into organic binder, injection molding for shaping the component, removing (debinding) the binder from the component, and sintering that consolidates the final component [1].

Each step is of the same importance as the defects occurring in the previous steps cannot be eliminated in the subsequent steps thus terminating in appearance of cracks, internal stresses, dimensional distortion (warpage), etc. [2]. Therefore, the process starts with a choice of appropriate feedstock. Ahn et al. [3] demonstrate that binder selection is more critical than powder selection. German [4] and Li et al. [5] recommend to use a binder which viscosity does not exceed 0.1 Pa.s thus ensuring moderate viscosity (<1000 Pa·s) of the feedstock under the shear rates applied during injection molding. According to Fang et al. [6] only particles smaller than 20 μm are suitable for PIM, and finer powders are beneficial to improve the homogeneity. Every feedstock should exhibit shear thinning, i.e. viscosity decreases under shear strain. Nevertheless, a rate of shear thinning is a crucial point as e.g. for higher

rates a cavity filling of complicated geometry requires less energy, but on the other hand, it can facilitate powder-binder separation [7].

Characterization of the powder-binder system is the introductory essential approach in modeling the PIM process complicated by the fact that the composition of PIM feedstocks typically range from 45 to 75 vol% filler content. Kate et al. [8] summarized empirical models for a prediction of a series of feedstock properties including their comparison with literature data on powder-polymer mixtures. They also presented the models for evaluating feedstock viscosity.

Rheological characterization gets more complicated during the second step: injection molding. This justifies an increased attention to a description of rheological behavior of the feedstock during injection molding as this characterization serves as one of the entries. Rheology of the feedstocks during injection molding was analyzed e.g. by [9–17].

As trial-and-error experiments are time-consuming and cost demanding, the computer simulation procedures not requiring performing the entire PIM process were proposed (e.g. [9,18,19]). The modeling of injection molding process with various molding parameters and complex material characterization was carried out by He et al. [20]. The simulations were in a good accordance with the experimental observations, however measured powder concentration within injected feedstocks was approximately 5–6% lower than simulated.

Such differences may be caused by no-slip conditions set in the most of models, while during real processing a contact between feedstock and channel walls results in the occurrence of so called slip layer (thickness attaining approximately 1/14–1/25 of a capillary diameter, details in [10,11]), containing only the pure binder system while

* Corresponding author at: Dept. of Production Engineering, Faculty of Technology, Tomas Bata University in Zlin, nam. T.G.Masaryka 5555, 760 01 Zlin, Czech Republic.
E-mail address: hausnerova@ft.utb.cz (B. Hausnerova).

the feedstock (with viscosity by orders higher) as a bulk material occupies most of the flow region [21,22], therefore special emphasis is necessary to pay to slip phenomenon that is the most notable rheological characteristic.

It was found [23] that no-slip condition leads to inaccurate simulation even in a simple pipe flow. In this respect, a method to determine wall slip layer thickness instead wall slip velocity was proposed [23]. Nevertheless, the wall slip correction model is still used solely if micro injection molding is simulated, because the wall slip is well pronounced in small flow channels. Choi and Kim [24] have shown that an implementation of a wall slip into flow simulations is necessary for channel diameters <10 μm.

Geometrical arrangement of the capillary dies participates significantly in the obtained rheological characteristics. An application of flat or conical dies changes both slip layer thickness and slip velocity. No obstacles as flat dies are encountered in the PIM process and rather smooth injection molding is met. The literature comparing flat and conical dies in connection with wall slip effect is rather scarce. Liang [25] and Ardakani et al. [26] tested changes in pressure drop with different capillary angles during extrusion. It was found that under constant pressure, shear rate increased with higher capillary entrance angle. The aim of this contribution is to compare rheological characterization of feedstocks obtained for both geometries of a capillary die and to show that a usage of the conical die is in better compliance with the analyses presented in the literature.

2. Experimental

2.1. Materials

Four types of commercially available PIM feedstocks (abbreviated P316L, P17-4PH, C316L, and C17-4PH, where P and C stands for two different binders, were used. The feedstocks are based on gas atomized spherical shaped stainless steel 316L and 17-4PH particles with sintered densities 7.75 g/cm³ and 7.65 g/cm³ for the binder P, respectively (P 316L , P 17-4PH), and 7.96 g/cm³ and 7.67 g/cm³ for the binder C, respectively (C316L, C17-4PH). The chemical composition of powders is depicted in Table 1. The feedstocks were prepared from the master alloys and carbonyl iron powder (ratio 1:3) having distributions of powder sizes $>D_{90}$ 26 μm/D_{50} 9 μm/D_{10} 3 μm, and $>D_{90}$ 8 μm/D_{50} 5 μm/D_{10} 2 μm, respectively.

The transition temperatures characterizing both polymer binders were obtained using a differential scanning calorimeter Mettler Toledo DSC1 Star. Fig. 1 depicts the results obtained, after cooling the samples to 0 °C, from second heating scan at a rate of 10 °C/min in the temperature range from 0 to 250 °C in a nitrogen atmosphere.

2.2. Rheological investigation

Two capillary rheometers with the dies of different entrance angles were used for an evaluation of the wall slip effect (Fig. 2). A Goettfert RHEOGRAPH 50 rheometer was equipped with 3 flat dies (180° entrance angle) of the same length-to-diameter (L/D) ratio (20/2, 10/1 and 5/0.5 in mm), a Rosand RH 2000 was used with 2 conical dies (90° entrance angle) of the same aspect ratio (16/1 and 8/0.5 in mm).

In the following we use the traditional Mooney method for the determination of the wall slip velocities. This method is based on changing the surface-to-volume ratio of the capillary dies, in other words, on changing a length L and radius R of the dies with fixing their ratio. In brief, we outline an evaluation of the experimental data.

Table 1
Composition of 316L and 17-4PH stainless steel powders (in wt%).

Powder	Fe	C	Ni	Mn	Si	Cu	Mo	Cr
17-4PH	Balance	<0.07	3.0–5.0	<0.1	<1.0	3.0–5.0	–	–
316L	Balance	<0.03	10.0–14.0	<2.0	<1.0	–	2.0–3.0	16–18
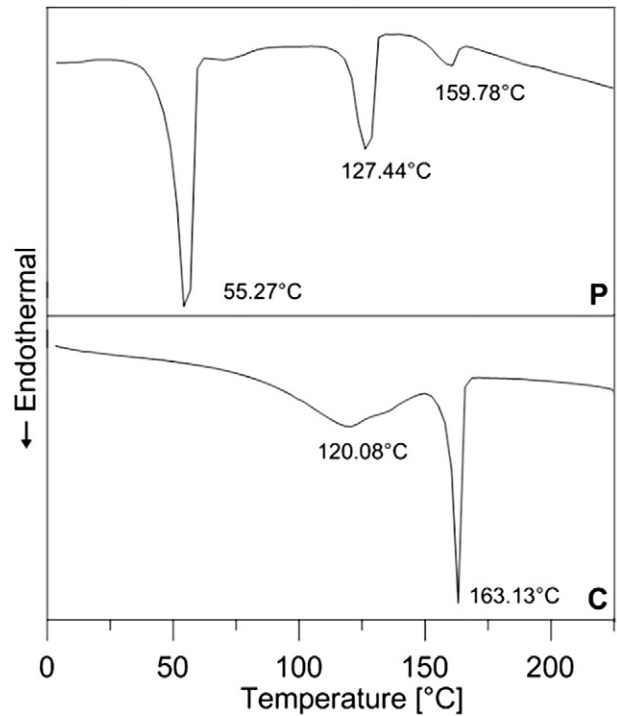
Fig. 1. Transition temperatures of both binders P and C (second heating scan at 10 °C/min in nitrogen atmosphere).

In a circular die an apparent wall shear rate $\dot{\gamma}_a$ and an apparent wall shear stress τ_a are determined by the relations

$$\dot{\gamma}_a = \frac{4\dot{Q}}{\pi R^3}; \tau_a = \frac{\Delta p R}{2L} \tag{1}$$

where $\dot{Q}$ is the volumetric flow rate and Δp is the measured pressure drop.

Consequently, a true average velocity is given by the difference of an average v_{av} ($=\dot{Q}/\pi R^2$) and slip v_{slip} velocities

$$v_{true} = v_{av} - v_{slip} \tag{2}$$

Multiplying this relation by $4/R$ and using rel. (1) we obtain a dependence of the true apparent shear rate on the measured apparent shear rate and wall slip velocity

$$\dot{\gamma}_{a,\,slip-corrected} = \dot{\gamma}_a - \frac{4v_{slip}}{R} \tag{3}$$
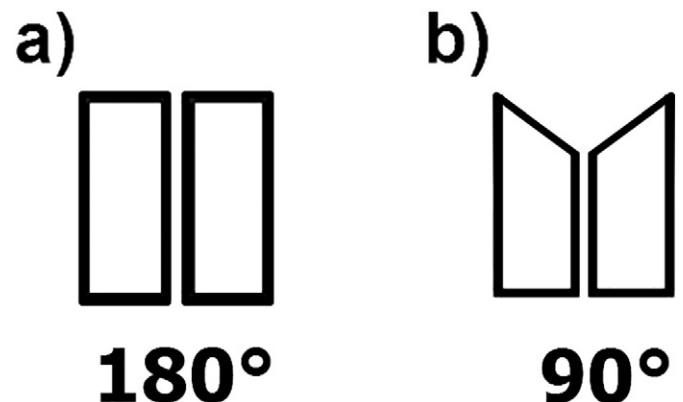
Fig. 2. Schematic representation of flat (a) and conical (b) testing capillaries.

or in other form

$$(intercept) = \frac{4\dot{Q}}{\pi R^3} - (slope)\frac{4}{R} \quad (4)$$

Geometrical interpretation of the last two relations is illustrated in Fig. 3.

3. Results and discussion

As mentioned in the Introduction, injection molding which shapes the components to their final form represents the second step in the PIM process after mixing the powder into the polymer binder. Proper rheological characterization of flow behavior of the feedstocks in this second step, i.e. flow into a mold and its uniform filling, is an important point in modeling the whole process. Geometrical arrangement of the rheometers could be free of obstacles not encountered during molding. Therefore, two different dies are examined in rheological characterization. The first one, commonly used, is a capillary with a flat 180° entrance die and the second one is a capillary with a conical 90° die. Suitability of each die will be evaluated with respect to compatibility of the obtained results with the general findings on wall slip issue stated in the literature.

For the flat 180° entrance die both 316L and 17-4PH stainless steel feedstocks based on two binder systems (C and P) exhibited pseudoplastic behavior in the measured range of shear rates which is an indispensable assumption for satisfactory course of injection molding process, see Fig. 4. The viscosity curves for the C binder system occupy a smaller range of apparent shear rate under imposed pressure in comparison with the P binder system. It implies lower tendency to a wall slip of the C binder system composed of polymers with higher transition temperatures. On the other hand, P binder with more pronounced wall slip is less sensitive to phase separation due to the lower shear rate gradients generated by slip.

Fig. 5 presents the Mooney plots of apparent shear rate as a function of reciprocal radius of the capillary dies, the slip velocity is determined according to the approach described in the Experimental. It is obvious that the slopes of the fitting lines increase with increasing pressure (and apparent wall shear stress) and hence, the slip velocity v_s is an increasing function of shear stress.

Fig. 6 shows the slip velocity at the wall as a function of apparent shear stress. In accordance with Fig. 4 both feedstocks (316L and 17-4PH) based on the P binder system having lower transition temperatures exhibited multiple slip velocity at the wall in comparison with the C binder system. Further, the slip velocities of both binder systems with 17-4PH powder are slightly higher than those with 316L compounds. When considering rounded shape of all types of powders (gas atomized) and also their similar particle distributions, the interactions between binder and different chemical compositions of powder (Table 1) plays a negligible role in a wall slip evaluation.
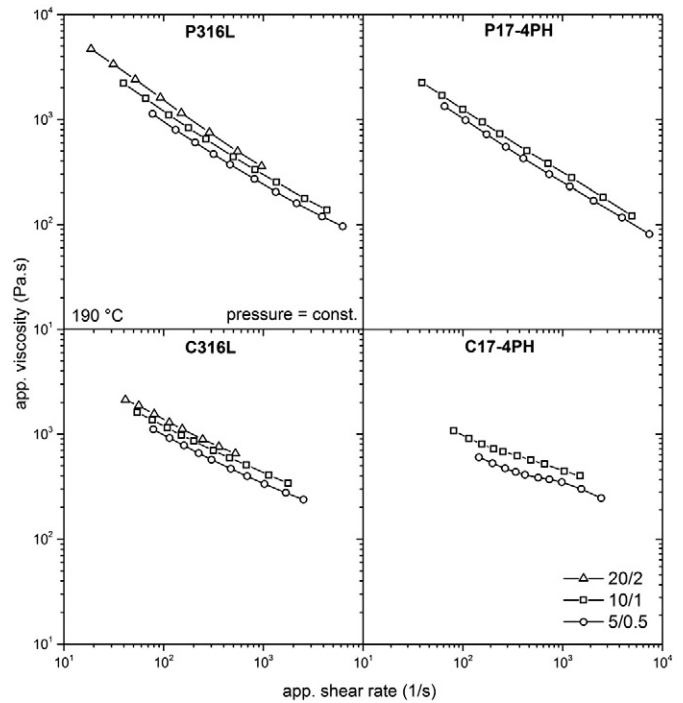
Fig. 4. Relation of apparent viscosity to apparent shear rate for three flat (180°) entrance dies (L/D = 20/2, 10/1 and 5/0.5 in mm).

The same procedure as above was carried out with the conical 90° entrance dies, see Fig. 7. The lower (conical) entrance angle decreases the wall slip velocity. Similar observations have been done for viscoelastic materials as rubber [25] or toothpaste [26] compounds.

Fig. 5. Graphical interpretation of Mooney approach for three flat (180°) entrance dies (L/D = 20/2, 10/1 and 5/0.5 in mm).
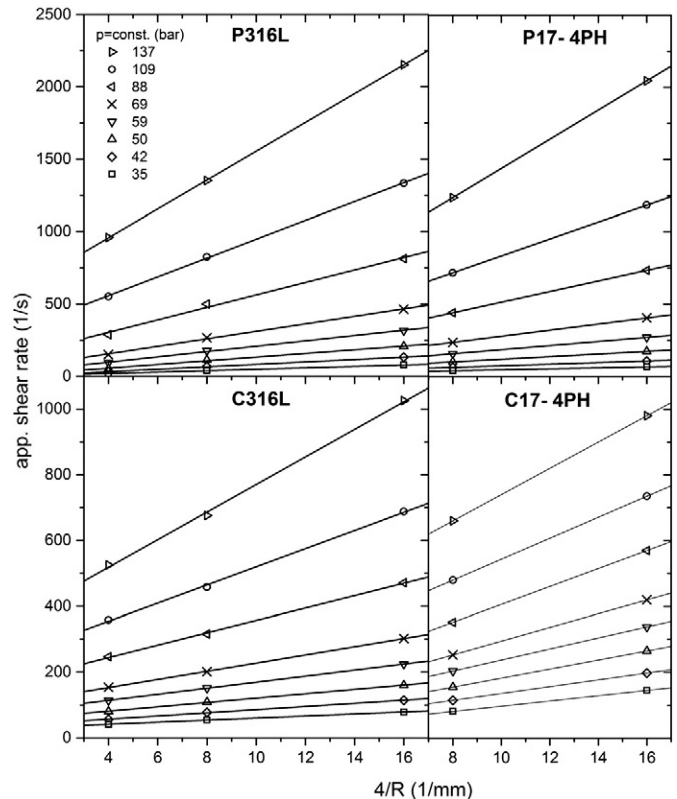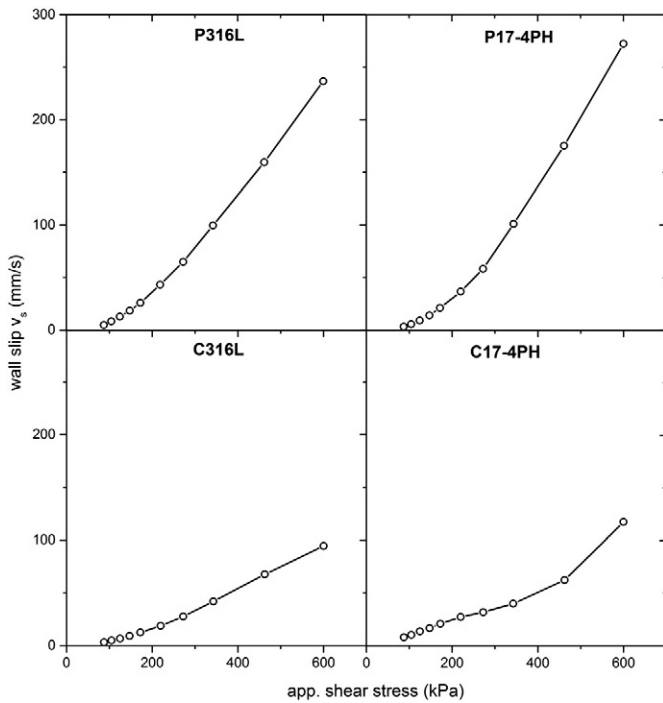

Fig. 3. Calculation of wall slip velocity using Mooney approach.

Fig. 6. Wall slip velocity as a function of apparent shear stress based on using flat (180°) entrance dies.

Furthermore, the main finding is the better linear proportionality between the wall slip velocity and the shear stress obtained with 90° entrance dies. The relation has been proposed by Yilmazer and Kalyon [24] and Soltani and Yilmazer [14] for concentrated suspensions

$$\upsilon_{slip} = a(T) \cdot \tau \tag{5}$$
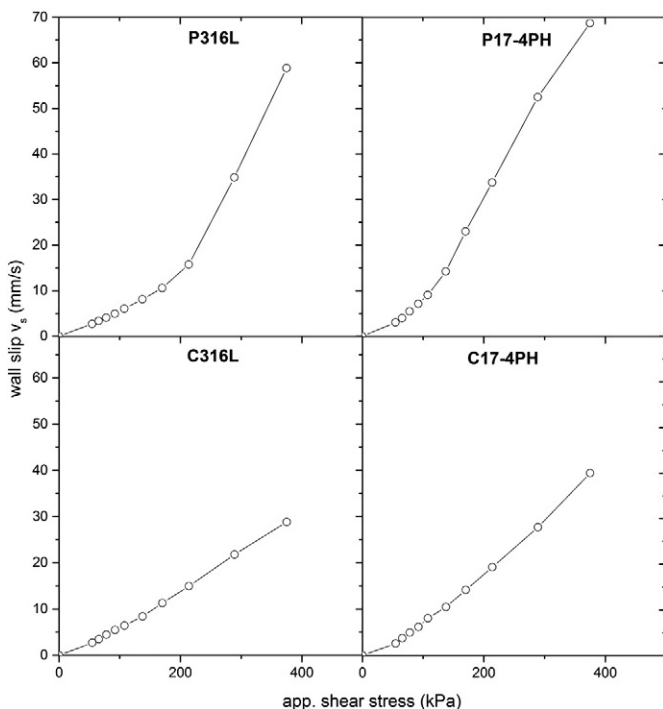
where $a(T)$ is the temperature dependent coefficient.

Fig. 7. Wall slip velocity as a function of apparent shear stress based on using conical (90°) entrance dies.

We can see that only the experimental findings obtained for the conical die (Fig. 7) comply with the above linear relation (especially for the C binder system). No such relation can be derived for the plane entrance angle depicted in Fig. 6. This justifies the applicability of the conical entrance dies in simulations of PIM feedstocks flow. The flat 180° entrance die enhance the tendency of feedstock to the separation of polymer binder and powder, which is then accumulated in the dead zones (edges) above the die. In addition, the sharp edges cause rapid changes in shear rate which further support separation of feedstocks (binder and powder) components [12,27,28] resulting in higher wall slip velocities.

4. Conclusion

Wall slip as a crucial rheological phenomenon influencing injection molding of PIM compounds has been evaluated aiming at geometry of flow channels. Reliable determination of wall slip strongly participates on successful simulations of PIM process. It has been shown that the application of the flat entrance capillaries, used in overwhelming majority of rheological studies, provide overstated values of slip velocities. This is caused by a 180° entrance angle obstacle, which does not comply with geometrical arrangements during PIM process. An application of conical dies seems to be more beneficial as the corresponding rheological measurements are in accordance with linear proportionality rule between wall slip velocity and shear stress.

Acknowledgments

References

[1] R.M. German, A. Bose, Injection Molding of Metals and CeramicsMetal Powder Industry, 1997, ISBN 978-1878954619.
[2] R.T. Fox, D. Lee, Analysis of temperature effects during cooling in powder injection-molding, Int. J. Powder Metall. 30 (1994) 221–229.
[3] S. Ahn, S.J. Park, S. Lee, S.V. Atre, R.M. German, Effect of powders and binders on material properties and molding parameters in iron and stainless steel powder injection molding process, Powder Technol. 193 (2009) 162–169.
[4] R.M. German, Homogeneity effects on feedstock viscosity in powder injection molding, J. Am. Ceram. Soc. 77 (1994) 283–285.
[5] Y. Li, B. Huang, X. Qu, Viscosity and melt rheology of metal injection moulding feedstocks, Powder Metall. 42 (1999) 86–90.
[6] W. Fang, X.B. He, R.J. Zhang, X.M. You, X.H. Qu, Effects of particle characteristics on homogeneity of green bodies in powder injection moulding, Powder Metall. 57 (2014) 274–282.
[7] R. Supati, N.H. Loh, K.A. Khor, S.B. Tor, Mixing and characterization of feedstock for powder injection molding, Mater. Lett. 46 (2000) 104–114.
[8] K.H. Kate, R.K. Enneti, S.J. Park, R.M. German, S.V. Atre, Predicting powder-polymer mixture properties for PIM design, Crit. Rev. Solid State. 39 (2014) 197–214.
[9] P. Suri, R.M. German, J.P. De Souza, S.J. Park, Numerical analysis of filling stage during powder injection moulding: effects of feedstock rheology and mixing conditions, Powder Metall. 47 (2004) 137–143.
[10] D.M. Kalyon, S. Aktas, Factors affecting the rheology and processability of highly filled suspensions, Annu. Rev. Chem. Biomol. 5 (2014) 229–254.
[11] F. Soltani, U. Yilmazer, Slip velocity and slip layer thickness in flow of concentrated suspensions, J. Appl. Polym. Sci. 70 (1998) 515–522.
[12] J.M. Jang, H. Lee, W. Lee, Y.I. Kim, S.H. Ko, J.H. Kim, J.S. Lee, J.P. Choi, Evaluation of feedstock for powder injection molding, Jpn. J. Appl. Phys. 53 (2014).
[13] S. Ahn, S.T. Chung, S.V. Atre, S.J. Park, R.M. German, Integrated filling, packing, and cooling CAE analysis of powder injection molding parts, Powder Metall. 51 (2008) 318–326.
[14] D.M. Kalyon, Apparent slip and viscoplasticity of concentrated suspensions, J. Rheol. 49 (2005) 621–640.
[15] T.H. Kwon, S.Y. Ahn, Slip characterization of powder/binder mixtures and its significance in the filling process analysis of powder injection molding, Powder Technol. 85 (1995) 45–55.
[16] Y.C. Lam, Z.Y. Wang, X. Chen, S.C. Joshi, Wall slip of concentrated suspension melts in capillary flows, Powder Technol. 77 (2007) 162–169.
[17] U. Yilmazer, D.M. Kalyon, Slip effects in capillary and parallel disk torsional flows of highly filled suspensions, J. Rheol. 33 (1989) 1197–1212.
[18] S.J. Park, S. Ahn, T.G. Kang, S.T. Chung, Y.S. Kwon, S.H. Chung, S.G. Kim, S. Kim, S.V. Atre, S. Lee, R.M. German, A review of computer simulations in powder injection molding, Powder Metall. 46 (2010) 37–45.

[19] C.J. Hwang, T.H. Kwon, A full 3D finite element analysis of the powder injection molding filling process including slip phenomena, Polym. Eng. Sci. 42 (2002) 33–50.

[20] H. He, Y. Li, J. Lou, D. Li, Ch. Liu, Prediction of density variation in powder injection moulding-filling process by using granular modelling with interstitial power-law fluid, Powder Technol. 291 (2016) 52–59.

[21] V. Ramamurthy, Wall slip in viscous fluids and influence of materials of construction, J. Rheol. 30 (1986) 337–357.

[22] S. Kalika, M.M. Denn, Wall slip and extrudate distortion in linear low-density polyethylene, J. Rheol. 31 (1987) 815–834.

[23] T.H. Kwon, S.Y. Ahn, Slip characterization of powder/binder mixture and its significance in the filling process of powder injection molding, Powder Technol. 85 (1995) 45–55.

[24] S.J. Choi, S.K. Kim, Multi-scale filling simulation of micro-injection molding process, J. Mech. Sci. Technol. 25 (2010) 117–124.

[25] J.Z. Liang, Influence of die angles on pressure drop during extrusion of rubber compound, J. Appl. Polym. Sci. 80 (1999) 1150–1154.

[26] H.A. Ardakani, E. Mitsoulis, S.G. Hatzikiriakos, Thixotropic flow of toothpaste through extrusion dies, J. Non-Newton. Fluid. 166 (2011) 1262–1271.

[27] M. Thornagel, MIM-simulation: a virtual study on phase separation, Euro PM 2009 (2009) 135–140.

[28] J.Z. Liang, J.S.F. Chan, E.T.T. Wong, Effects of operation conditions and die angles on the pressure losses in capillary flow of polystyrene melt, J Mater Process Tech. 114 (2001) 118–121.

Paper III

Online Rheometry Investigation of Flow/Slip Behavior of Powder Injection Molding Feedstocks

Daniel Sanetrnik [1,2], Berenika Hausnerova [1,2,*] and Vladimir Pata [1]

[1] Dept. of Production Engineering, Faculty of Technology, Tomas Bata University in Zlin, nám. T. G. Masaryka 5555, 760 01 Zlín, Czech Republic; dsanetrnik@utb.cz (D.S.); pata@utb.cz (V.P.)

[2] Centre of Polymer Systems, University Institute, Tomas Bata University in Zlin, Trida T. Bati 5678, 760 01 Zlín, Czech Republic

* Correspondence: hausnerova@utb.cz

Abstract: Wall slip in the flow of powder injection molding (PIM) compounds can be the cause of unrealistically low viscosity values, and can lead to a failure of flow simulation approaches. Regardless of its importance, it has been considered only scarcely in the rheological models applied to PIM materials. In this paper, an online extrusion rheometer equipped with rectangular slit dies was used to evaluate the slip velocity of commercial as well as in-house-prepared PIM feedstocks based on metallic and ceramic powders at close-to-processing conditions. The tested slit dies varied in their dimensions and surface roughness. The wall-slip effect was quantified using the Mooney analysis of slip velocities. The smaller gap height (1 mm) supported the wall-slip effect. It was shown that both the binder composition and the powder characteristic affect slip velocity. Slip velocity can be reduced by tailoring a powder particle size distribution towards smaller particle fractions. The thickness of the polymer layer formed at the channel wall is higher for water-soluble feedstocks, while in the case of the catalytic polyacetal feedstocks the effect of surface roughness was manifested through lower viscosity at smooth surfaces.

1. Introduction

Powder injection molding (PIM) currently gains enhanced attention due to its merging with additive manufacturing. The PIM process consists of four steps whose accomplishment allows for the production of small and complex-shaped metal or ceramic parts that is often hardly achievable with traditional metallurgical methods [1,2]. During the first step, homogeneous highly filled polymer melt (feedstock) is prepared by compounding metal/ceramic powder into a polymer binder. The binder is an at least three-component system ensuring processability of feedstocks by injection molding, which is followed by its removal from injected parts. This step is called debinding, and can be thermal, solvent, or thermal/solvent combined. Finally, a porous powder structure is sintered to its final density.

Highly filled polymers such as those used in PIM technology belong to rheologically complex systems. Although PIM compounds are high-viscosity (typically 10^3–10^5 Pa·s [1]) materials, many published studies report their viscosity values in the order of flowability of low-molecular weight fluids (tens and hundreds Pa·s) [3,4]. Such low viscosity values can be attributed to a wall slip appearing during the flow in capillaries. Rheological characterization is essential for the process optimization; however, a no-slip condition is set in most rheological models and simulations of the injection molding step of PIM [5].

According to Denn [6], all highly filled materials slip at the wall at certain rates and stresses. Delime and Moan [7] showed that during shearing, a low-viscosity polymer layer with a typical thickness of 0.1–10 μm is formed near flow channel walls as powder particles migrate away from walls during flow [6,8,9]. Kalyon and Aktas [10], as well as Soltani and Yilmazer [11], reported that the thickness of the layer is about 1/14–1/25 of a capillary diameter. This is known as an apparent slip [12]. Delime and Moan, in the abovementioned study [7], further suppose that the migration of solid particles is initiated by the failure of Brownian movement near the walls, which is supported by shear rate gradients which promote particle collision. For PIM feedstocks, Thornagel [13] assumes that particles present in the regions of high shear rate gradients try to leave these areas and concentrate in the middle of the flow channel, which results in so-called powder/binder separation. [14,15].

Soltani and Yilmazer [11] tested the tendency of hydroxyl-terminated polybutadiene (HTPB) filled with glass spheres to wall slip on a parallel-plate rheometer, and found the slip layer thickness to be independent of temperature, but enhanced with the size of the particles. On the other hand, the slip velocity increased with increasing temperature, which was attributed to lower polymer viscosity. Increasing wall-slip velocity with rising particle size was reported by Gulmus and Yilmazer [16] for poly(methyl methacrylate) (PMMA) particles in HTPB as a result of the steric hindrance effect of the particles—larger particles cannot get very close to the wall and this causes the slip layer thickness (and consequently slip velocity) to increase.

Concerning the effect of the processing tool (the chemical nature of materials and roughness), Chen et al. [17] tested linear low-density polyethylene (LLDPE) and concluded that its wall-slip velocity increases in the following manner: aluminum < glass < copper < stainless steel. As can be seen, the stainless-steel die, which is mostly used for processing tools, is prone to wall slip. This was attributed to a relatively small work of adhesion, and also a smooth capillary surface in comparison to a rough surface of aluminum, which improved the material's adhesion to the wall. A similar effect of surface roughness was confirmed by carrying out studies using poly(butadiene-acrylonitrile-acrylic acid) terpolymer mixes with glass spheres (85.4 and 35.3 μm) [18] or HTPB filled with PMMA [19]. According to Medhi et al. [20], in the case of a rough wall, solid particles can move into the groove, therefore, the whole material flow as a continuum and formation of low molecular layer is suppressed.

Concerning the geometry of measuring tools, Kalyon [21] proposed methodology to provide the slip-corrected shear viscosity of concentrated suspensions in Couette, capillary, and rectangular slit flows on the basis of the apparent slip mechanism. The influence of the entrance angle of capillary dies was tested recently [22] with the conclusion that the application of conical dies seems to be more beneficial as the corresponding rheological measurements are in accordance with general wall-slip findings. Finally, in the study published by Walter et al. [23], the relation between slip and static axial preload, as well as the measuring frequency of a parallel-plate rotational rheometer, was tested on two-component silicone rubber. The wall-slip velocity was rather sensitive to the applied preload—higher preload force resulted in a delay in the onset of wall slip. On the other hand, only a slight dependence of wall-slip on frequency was found.

As pointed out by Kwon and Ahn [24], disregarding slip leads to inaccurate simulations of the PIM process. Very recently, the slip of PIM compounds was considered by Liu et al. [25] for micro-PIM of zirconia feedstock with the clear conclusion that it cannot be ignored in numerical simulations. In the following work, Liu et al. [26] supported this finding when comparing the simulations of temperature, viscosity, and pressure gradient distributions during mold filling, including/excluding wall slip.

The present study was performed on an online rheometer with slit dies of different sizes and surface roughness. The purpose of this study is to point out the importance of the wall-slip effect and to show that it is the typical effect for PIM compounds, occurring for the most-often employed PIM feedstocks and, thus, it should always be examined when performing rheological characterization of these highly filled polymers. Concerning PIM compounds, there are—to our best knowledge—no studies considering the dimensions and surface roughness of the processing dies. Also, there are no wall-slip studies performed on commercially available feedstocks.

2. Materials and Methods

2.1. Materials

The research covered both in-house-prepared and commercially available PIM feedstocks; their composition can be seen in Table 1. Commercial compounds P316L, P17-4PH, C316L, and C17-4PH were based on gas-atomized stainless steels 316L and 17-4PH, and differed in polymer binders (abbreviated P and C for partly water soluble and catalytic polyacetal binder systems, respectively), as can be seen from the transition temperatures obtained from the second heating scan (Mettler Toledo DSC1 Star, temperature range from 0 to 250 °C, nitrogen atmosphere, 10 °C/min) depicted in Figure 1. All these compounds had powder volumetric concentrations higher than 60%.

Table 1. Investigated powder injection molding (PIM) feedstocks.

Abbreviation of Feedstock	Type of Powder	Type of Binder	Commercial Name	Producer
P316L	Stainless steel 316L	Partly water soluble (PEG based)	PolyMIM 316L D 110 E	PolyMIM GmbH
P17-4PH	Stainless steel 17-4PH	Partly water soluble (PEG based)	PolyMIM 17-4PH D 110 E	PolyMIM GmbH
C316L	Stainless steel 316L	Catalytic (Poly-acetal based)	Catamold 316 L G	BASF
C17-4PH	Stainless steel 17-4PH	Catalytic (Poly-acetal based)	Catamold 17-4PH G	BASF
ZrO_2	Ceramic ZrO_2	LDPE [1] + EVA [2] + PW [3]	in-house	see bellow
Al_2O_3	Ceramic Al_2O_3	LDPE [1] + EVA [2] + PW [3]	in-house	see bellow

[1] ExxonMobil™ LDPE LD 650 Low Density Polyethylene Resin, [2] ExxonMobil™ Escorene™ Ultra UL 40028CC Ethylene Vinyl Acetate Copolymer Resin, [3] FAGRON Paraffinum solidum
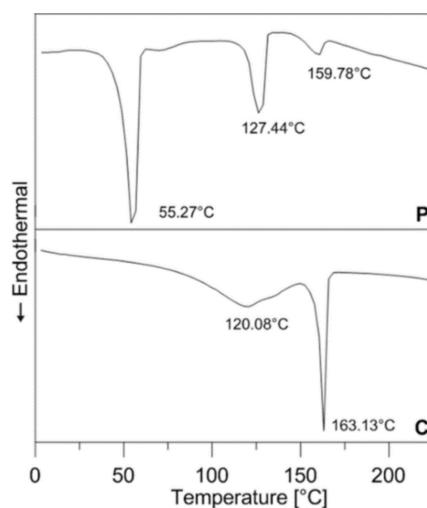
Figure 1. DSC of partly water soluble (P) PolyMIM binder, and catalytic polyacetal (C) Catamold (BASF) binder systems (10 °C/min, second heating scan).

On the other hand, ceramic powders—zirconium oxide (ZrO_2) and aluminum oxide (Al_2O_3)—were admixed to an in-house-prepared binder system at the loading level of 50 vol %. Particle size distributions were measured with the laser diffraction particle size analyzer Malvern Mastersizer 3000 (Malvern, UK). The particle size distribution of ceramic powders was (in μm) D_{10}—0.3, D_{50}—0.56, D_{90}—2.5; and D_{10}—0.19, D_{50}—0.3, D_{90}—0.47 for Al_2O_3 and ZrO_2 powders, respectively. Feedstocks produced by PolyMIM exhibited a particle size distribution of D_{10}—3, D_{50}—9, D_{90}—26, and Catamold feedstocks of D_{10}—7, D_{50}—15, D_{90}—28.

2.2. Preparation of In-House Feedstocks

First, the critical solid loading of powders was determined with a torque rheometer at 160 °C. In the process, the concentration of powder in the mixing chamber was gradually increased by 1 vol % until an unstable and rapidly increased torque signalized critical solid loading. Then, the feedstocks were mixed on a Brabender plastometer with a twin-screws extruder setup. Along the screw, the temperature changed. In the first zone it was set to 140 °C, in the second zone to 150 °C, and at the end of the screw the temperature was increased to 160 °C. A stable temperature profile during the mixing process was maintained, regardless of high dissipation energy, in order to ensure the homogeneity of the mixtures. Extruded feedstocks were subsequently granulated on a grinding machine.

2.3. Rheological Investigation

For slip evaluation, an online Brabender Extrusion Lab (19/25D) rheometer (Duisburg, Germany) and four slit dies of different dimensions and surface roughness were employed, as demonstrated in Table 2. For ceramic powder feedstocks, which are generally considered to be more abrasive than metal-based compounds, we used higher surface roughness and modified geometry of slit dies. The surface roughness of the dies was quantified with an optical surface profiler ZYGO NEWVIEW 9000 (Berwyn, PA, USA) based on coherence scanning interferometry, which provides non-contact real topography maps of smooth, highly reflective surfaces of sub-10 nm roughness. In Table 2, the channel surface properties are described with the 3D roughness parameter *Sa*.

Table 2. Characteristics of slit dies used.

Metal Powder Feedstocks			Ceramic Powder Feedstocks		
Geometry (mm)	Surface	Roughness *Sa* (µm)	Geometry (mm)	Surface	Roughness *Sa* (µm)
$10 \times 0.5 \times 100$	smooth	0.25 ± 0.03	$10 \times 1 \times 100$	smooth	0.81 ± 0.03
	roughened	0.95 ± 0.02		roughened	9.65 ± 0.18
$15 \times 1 \times 100$	smooth	0.07 ± 0.00	$10 \times 2 \times 100$	smooth	0.82 ± 0.04
	roughened	0.77 ± 0.03		roughened	7.87 ± 0.70

The measurements were carried out on an online rheometer, schematically presented in Figure 2.
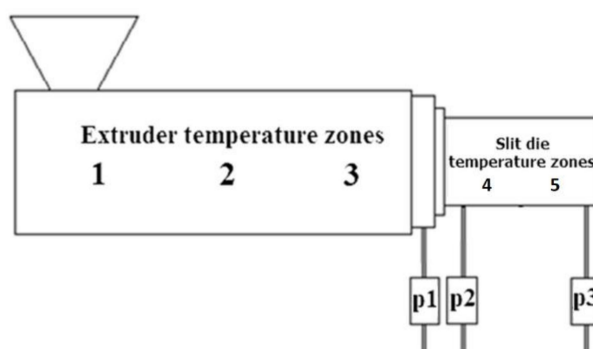
Figure 2. Scheme of the testing online rheometer.

As can be seen, the pressure profile was detected by three pressure transducers. For metal powder feedstocks, the individual screw zones (1 to 3) were set to 170, 180, and 190 °C, respectively, and in the slit die (zones 4 and 5) the temperature was 190 °C. For ceramic powder feedstocks the corresponding temperature profile was (140–150–160–160–160) °C.

The method for wall-slip evaluation from capillary data was proposed by Mooney as early as in 1931 [27]. The slip velocity was calculated from the slope of the apparent shear rate as a function of the reciprocal capillary radius data determined at the constant apparent wall shear stress. In order to obtain

experimental data at close-to-processing conditions, this method was modified by Kalyon et al. [28] for measurements on an online slit die rheometer with an adjustable die gap.

In calculations for on an online rheometer, the shear stress τ (Pa) was derived from

$$\tau = \frac{(p_2 - p_3)H}{2L} \tag{1}$$

where H (mm) represents the height of the slit die and L (mm) is the length between the transducers p_2 and p_3 (Figure 2).

The shear rate was calculated as

$$\dot{\gamma}_a = \frac{6\dot{Q}}{WH^2} \tag{2}$$

where W (mm) is the width of the slit die, and $\dot{Q}$ (mm^3/s) stands for the volumetric flow rate.

Figure 3 demonstrates the calculation of the wall-slip velocity according to the Mooney method.
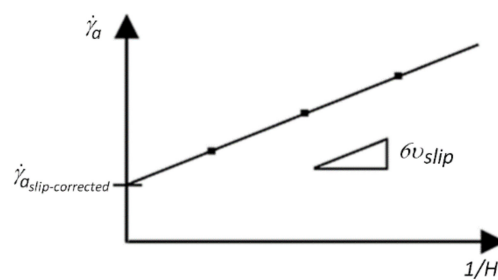
Figure 3. Calculation of wall-slip velocity.

The volumetric flow rate $\dot{Q}$ is related to the calculated average velocity v_{av} in the capillary die as

$$v_{av} = \frac{\dot{Q}}{WH} \tag{3}$$

The calculated average velocity v_{av} in the die is related to the slip-corrected average velocity v_{true} through the slip velocity v_{slip} as

$$v_{true} = v_{av} - v_{slip} \tag{4}$$

To obtain the relationship between the slip-corrected apparent shear rate $\dot{\gamma}_{a,\,slip-corrected}$ and the measured apparent shear rate $\dot{\gamma}_a$, we have to multiply by $6/H$:

$$\dot{\gamma}_a = \frac{6v_{av}}{H} = \frac{6\dot{Q}}{WH^2} \tag{5}$$

$$\frac{6v_{true}}{H} = \frac{6v_{av}}{H} - \frac{6v_{slip}}{H} \tag{6}$$

Then, after rearranging, we obtain

$$\dot{\gamma}_{a,slip-corrected} = \frac{6\dot{Q}}{WH^2} - \frac{6v_{slip}}{H} \tag{7}$$

3. Results and Discussion

The dependence of viscosity on the surface roughness and die geometry is an indicator of wall slip occurring in the flow of highly filled compounds. All tested PIM feedstocks exhibited slip during shear deformation. The feedstocks based on stainless-steel powders (Figure 4) showed the same trend in the slip dependence on die dimension regardless of surface roughness. However, the feedstock

with the partly water-soluble binder (P316L and P17-4PH) shows a stronger influence of flow channel geometry on viscosities than that with the catalytic binder, indicating an enhanced tendency to slip.
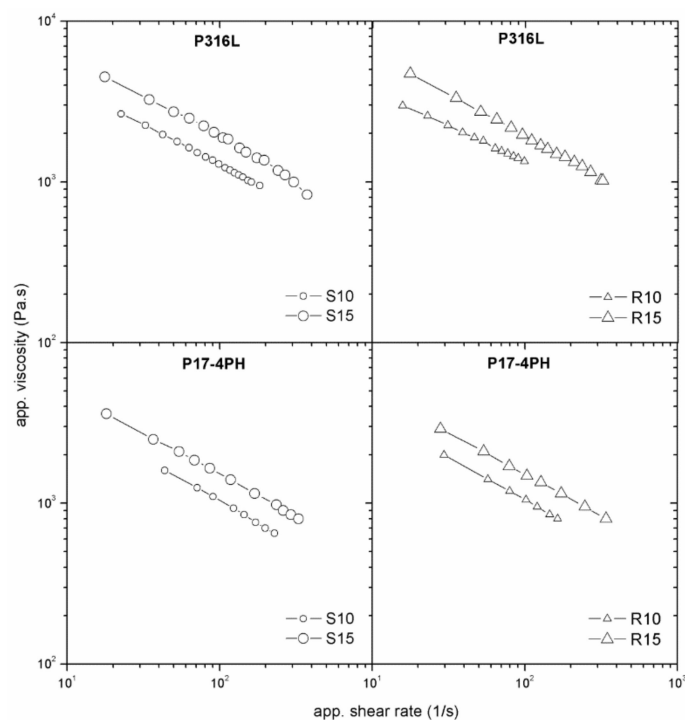
Figure 4. Effect of die dimensions on flow properties of stainless-steel powders 316L (P316L) and 17-4PH (P17-4PH) in the partly water-soluble binder system PolyMIM (P).

Let us move now to the effect of surface roughness. As can be seen from Figure 4 (R10, R15) and Figure 5, the presence of a water-soluble binder in the feedstock resulted in an imperceptible influence of the surface roughness. This means that the thickness of the polymer layer formed at the channel wall was higher than the surface irregularities [12,20] of the tested slit dies.
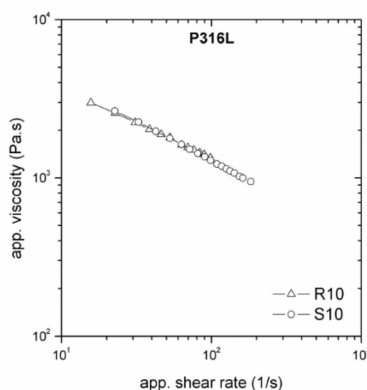
Figure 5. Effect of surface roughness on flow properties of P316L, stainless-steel powder 316L, in the partly water-soluble binder system PolyMIM (P).

On the other hand, for both types of metal powders in the catalytic binder (Figure 6), the effect of surface roughness was evident—a lower viscosity was obtained for a smooth surface. The observed trend is in agreement with the simulations performed by Papanikolaou et al. [29], where parallel liquid layers that formed near a smooth wall surface were disturbed in case of a roughened surface (leading to a higher viscosity).
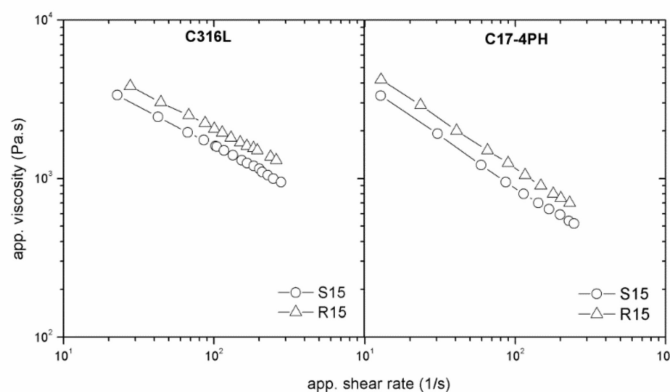
Figure 6. Effect of surface roughness on flow properties of stainless-steel powders 316L (C316L) and 17-4PH (C17-4PH) in catalytic polyacetal Catamold binder system (C).

Furthermore, we compared the effect of the rheometer type. For metal powder feedstocks, the slip behavior obtained on an online rheometer corresponded with our previous findings [22] achieved on a capillary rheometer. Feedstocks based on a partly water-soluble binder exhibited a higher wall-slip velocity (a thicker polymer layer formed on the flow channel wall) in comparison with catalytic feedstocks, where a lower wall-slip velocity was observed. In this case, however, due to the considerable pressure fluctuations, $(10 \times 0.5 \times 100)$ mm geometry has been disregarded for catalytic feedstocks, where, similarly to ceramic feedstocks, for further testing the gap was enlarged to $(10 \times 1 \times 100)$ mm.

Using roughened surfaces of the processing tools should diminish, or even eliminate, wall slip because powder particles (in case of an apparent slip) or polymer chains (in case of true slip) can move into the grooves, polymer layer is eliminated, and the suspension can flow as a continuum [20]. For pure polymer melts, this theoretical finding was confirmed for LLDPE, where a smooth capillary surface revealed the wall-slip velocities 50 % to 150 % greater than roughened dies [17]. In case of highly filled compounds, we obtained the same trend in testing ZrO_2 feedstocks (Figure 7) where, due to higher abrasion of ceramics, the surface roughness was increased for the smooth as well as for the rough surface, to capture the difference.
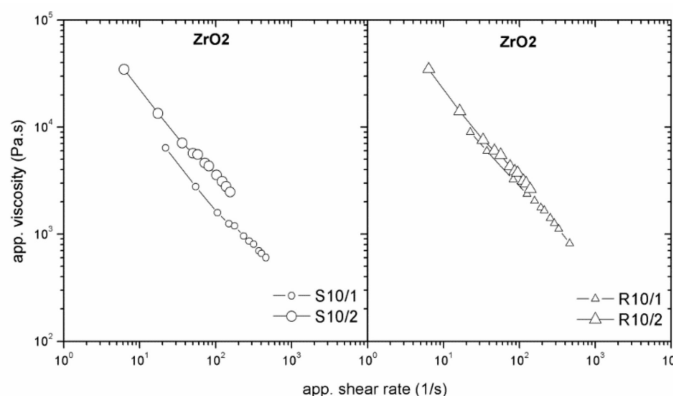
Figure 7. Effect of surface roughness on the flow properties of zirconium oxide (ZrO_2)/LDPE+EVA+PW feedstock.

Another factor influencing wall slip could be the die geometry. As can be seen from Figure 8, the smaller gap height (1 mm) supported the wall-slip effect, while this was substantially reduced for a 2 mm gap.
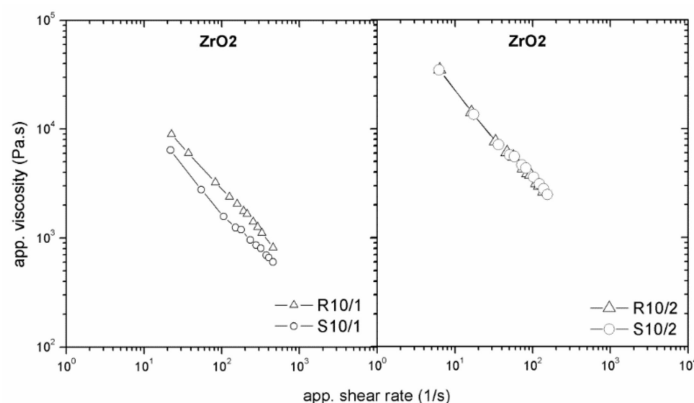
Figure 8. Effect of die dimension on the flow properties of zirconium oxide (ZrO_2)/LDPE+EVA+PW feedstock.

These measurements again correspond to findings on pure linear low-density polyethylene in the capillary flow with different surface roughness [17]. Further, this behavior is in agreement with that of suspensions containing polymer matrix poly(butadiene-acrylonitrile-acrylic acid) filled with glass spheres (particles with a mean size of 35.3 m and 85.4 m) [18] and poly(methyl methacrylate) solid spheres (121.2 m) in hydroxyl-terminated polybutadiene [16], where smooth flow channel walls and small channel geometry [8,30] were found to be the most significant factors causing wall slip.

The influence of the surface roughness on the slip velocity for ceramic powder feedstocks is presented in Figure 9.
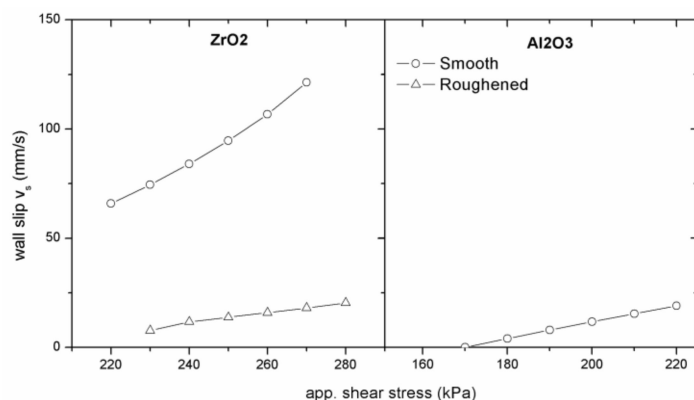
Figure 9. The effect of surface roughness on wall-slip velocity of zirconium oxide (ZrO_2) and aluminum oxide (Al_2O_3) powders in LDPE+EVA+PW binder.

As can be seen, the slip velocity in the roughened die is substantially lower than in the smooth-wall die. The measurement of the rheological behavior in smooth dies results in greater underestimated viscosity, however, as shown in the studies [13,14], due to lower shear rate gradients, slipping at the wall might positively affect the tendency of PIM feedstocks towards powder and binder separation. Figure 9 demonstrates that the values of slip velocities obtained for Al_2O_3 powder in the smooth slit die are comparable with the slip velocities of ZrO_2 feedstock in the roughened slit die; the tendency of Al_2O_3 feedstock to wall slip as a function of the die geometry and surface roughness is generally less pronounced than for ZrO_2 compound, although as we showed recently [31], their surface characteristics (surface energies) were fairly similar—44 and 47 J/m^2 for ZrO_2 and Al_2O_3, respectively.

4. Conclusions

Online rheological investigation of PIM compounds was focused on the wall-slip phenomenon. As could be seen, all tested highly filled materials exhibited wall slip. Thus, neglecting this

phenomenon may lead to inaccurate flow data and, as a consequence, to non-realistic simulations of the injection molding step of the PIM process. The results reveal the importance of surface roughness to wall-slip development if surface irregularities are higher than polymer layers formed at flow channel walls. Generally, the wall-slip velocity decreases with increasing surface roughness. Furthermore, the higher tendency of materials to wall slip was observed in smaller dies. Therefore, both parameters—surface roughness and geometry of the flow channels—are important for reliable testing of highly filled materials.

Author Contributions: D.S. and B.H. designed experiments, analyzed and evaluated data, and wrote the paper together. D.S. performed laboratory tests. The author V.P. evaluated the surface properties of the dies.

Conflicts of Interest: The authors declare no conflict of interest.

References

1. German, R.M.; Bose, A. *Injection Molding of Metals and Ceramics*, 1st ed.; Metal Powder Industry Federation: Princeton, NJ, USA, 1997.

2. German, R.M. *Powder Metallurgy and Particulate Materials Processing*, 1st ed.; Metal Powder Industry Federation: Princeton, NJ, USA, 2005.

3. Thavanayagam, G.; Pickering, K.L.; Swan, J.E.; Cao, P. Analysis of rheological behaviour of titanium feedstocks formulated with a water-soluble binder system for powder injection molding. *Powder Technol.* **2014**, *269*, 227–232. [CrossRef]

4. Zauner, R.; Binet, C.; Heaney, D.F.; Piemme, J. Variability of feedstock viscosity and its correlation with dimensional variability of green powder injection moulded components. *Powder Metall.* **2004**, *47*, 151–156. [CrossRef]

5. He, H.; Li, Y.; Lou, J.; Li, D.; Liu, C. Prediction of density variation in powder injection moulding-filling process by using granular modelling with interstitial power-law fluid. *Powder Technol.* **2016**, *291*, 52–59. [CrossRef]

6. Denn, M.M. Extrusion instabilities and wall slip. *Annu. Rev. Fluid. Mech.* **2001**, *33*, 265–287. [CrossRef]

7. Delime, A.; Moan, M. Lateral migrations of solid spheres in tube flow. *Rheol. Acta* **1991**, *30*, 131–139. [CrossRef]

8. Barnes, H.A. A review of the slip (wall depletion) of polymer solutions, emulsions and particle suspensions in viscometers: Its cause, character, and cure. *J. Non-Newton. Fluid* **1995**, *56*, 221–251. [CrossRef]

9. Bryan, M.P.; Rough, S.L.; Wilson, D.I. Investigation of static zone and wall slip through sequential ram extrusion of contrasting micro-crystalline cellulose-based pastes. *J. Non-Newton. Fluid* **2015**, *220*, 57–68. [CrossRef]

10. Kalyon, M.; Aktas, S. Factors Affecting the Rheology and Processability of Highly Filled Suspensions. *Annu. Rev. Chem. Biomol.* **2014**, *5*, 229–254. [CrossRef] [PubMed]

11. Soltani, F.; Yilmazer, U. Slip velocity and slip layer thickness in flow of concentrated suspensions. *J. Appl. Polym. Sci.* **1998**, *70*, 515–522. [CrossRef]

12. Lam, Y.C.; Wang, Z.Y.; Chen, X.; Joshi, S.C. Wall slip of concentrated suspension melts in capillary flows. *Powder Technol.* **2007**, *77*, 162–169. [CrossRef]

13. Thornagel, M. MIM-Simulation: A virtual study on phase separation. *Proc. EURO PM 2009* **2009**, *2*, 135–140.

14. Hausnerova, B.; Marcanikova, L.; Filip, P.; Saha, P. Wall-slip velocity as a quantitative measure of powder-binder separation during powder injection moulding. In Proceedings of the World Powder Metallurgy Congress and Exhibition, World PM 2010, Florence, Italy, 10–14 October 2010; pp. 557–562.

15. Hausnerova, B.; Sanetrnik, D.; Ponizil, P. Surface structure analysis of injection molded highly filled polymer melts. *Polym. Comp.* **2013**, *34*, 1553–1558. [CrossRef]

16. Gulmus, S.A.; Yilmazer, U. Effect of volume fraction and particle size on wall slip in flow of polymeric suspension. *J. Appl. Polym. Sci.* **2005**, *98*, 439–448. [CrossRef]

17. Chen, Y.; Kalyon, D.M.; Bayramli, E. Effects of surface roughness and the chemical structure of materials of construction on wall slip behavior of linear low density polyethylene in capillary flow. *J. Appl. Polym. Sci.* **1993**, *50*, 1169–1177. [CrossRef]

18. Aral, B.K.; Kalyon, D.M. Effects of temperature and surface roughness on time-dependent development of wall slip in steady torsional flow of concentrated suspension. *J. Rheol.* **1994**, *38*, 957–972. [CrossRef]

19. Gulmus, S.A.; Yilmazer, U. Effect of the surface roughness and construction material on wall slip in the flow of concentrated suspensions. *J. Appl. Polym. Sci.* **2006**, *103*, 3341–3347. [CrossRef]

20. Medhi, B.J.; Kumar, A.A.; Singh, A. Apparent wall slip velocity measurement in free surface flow of concentrated suspensions. *Int. J. Multiph. Flow* **2011**, *37*, 609–619. [CrossRef]

21. Kalyon, D.M. Apparent slip and viscoplasticity of concentrated suspensions. *J. Rheol.* **2005**, *49*, 621–640. [CrossRef]

22. Sanetrnik, D.; Hausnerova, B.; Filip, P.; Hnatkova, E. Influence of capillary die geometry on wall slip of highly filled powder injection molding compounds. *Powder Technol.* **2018**, *325*, 615–619. [CrossRef]

23. Walter, B.L.; Pelteret, J.P.; Kaschta, J.; Schubert, D.W.; Steinmann, P. On the wall slip phenomenon of elastomers in oscillatory shear measurement using parallel-plate rotational rheometry: II. Influence of experimental conditions. *Polym. Test.* **2017**, *61*, 455–463. [CrossRef]

24. Kwon, T.H.; Ahn, S.Y. Slip characterization of powder/binder mixtures and its significance in the filling process analysis of powder injection molding. *Powder Technol.* **1995**, *85*, 45–55. [CrossRef]

25. Liu, L.; Ma, Y.H.; He, Z.Y. Rheological behavior of zirconia feedstock flowing through various channels considering wall-slip. *Ceram. Int.* **2018**, *44*, 22387–22392. [CrossRef]

26. Liu, L.; Gao, Y.Y.; Qi, X.T.; Qi, M.X. Effect of wall slip on ZrO_2 rheological behavior in micro powder injection molding. *Ceram. Int.* **2018**, *44*, 16282–16294. [CrossRef]

27. Mooney, M. Explicit formulas for slip and fluidity. *J. Rheol.* **1931**, *2*, 210–222. [CrossRef]

28. Kalyon, D.; Gevgilili, H.; Kowalczyk, J.E.; Prickett, S.; Murphy, C. Use of adjustable-gap on-line and off-line slit rheometers for the characterization of the wall slip and shear viscosity behavior of energetic formulations. *J. Energ. Mater.* **2006**, *24*, 175–193. [CrossRef]

29. Papanikolaou, M.; Frank, M.; Drikakis, D. Effects of surface roughness on shear viscosity. *Phys. Rev. E* **2017**, *95*. [CrossRef] [PubMed]

30. Jeong, M.; Kim, Y.; Zhou, W.; Tao, W.Q.; Ha, M.Y. Effects of surface wettability, roughness and moving wall velocity on the Couette flow in nano-channel using multi-scale hybrid method. *Comput. Fluids* **2017**, *147*, 1–11. [CrossRef]

31. Hausnerova, B.; Bleyan, D.; Kasparkova, V.; Pata, V. Surface adhesion between ceramic injection molding feedstocks and processing tools. *Ceram. Int.* **2016**, *2016 42*, 460–465. [CrossRef]

Paper IV

Rheological and thermal debinding properties of blended elemental Ti-6Al-4V powder injection molding feedstock

Dongguo Lin [a], Daniel Sanetrnik [b,c], Hanlyun Cho [a], Seong Taek Chung [d], Young Sam Kwon [d], Kunal H. Kate [e], Berenika Hausnerova [b,c], Sundar V. Atre [e], Seong Jin Park [a,*]

[a] Department of Mechanical Engineering, Pohang University of Science and Technology (POSTECH), Pohang, Gyeongbuk, South Korea
[b] Department of Production Engineering, Faculty of Technology, Tomas Bata University in Zlin, 760 01 Zlin, Czech Republic
[c] Centre of Polymer Systems, Tomas Bata University in Zlin, Trida T. Bati 5678, 760 01 Zlin, Czech Republic
[d] CetaTech, Inc., TIC 296-3, Sacheon, Gyeongnam, South Korea
[e] Materials Innovation Guild, Department of Mechanical Engineering, University of Louisville, Louisville, KY, USA

A B S T R A C T

The rheological and thermal debinding properties of a feedstock play an important role in the molding and debinding stage of powder injection molding (PIM), and can directly determine the quality of final PIM product. This work focuses on the rheological and thermal debinding properties of blended elemental Ti-6Al-4V (BE Ti64) PIM feedstock with a comparison study of pure titanium (Ti) feedstock. The effects of 60Al-40V alloy addition, on the attributes of BE Ti64 feedstock; including critical solids loading, rheological behavior, and binder decomposition behavior, were studied using torque rheometry, capillary rheometry, and thermogravimetric analysis. The critical solids loading of BE Ti64 (66 vol.%) was somewhat lower value than the Ti feedstock (69 vol.%), due to the different in particle characteristics. Both BE Ti64 and Ti feedstocks exhibited non-Newtonian shear-thinning behavior. The difference in flow activation energies for the two feedstocks indicates that the BE Ti64 feedstock is more sensitive to temperature compared to the Ti feedstock. During thermal debinding, both the feedstocks exhibited a dual-sigmoid, binder-decomposition behavior with only minor differences in activation energy.

© 2017 Elsevier B.V. All rights reserved.

1. Introduction

Titanium and its alloys exhibit a useful combination of properties such as high strength, corrosion resistance, high temperature endurance, lightweight and biocompatibility [1,2]. These properties of titanium can find many applications in medical, automotive and aerospace applications [3,4]. However the use of these materials especially in the manufacturing of complex parts in high production volumes is limited due to processing challenges as well as high material cost [4–7].

Powder injection molding (PIM) technology is one possible process candidate that can potentially provide a reduction of the manufacturing cost of large production volume net-shape titanium products [1,5,8]. In PIM, the metal powder is mixed with suitable polymer binders that should have good interactions with metals, enable easy debinding and be environmentally safe. Next, the powder-binder mixture (called feedstock) is injected into the cavity with desired shape. After injection molding, the polymer binder is removed and the samples are sintered into the final metal parts with density over 95% of theoretical [9,10].

The type of binder system significantly affects the feedstock homogeneity and rheology, consequently affecting the quality of the final parts [11–13]. Therefore, the appropriate mixing conditions and thermal characteristics of feedstock need to be identified as important features of the PIM process [7,11]. Prior to mixing, the optimal powder/binder ratio must be found, which determines the quality of the whole PIM process. Three levels of powder/binder ratio can be distinguished within PIM feedstock; binder deficit, binder excess, and optimal loading. Binder deficit limits the moldability of the feedstock due to high viscosity and also causes defects during sintering. On the other hand, the excess of binder can lead to binder separation from a powder during injection molding, structural collapse during debinding, and large shrinkage and distortion during sintering. At a critical solids loading, the powders are uniformly surrounded by the binder and are packed in close contact without any voids. A powder/binder ratio that is slightly less than (approximately 2– 5 vol.%) the critical solids loading is generally considered to be an optimal loading for PIM [9,14].

Titanium (abbreviated as Ti) is usually processed as alloys, one of the most commonly used titanium alloy being Ti-6Al-4V (abbreviated as Ti64). The addition of Al and V causes significantly higher strength with the same stiffness and thermal properties as pure Ti [15]. In

---

* Corresponding author.
  E-mail address: sjpark87@postech.ac.kr (S.J. Park).

traditional powder metallurgy, pre-alloyed (PA) or blended elemental (BE) Ti64 powders are two main types of Ti64 powders used to produce Ti64 alloy parts. Compared to the spherical shape of PA Ti64 powder, the BE Ti64 powder usually has an irregular shape and a non-uniform size distribution. Products made by BE Ti64 powder exhibit inferior mechanical properties, however, it is considered to be more cost-effective than PA Ti64.

Particle size has been reported to influence defects in the sintered parts [16–19]. Hausnerova et al. [18] studied the homogeneity of molded samples by atomic force microscopy and noticed that larger particles are more prone to phase separation. This finding was also confirmed by Shivashankar et al. [19] who used rheological measurement for investigation of phase separation. The size of particles affects not only the homogeneity of molded samples, additionally finer particles reduce sintering time and increase mixing viscosity, sintering shrinkage and agglomeration [20].

As demonstrated in this study, the powder morphology affects the critical solids loading. The higher powder loading leads to a higher sintered density in the final product. On the other hand, if porosity is desired, a lower powder loading can be used [21,22]. Spherical particles with broad distribution usually exhibit higher packing density, resulting in a higher critical solids loading and improved mechanical properties. Gulsoy et al. [23] reported the sintered density of spherical Ti64 to be 99.3% of theoretical, while irregularly shaped Ti64 powder could only be sintered to 97.9% of the theoretical density. However, irregular particles are more cost effective and they have been reported to improve the retention of the final shape of sintered products due to a higher interparticle friction [23–25].

In this study, a Ti-6Al-4V PIM feedstock was prepared using blended elemental (BE) powders and a wax-polymer binder system. The rheological and thermal debinding properties of the BE Ti64 feedstock were studied and compared to the performance of pure titanium (Ti) feedstock.

2. Experimental

2.1. Materials

The powder used in this work is BE Ti64 prepared by mechanical blending of 90 wt.% of plasma-atomized Ti powder and 10 wt.% of

Table 1
Particle size characteristics of pure Ti, 60Al-40V alloy, and BE Ti64 powders.

Type of powder	Mean particle size (µm)	D_{10} (µm)	D_{50} (µm)	D_{90} (µm)
Ti	28.4	13.2	26.5	45.6
60Al-40V alloy	23.3	6.0	20.6	44.6
BE Ti64	25.5	11.3	24.4	41.0

mater alloy powder. The Ti and 60Al-40V powders were blended with stainless steel balls using a turbula shaker-mixer for 30 min. The particle size distributions for pure Ti, 60Al-40V, and BE Ti64 were measured using a laser scattering particle size analyzer (Horiba LA 960) as shown in Fig. 1, and the results are summarized in Table 1. The mean particle size for BE Ti64 powder was 25.5 µm, a smaller value comparing to Ti powder (28.4 µm). This is due to the addition of the 60Al-40V powder (20.6 µm). The morphologies of pure Ti, 60Al-40V, and BE Ti64 powders were observed under a scanning electronic microscope (SEM) as shown in Fig. 2. It can be observed that the pure Ti powder had a spherical shape while the 60Al-40V powder had an irregular shape, which can also be distinguished easily in BE Ti64 powder as shown in Fig. 2 (c).

The binder system used in this work is a wax-polymer binder system, which includes 57.5 wt.% of paraffin wax (PW), 25 wt.% of polypropylene (PP), 15 wt.% of polyethylene (PE), and 2.5 wt.% of stearic acid (SA). The physical properties of each binder composition provided by each supplier are listed in Table 2.

2.2. Feedstock preparation

In this study, the feedstock critical solids loading was measured by torque rheometry to determine the optimal solids loading for each feedstock. The experiments were conducted using a twin-screw torque rheometer (HAAKE PolyLab QC) at a temperature of 150 °C and a mixing speed of 150 rpm. In the mixing chamber, the volume of binder was fixed and the concentration of powder was continuously increasing by 1 vol.% of solids loading until the mixing torque rapidly increased or didn't stabilize. The optimum solids loading was set as 2 vol.% lower than critical solids loading value to provide sufficient processing flexibility.
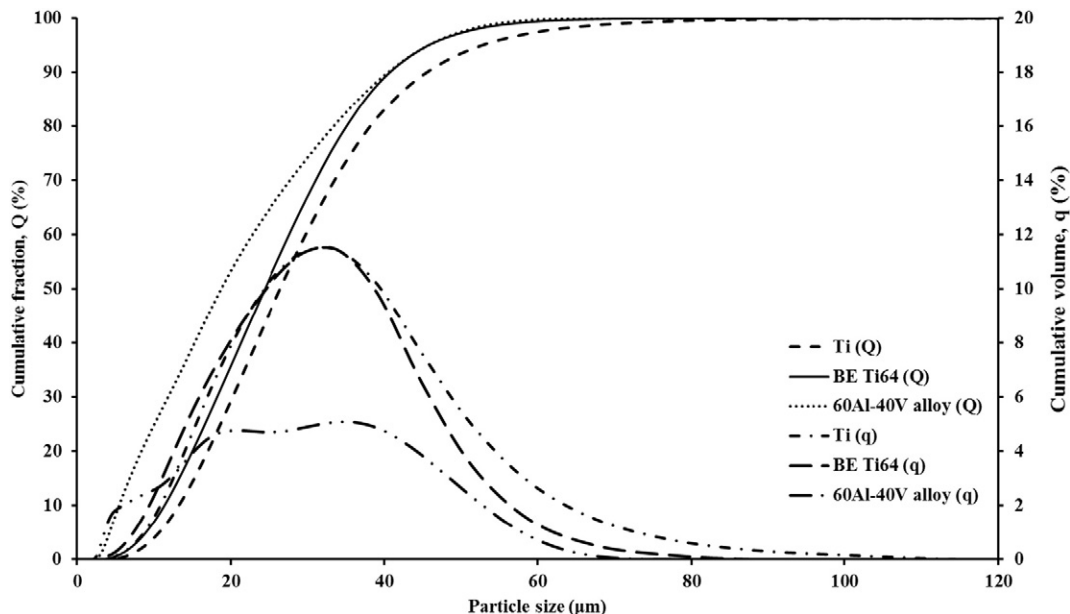

Fig. 1. Particle size distribution curves for pure Ti, BE Ti64, and 60Al-40V alloy powders.
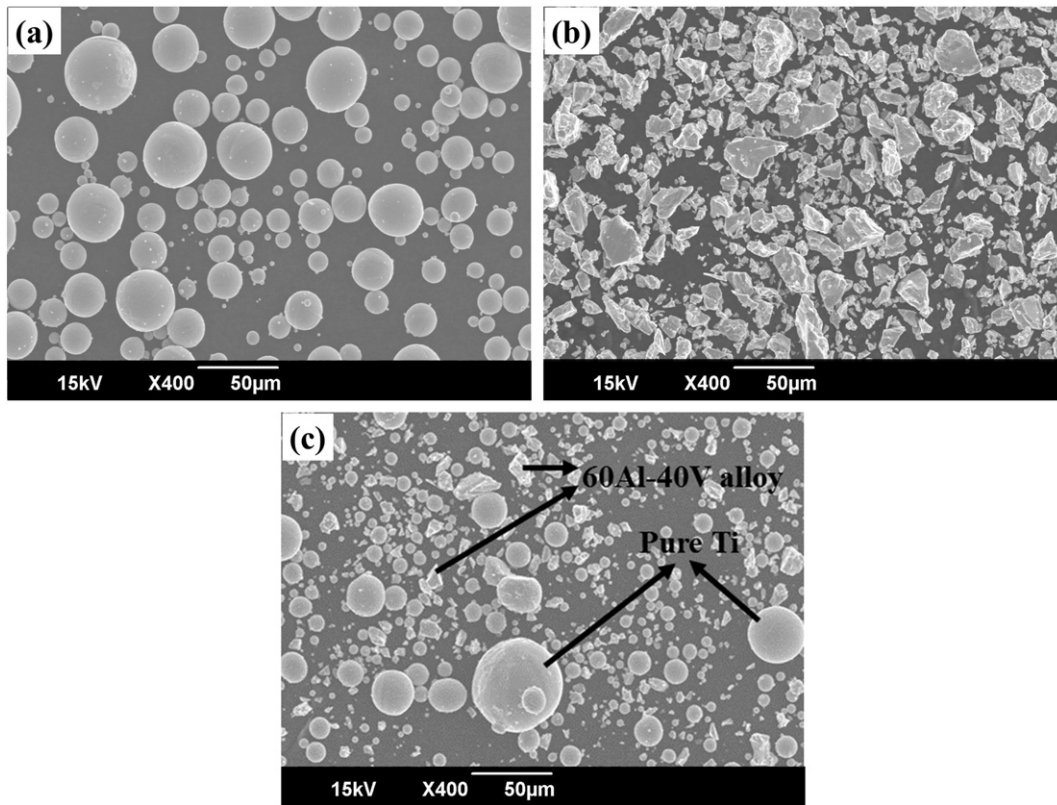
Fig. 2. Powder morphologies of different powders: (a) pure Ti powder, (b) 60Al-40V alloy powder, (c) BE Ti64 powder.

Mixing homogeneity is another important feedstock parameter. To achieve a homogeneous feedstock by mixing, the Ti and BE Ti64 powders were mixed with the binder system at designed optimal solids loading using a twin-screw extruder (CetaTech Inc.). The mixing was performed at a temperature of 160 °C and a mixing speed of 30 rpm. According to our previous research [13], the process was repeated three times to prepare the adequately homogeneous Ti and BE Ti64 feedstocks.

2.3. Feedstock characterization

The rheological behavior and moldability of the feedstock during injection molding can be expressed by its viscosity changes under different temperature and shear rate conditions. A twin-bore barrel capillary rheometer (Rosand RH7) with the Φ (1 × 16) mm die in measuring bore and Φ (1 × 0.25) mm die in correction bore, was used to measure the viscosity for prepared feedstocks at a high shear rate ranging from 100 to 5000 s^{-1}. In order to analyze the effects of molding temperature on their rheological properties, the rheometry experiments were performed under three different temperatures, i.e. 150, 160 and 170 °C.

The thermal debinding properties of prepared feedstocks were analyzed through thermos-gravimetric analysis (TGA). The TGA experiment for each feedstock was conducted using a thermal gravity analyzer (Mettler Toledo TGA/DSC 1). The feedstock was heated up from 30 to 700 °C at three different heating rates; 2, 5, and 10 °C/min. The weight loss curve was analyzed to understand its thermal debinding properties.

3. Results and discussion

3.1. Critical solids loadings

Fig. 3 (a) and (b) show the relationship between mixing torque and time for Ti and BE Ti64 feedstocks, respectively. Critical solids loading is

the composition where the powders are packed as tightly as possible without external pressure and all space between the powders is filled with binder. Below the critical solids loading, the mixing torque increases slowly with increasing of solids loading values. However, once the solids loading value exceeds a critical point, the mixing torque increases drastically, and was designated as the critical solids loading point [9].

In order to analyze the change of mixing torque values as a function of solids loading, the torque values after stabilization at each solids loading point for each feedstock were plotted as shown in Fig. 4 (a) and (b). In Fig. 4 (a), the mixing torque increased slowly as the solids loading increased, and after the solids loading reached 69 vol.%, the torque increased rapidly indicating the critical solids loading for Ti feedstock was 69 vol.%. Similarly, in Fig. 4 (b), the critical solids loading for BE Ti64 was 66 vol.%, which was 3 vol.% lower than that of Ti feedstock. This difference in the critical solids loading can be attributed to the characteristics of two powder systems. In this work, the BE Ti64 feedstock was prepared by adding irregular 60Al-40V powder with a wide particle size distribution into spherical Ti powders with a relatively narrow particle size distribution. We suggest that irregular powders may disperse less uniformly in the binder, possibly generating a larger friction force during mixing, resulting in an increase in mixing torque. The mixing

Table 2
Physical properties of binders in wax-polymer binder system.

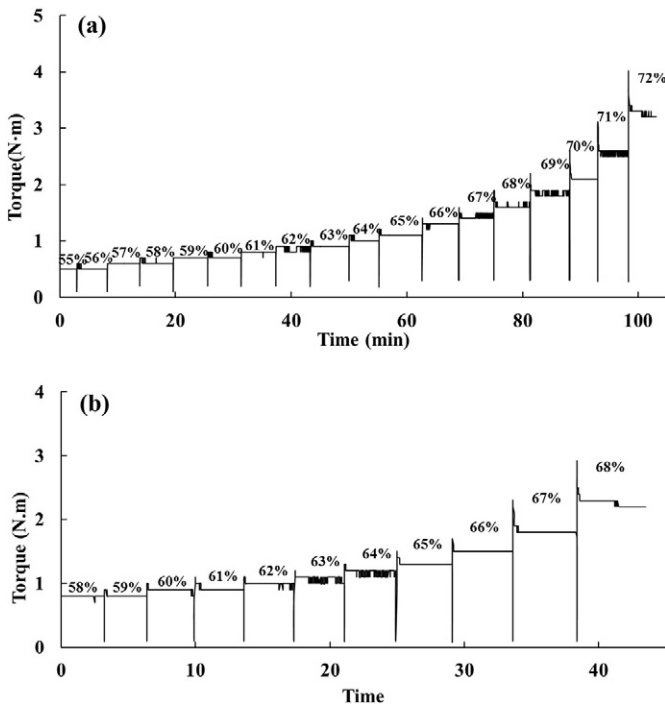| Type of polymer	Contents (wt.%)	Density (g/cm^3)	Melting temperature (°C)	Decomposition temperature (°C)
Paraffin wax	57.5	0.92	51	242–280
Polypropylene	25	0.92	78	464–481
Polyethylene	15	0.93	120	464–471
Stearic acid	2.5	0.95	53	246–275

Fig. 3. The mixing torque at different solids loading for: (a) Ti feedstock, (b) BE Ti64 feedstock.

torque of the Ti feedstock was lower than that of the BE Ti64 feedstock at the same solids loading, which can eventually decrease the critical solids loading. Such differences have been noted in several previous studies on the injection molding of Ti alloys [2,23], stainless steel [20], and alumina powders [17]. In this study, the optimal solids loading for Ti and BE Ti64 feedstocks were set as 67 vol.% and 64 vol.%, respectively, which were 2 vol.% lower than their critical solids loadings.
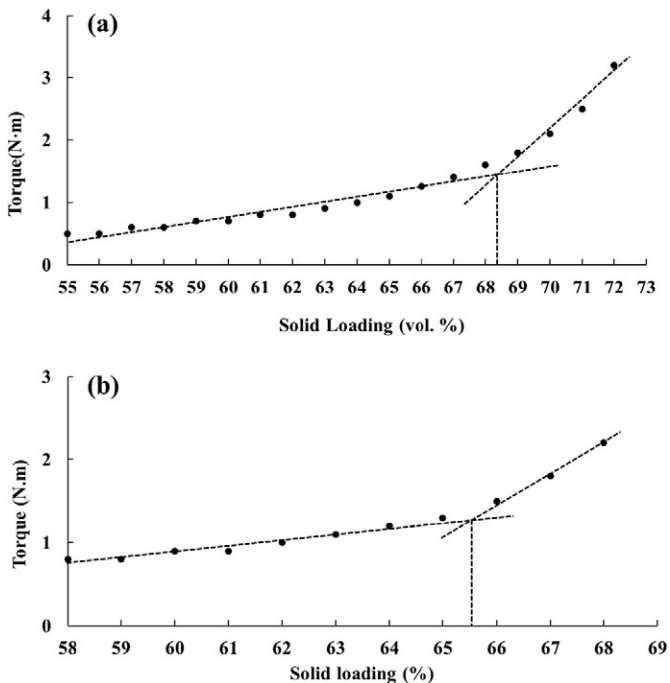

Fig. 4. The mixing torque after stabilization at different solids loading for: (a) 67 vol.% Ti feedstock, (b) 64 vol.% BE Ti64 feedstock.

3.2. Rheological properties

The rheological properties of feedstock can largely affect the success or failure of the mold-filling process. An improper rheological behavior would result in molding defects such as short-shot, flash, cracking, bubbling, warpage, and powder-binder separation. Based on capillary rheometry, the relationship between viscosity and shear rate for each feedstock was plotted.

Fig. 5 shows the relationship between viscosity and shear rate for the two feedstocks at 160 °C. In PIM, at the chosen injection temperature, the feedstock viscosity is recommended to be lower than 1000 Pa·s at a shear rate range between 100 and 10,000 s^{-1} [9]. As shown in Fig. 5, the viscosity values of Ti and BE Ti64 feedstocks were much lower than 1000 Pa·s at shear rates over than 100 s^{-1} indicating that both the feedstocks were suitable to be injection molded. Also, from Fig. 5, both feedstocks showed a pseudo-plastic behavior, where the viscosity decreased with increasing shear rate. However, at the same shear rate and temperature, the viscosity value for the 64 vol.% BE Ti64 feedstock was lower than that of the 67 vol.% Ti feedstock due to its lower solids loading percentage.

In order to evaluate the dependence of viscosity on temperature, rheological properties of the feedstocks were measured at 150, 160, and 170 °C. As shown in Fig. 6 (a) and (b), the viscosity of both feedstocks decreased with increasing temperature. An Arrhenius type power-law model was used to describe the dependence of viscosity on temperature as shown in Eq. (1) [26]:

$$\eta(\dot{\gamma}, T) = B \exp\left[\frac{E}{RT}\right]\dot{\gamma}^{n-1} \tag{1}$$

where n, B, E, and R represent the power-law exponent, the material specific reference factor (or reference viscosity), the flow activation energy for the Arrhenius temperature dependence of the viscosity, and the gas constant, respectively. The parameters in the above equation can be derived by curve fitting the experimental results. The value of n can be derived by fitting the viscosity and shear rate data as shown in Fig. 6 (a) and (b). The results showed that the values of power-law exponent n for the 67 vol.% Ti and the 64 vol.% BE Ti64 feedstocks were 0.55 and 0.57, respectively. The power-law exponent n is related to shear thinning, when $n < 1$, it indicated that both feedstocks have the properties of non-Newtonian shear-thinning fluid. In addition, the lower value of n for the BE Ti64 feedstock indicates that it has a lower shear thinning effect than Ti feedstock.

The flow activation energy, E, is a measure of temperature sensitivity of a feedstock. It can be determined by the material properties of binders, powders, as well as the solids loading percentage of powder in feedstock. The larger flow activation energy value means the
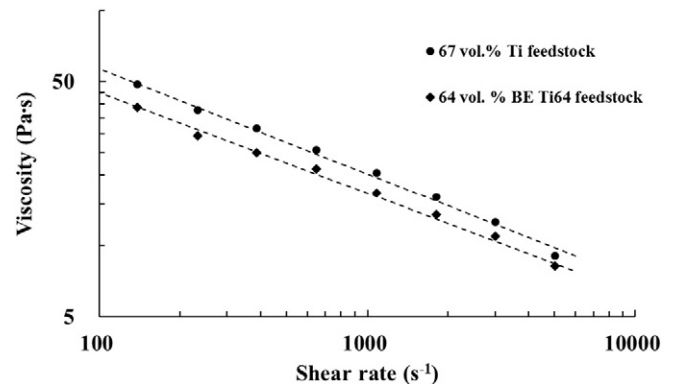

Fig. 5. Relationship between viscosity and shear rate for 67 vol.% Ti and 64 vol.% BE Ti64 feedstocks at 160 °C.
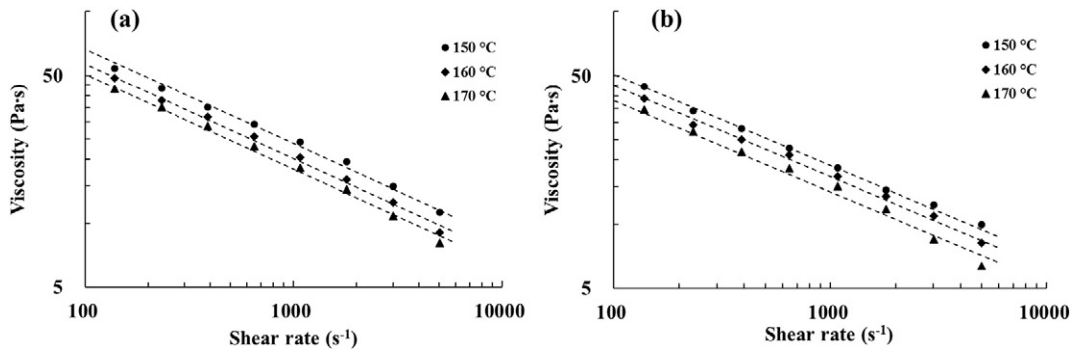
Fig. 6. Viscosity and shear rate data and its fitting results (the slope of dash line is n value) for different feedstocks at three different temperatures: (a) 67 vol.% Ti feedstock, (b) 64 vol.% BE Ti64 feedstock.

feedstock is more sensitive to temperature, to whom the control of temperature conditions such as injection temperature and mold temperature will be very important and should be monitored carefully. The parameter, E, can be derived by fitting the viscosity and temperature data as shown in Fig. 7 (a) and (b), where the values of flow activation energy for the 67 vol.% Ti and the 64 vol.% BE Ti64 feedstocks were 20 and 22 kJ/mol, respectively, indicating they have a similar sensitivity degree to temperature during molding process.

3.3. Thermal debinding properties

Thermal debinding is widely used in PIM to remove the backbone (higher molecular weight) binder component prior to sintering. Improper thermal debinding conditions can result in defects such as cracking, bloating, distortion, and contamination [27]. Especially, in Ti-PIM, more attention should be paid on the contamination issue due to the highly reactive properties of Ti and its alloy powders in a relatively high temperature [1]. At this point, the thermal debinding properties for both Ti and BE Ti64 feedstocks were evaluated through TGA results.

Fig. 8 (a) and (b) respectively show the weight loss curves of Ti and BE Ti64 feedstocks at three different heating rates. For both systems, the weight loss curve comprised of two sigmoids, where the first sigmoid is related to the decomposition of low molecular weight binder components (PW and SA), and second sigmoid relates to the decomposition of high molecular weight binder components (backbone binders-PE and PP). After the binders decomposed, the weight of both feedstocks increased at higher temperatures due to the reaction between Ti and BE Ti64 with carbon and atmospheric air. As claimed by S. Guo et al. [1], the oxygen level increases dramatically after a certain debinding temperature (around 600 °C) because of the reaction between titanium powders with oxygen in atmosphere to form titania (titanium oxide), which had a good agreement with the TGA curves as shown in Fig. 8 (a) and (b). Also, at a high temperature the titanium can react with the carbon, which may come from the impurities of experimental

environment but also from the polymer binder compositions, to form the titanium carbide. However, the stage between two sigmoids in the binder decomposition behavior of BE Ti64 feedstock showed a more gradual decline when comparing to Ti feedstock that has previously been speculated to result from catalytic effects of the powder surface [2,27].

The first-order reaction kinetics can be used to describe the decomposition of binders in PIM feedstock [28]. The remaining weight fraction of binder, α, can be expressed as Eq. (2):

$$\frac{da}{dt} = -Ka \tag{2}$$

where α is the weight fraction of remained binders, t is the time and K is the rate constant for thermal degradation, which can be expressed using the Arrhenius equation as shown in Eq. (3):

$$K = k_0 \exp\left(-\frac{Q}{RT}\right) \tag{3}$$

where, k_0 is the specific rate constant, Q is the apparent activation energy for thermal decomposition, R is the gas constant, and T is the absolute temperature.

The apparent activation energy Q can be calculated by the Kissinger method using the maximum temperature T_{max}, where the maximum rate of weight loss occurs. It can be described as shown in Eq. (4).

$$\frac{d}{dt}\left(-\frac{d\alpha}{dt}\right) = 0, (T = T_{max}) \tag{4}$$

Eq. (5) can be derived from Eqs. (2)–(4):

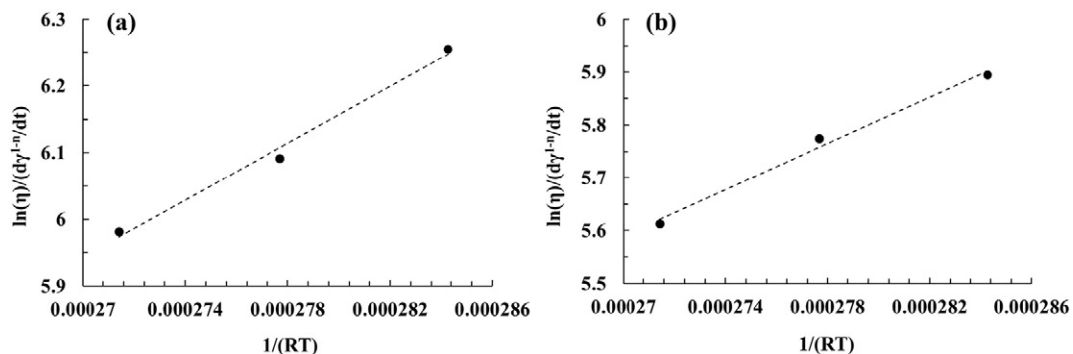$$\frac{rQ}{RT_{max}^2} k_0 \exp(-Q/RT_{max}), \left(r = \frac{dT}{dt}\right) \tag{5}$$

Fig. 7. Flow activation energy represented as the slopes of linear fit for (a) 67 vol.% Ti feedstock, (b) 64 vol.% BE Ti64 feedstock.
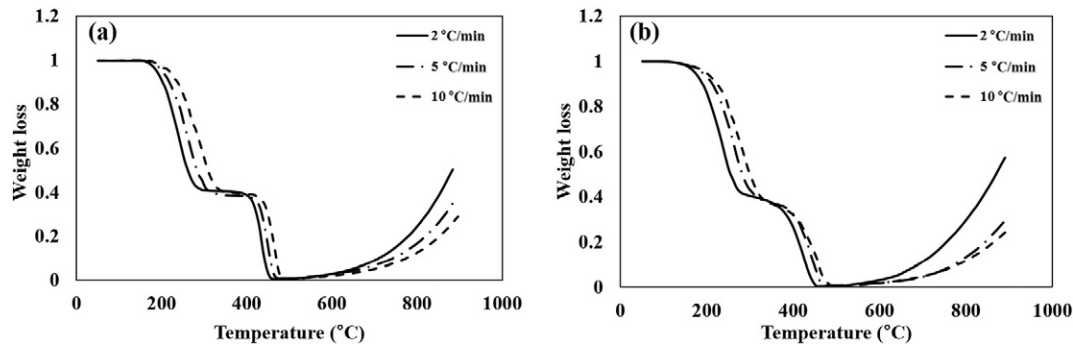
Fig. 8. Binder decomposition behaviors of different feedstocks at three different heating rates: (a) 67 vol.% Ti feedstock, (b) 64 vol.% BE Ti64 feedstock.
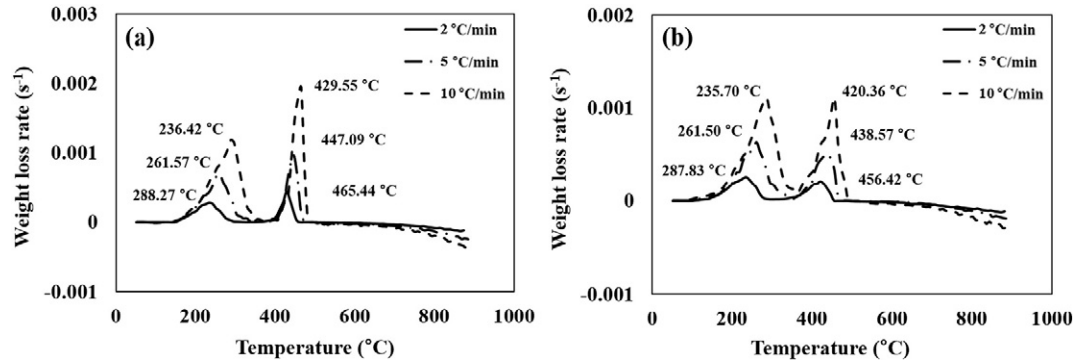

Fig. 9. Binder weight loss rate curves at three different heating rates: (a) 67 vol.% Ti feedstock, (b) 64 vol.% BE Ti64 feedstock.

where r represents the constant heating rate, which equals to the value in TGA experiments (i.e. 2, 5, 10 °C/min).

By taking logarithms on each side of Eq. (5), it can be derived into a form as shown in Eq. (6), where the values of activation energy Q and specific rate constant k_0 can be calculated by curve fitting.

$$\ln\left(\frac{r}{T_{max}^2}\right) = Q\left(-\frac{1}{RT_{max}}\right) - \ln\left(\frac{Q}{k_0 R}\right) \quad (6)$$

Fig. 9 (a) and (b) show the weight loss rate versus temperature of the Ti and BE Ti64 feedstocks at three different heating rates. As heating rate increased, the temperature for maximum weight loss (T_{max}) lagged due to the shorter heating time used for the feedstocks. Also, for the same heating rate, the T_{max} values for first sigmoid of the BE Ti64 feedstock were close to that of the Ti feedstock. However, the T_{max} values for first sigmoid of the BE Ti64 feedstock were higher than that of the Ti feedstock.

Fig. 10 (a) and (b) show the fitted plots to calculate the apparent activation energy Q from Eq. (6) for both the feedstocks. The apparent activation energy of first sigmoid (Q_1) for the BE Ti64 feedstock was 64 kJ/mol, comparable to that of the Ti feedstock (65 kJ/mol). The apparent activation energy of second sigmoid (Q_2) was 176 kJ/mol, was also only slightly lower value comparing to that of Ti feedstock (182 kJ/mol).

The rate constants K at different debinding temperatures can also be calculated using the relationships among the specific rate constant k_0 (determined by curve fitting), apparent activation energy Q (determined by curve fitting), and temperature T (specific temperature for first and second sigmoids) as shown in Eq. (3). Two specific temperatures, 250 and 450 °C, were selected for the first and second sigmoids to calculate the K values for both feedstocks, and the results are summarized in Table 3. It can be found that the calculated rate constants for the Ti and the BE Ti64 feedstocks at 250 °C (first sigmoid) were almost the same, having the values of 1.5×10^{-3} and 1.7×10^{-3} s^{-1}, respectively. However, the calculated rate constants at 450 °C (second sigmoid) for Ti and BE Ti64 feedstocks were slightly different, showing the values of
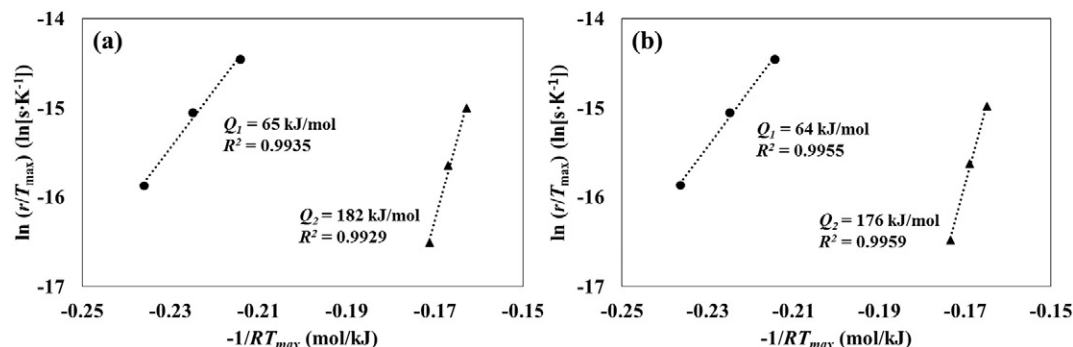

Fig. 10. Calculation of apparent activation energies for binder decomposition of different feedstocks: (a) 67 vol.% Ti feedstock, (b) 64 vol.% BE Ti64 feedstock.

Table 3
Thermal debinding properties of Ti and BE Ti64 feedstock.

	Q_1 (kJ/mol)	Q_2 (kJ/mol)	k_{01} (10^3 s^{-1})	k_{02} (10^{10} s^{-1})	K_1 (at 250 °C, 10^{-3} s^{-1})	K_2 (at 450 °C, 10^{-3} s^{-1})
Ti feedstock	165	1.4	4.8	4.8	1.5	3.4
BE Ti64 feedstock	165	1.4	4.2	2.8^0	1.7	5.4

3.4×10^{-3} and 5.4×10^{-3} s^{-1}, respectively. It suggests that the backbone binders (PE and PP) may be slightly more rapidly removed in BE Ti64 feedstock than in Ti feedstock, possible due to some mild catalytic effects of the Al-V powders on binder decomposition.

4. Conclusions

Rheological and thermal debinding properties of the BE Ti64 powder injection molding feedstock were characterized. The effects of 60Ti-40V alloy addition on the attributes of the BE Ti64 feedstock; including critical solids loading, rheological behavior, and binder decomposition behavior, were analyzed by comparison study with the Ti feedstock. The results showed that the critical solids loading of BE Ti64 was 66 vol.%, which was 3 vol.% lower than that of Ti feedstock (69 vol.%) affected by the change in powder characteristics as 60Ti-40V alloy powders, with irregular shape and wide particle size distribution, added into spherical Ti powders. The rheological properties of these two feedstocks exhibited non-Newtonian shear-thinning fluid with a relatively low viscosity during molding process, which would be suitable for both low and high pressure injection molding. The thermal debinding properties of BE Ti64 and Ti feedstocks exhibited a dual-sigmoid binder decomposition behavior. The estimated apparent activation energy for the BE Ti64 feedstock was similar to that of the Ti feedstock in thermal debinding. This result indicates that the BE Ti64 powder does not have a significant difference in the catalytic effects on the binder decomposition when compared to the Ti powder. Further, the binder decomposition rate constants of both Ti and BE Ti64 feedstocks for the first sigmoid were similar. However, for the second sigmoid, the BE Ti64 feedstock had a slightly higher rate constant compared to the Ti feedstock, possibly owing to minor catalytic effects in the blended powders.

References

[1] S. Guo, B. Duan, X. He, X. Qu, Powder injection molding of pure titanium, Rare Metals 28 (2009) 261–265.
[2] S.J. Park, Y. Wu, D.F. Heaney, X. Zou, G. Gai, R.M. German, Rheological and thermal debinding behaviors in titanium powder injection molding, Metall. Mater. Trans. A 40 (2009) 215–222.
[3] V. Friederici, M. Ellerhorst, P. Imgrund, S. Kramer, N. Ludwig, Metal injection moulding for medical applications, Powder Metall. 57 (2014) 5–8.
[4] G.C. Obasi, O.M. Ferri, T. Ebel, R. Bormann, Influence of processing parameters on mechanical properties of Ti-6Al-4V alloy fabricated by MIM, Mater. Sci. Eng. A 527 (2010) 3929–3935.
[5] J.H. Wang, Q.N. Shi, C.L. Wu, J. Xi, Rheological characterization of injection molded titanium alloy powder, Trans. Nonferrous Metals Soc. China 23 (2013) 2605–2610.
[6] H. Wang, M. Lefler, Z.Z. Fang, T. Lei, S. Fang, Titanium and titanium alloy via sintering of TiH$_2$, Key Eng. Mater. 436 (2010) 157–163.
[7] N.H. Mohamad Nor, N. Muhamad, A.K.A. Mohd Ihsan, K.R. Jamaludin, Sintering parameter optimization of Ti-6Al-4V metal injection molding for highest strength using palm stearin binder, Procedia Eng. 68 (2013) 359–364.
[8] F.H. Froes, Advances in titanium metal injection molding, Powder Metall. Met. Ceram. 46 (2007) 303–310.
[9] R.M. German, A. Bose, Injection Molding of Metals and Ceramics, Metal Powder Industries Federation, New Jersey, 1997.
[10] R.M. German, Progress in titanium metal powder injection molding, Materials 6 (2013) 3641–3662.
[11] G. Thavanayagam, K.L. Pickering, J.E. Swan, P. Cao, Analysis of rheological behavior of titanium feedstocks formulated with a water-soluble binder system for powder injection molding, Powder Technol. 269 (2015) 227–232.
[12] B. Hausnerova, D. Sanetrnik, P. Ponizil, Surface structure analysis of injection molded highly filled polymer melts, Polym. Compos. 34 (2013) 1553–1558.
[13] D. Lin, S.T. Chung, Y.S. Kwon, S.J. Park, Preparation of Ti-6Al-4V feedstock for titanium powder injection molding, J. Mech. Sci. Technol. 30 (2016) 1859–1864.
[14] A. Mannschatz, S. Hohn, T. Moritz, Powder-binder separation in injection moulded green parts, J. Eur. Ceram. Soc. 30 (2010) 2827–2832.
[15] M. Qian, F.H. Froes, Titanium Powder Metallurgy, Science, Technology and Application, Elsevier, 2015.
[16] W. Fang, X.B. He, R.J. Zhang, X.M. You, X.H. Qu, Effects of particle characteristics on homogeneity of green bodies in powder injection moulding, Powder Metall. 57 (2014) 274–282.
[17] J. Bricout, J. Gelin, C. Ablitzer, P. Matheron, M. Brothier, Influence of powder characteristics on the behaviour of PIM feedstock, Chem. Eng. Res. Des. 91 (2013) 2484–2490.
[18] B. Hausnerova, L. Cucova, A. Sorrentino, Effect of carbide powder characteristics on the PVT behavior of powder injection molding compounds, Powder Technol. 237 (2013) 627–633.
[19] T.S. Shivashankar, R.K. Enneti, S.J. Park, R.M. German, S.V. Atre, The effects of material attributes on powder-binder separation phenomena in powder injection molding, Powder Technol. 243 (2013) 79–84.
[20] M.E. Sotomayor, A. Varez, B. Levenfeld, Influence of powder particles size distribution on rheological properties of 316 L powder injection moulding feedstocks, Powder Technol. 200 (2010) 30–36.
[21] M. Aslam, F. Ahmad, P.S.M.B.M. Yusoff, K. Altar, M.A. Omar, H.P.S.A. Khalil, M.R. Raza, Investigation of rheological behavior of low pressure injection molded stainless steel feedstocks, Adv. Mater. Sci. Eng. 2016 (2016) 1–9.
[22] E. Nyberg, M. Miller, K. Simmons, K.S. Weil, Microstructure and mechanical properties of titanium components fabricated by a new powder injection molding technique, Mater. Sci. Eng. C 25 (2005) 336–342.
[23] H.O. Gulsoy, N. Gulsoy, R. Calisici, Particle morphology influence on mechanical and biocompatibility properties of injection molded Ti alloy powder, Biomed. Mater. Eng. 24 (2014) 1861–1873.
[24] J. Bricout, J.C. Gelin, C. Ablitzer, P. Matheron, M. Brothier, Influence of powder characteristics on the behavior of PIM feedstock, Chem. Eng. Res. Des. 91 (2013) 2484–2490.
[25] B. Hausnerova, T. Kitano, I. Kuritka, J. Prindis, L. Marcanikova, The role of powder particle size distribution in the processability of powder injection molding compounds, Int. J. Polym. Anal. Charact. 16 (2011) 141–151.
[26] Y. Li, B. Huang, X. Qu, Viscosity and melt rheology of metal injection moulding feedstocks, Powder Metall. 42 (1999) 86–90.
[27] R.K. Enneti, S.J. Park, R.M. German, S.V. Atre, Review: thermal debinding process in particulate materials processing, Mater. Manuf. Process. 27 (2012) 103–118.
[28] Z. Shi, Z.X. Guo, J.H. Song, A diffusion-controlled kinetic model for binder burnout in a powder compact, Acta Mater. 50 (2002) 1937–1950.

Paper V

Surface Properties of Powder Injection Moulded Parts Related to Processing Conditions

Berenika Hausnerová[1,2], Daniel Sanétrník[2] and Vladimír Pata[1]

[1]Dept. of Production Engineering, Faculty of Technology, Tomas Bata University in Zlin, nam. T.G.Masaryka 5555, 760 01 Zlin, Czech Republic, E-mail: hausnerova@utb.cz

[2]Centre of Polymer Systems, University Institute, Tomas Bata University in Zlin, Trida T. Bati 5678, 760 01 Zlin, Czech Republic

The surface quality of ceramic items produced via powder injection moulding (PIM) at processing conditions varying in injection moulding temperature and debinding route is investigated. The analysis is performed on aluminium oxide part design containing complicated rotational areas, where a smooth surface of an internal spiral is a critical quality factor. Surface properties of the final sintered parts are examined with the help of a contactless scanner. Then, the obtained surface roughness data are treated with suitable statistical analytical tools in order to reveal the effect of the processing conditions during the PIM process on the final parts. Relating surface properties of final sintered parts to processing parameters might provide a powerful tool to control particular steps of PIM process.

Keywords: Quality, Powder injection moulding, Contactless scanning, Roughness evaluation

1 Introduction

Powder injection moulding (PIM) is a valuable alternative to traditional metal and ceramic forming methods [1]. Surface properties of the sintered powder injection moulding (PIM) parts have recently gained increasing attention [2]. PIM process consists of four main steps: preparation of ceramic (CIM) or metallic (MIM) feedstocks, their manufacturing via injection moulding followed with debinding and approaching to final sintering.

Although the surface roughness is generally smaller for ceramics than metals due to their relatively smaller powder sizes available, there is an increasing number of applications (especially in μ-PIM [3]), where the surface forces become dominant at the surface-to-volume ratio encountered in ceramic parts. Such forces (e.g. friction, viscous drag and surface tension) are encountered in particular for applications involving fluid flow, surface reaction, wear and lubrication at the interface [4-6].

Currently, surface roughness values in the range of Ra = 0.3 - 0.6 μm and Rz = 2 - 5 μm are reached in μPIM, depending on the material and powder particle size [7, 8]. The best surface qualities obtained were Rmax = 2 - 3 μm with ultrafine ceramic powders [9]. Lower values of surface finish are likely to be achieved as the μPIM process develops and new advanced feedstock systems are introduced [10].

Surface properties of the sintered powder injection moulding parts are dictated above all by sintering conditions (atmosphere, temperature-time profile and heat flow distribution). Sintering affects the surface roughness of the final part since the roughness of sintered components is the highest surface roughness observed throughout the process chain [11]. However, the effect of debinding conditions on resulting surface roughness has been investigated as well. Liu et al. [5] showed that using higher heating rates during debinding increased the weight loss of rebound 316 L stainless steel microstructured parts. The debound parts of higher weight loss gave better surface finish after sintering. Comparing the increase of sintering time and temperature, the surface finish improvement was more significant for increasing temperature.

On the other hand, the surface roughness of the mould was shown to have a negligible influence on the surface quality of sintered components. If the surface roughness Ra of the mould, the green parts and the sintered parts were compared for different sintering conditions, it has turned out that whilst the roughness of the green part increased slightly compared to the mould roughness, the surface roughness values of the sintered part was orders of magnitude higher than the mould values [4].

The weak point of majority studies concerning the investigation of surface properties generally lies in the leak of reliable quantification methods and their employment [12-16]. Therefore, the intent of this paper is to present the quantitative study of sintered ceramic parts at critical conditions, where the statistical tools available will be tested and compared. For this purpose, the possible effect of injection moulding temperature and debinding method were selected to demonstrate the sensitivity of the approaches employed. The non-destructive testing [17] has been selected as a proper tool to achieve this task. The additional aim of this article is to find suitable statistical metrological methods describing the properties of samples produced by PIM technology under specified repeatability conditions in accordance with ISO 4287 and ISO 4288.

2 Experimental

In this study, highly compressive super ground aluminium oxide (alumina) powder MARTOXID® MR70 (Albemarle Corporation, USA) with a specific surface area (BET) 6–10 m²/g, bulk density ~0.90 g/cm³, green density 2.20−2.40 g/cm³ and fired density (1,600 °C, 2h) 3.80−3.92 g/cm³ was used to produce the ceramic item containing complicated rotational areas, where a smooth surface of an internal spiral is a critical quality factor (see Fig. 1).

Fig. 1 *Design of tested aluminium oxide PIM part*

The powder was compounded with a commercial multi-component binder Licomont EK 583-G (Clariant, Switzerland) which is partially water-soluble with a density 1.05−1.15 g/cm^3 and the softening point at 105−115 °C. During mixing in a blade kneader at 160 °C for 2h, a surfactant (1 wt.% oleic acid) was added. Subsequently, 60 vol.% feedstock in the form of pellets was acquired from a single-screw extruder.

Two series of samples were selected differing in (10±0.5) °C in moulding (nozzle) temperatures: 150 °C (Alu150) and 160 °C (Alu160), and debinding routes, where T in the abbreviation means that the samples were debound thermally, and ST stands for combined solvent/thermal binder removal.

Prior to testing the samples were cleaned in a technical gas stream connected to impurities separator. In order to obtain a quantitative analysis, a contactless 3D Chromatic Length Aberration (CLA) scanner (Talysurf 300, Taylor and Hobson, UK) equipped with Talymap ver.5.0.2 software has to be employed. Tested surfaces were subjected to a height measurement over a rectangular area (1 x 1) mm with the scanning rate of 100 μm/s and spacing 5 μm. Filtration of the scanning data was done with the help of Gaussian filter (0.25 mm) in accordance with ISO 4288.

3 Results
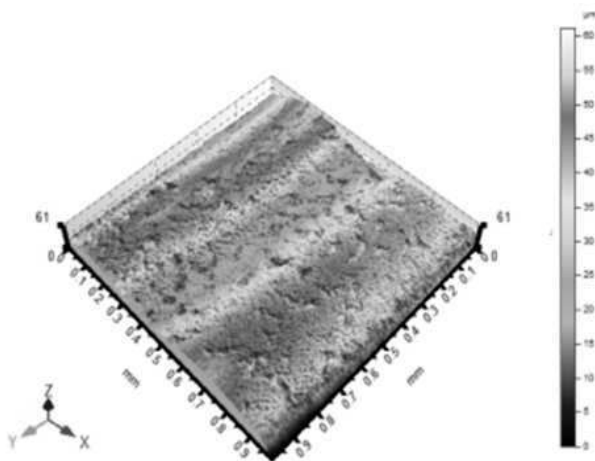
Fig. 2 *Example of surface reconstruction from contactless measurement on a 160ST sample*
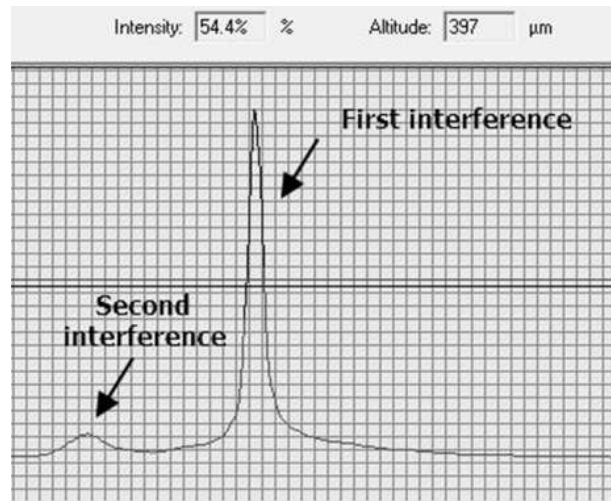
Fig. 3 *Interface Detection (FID) measurement mode applied to a 3D surface reconstruction*
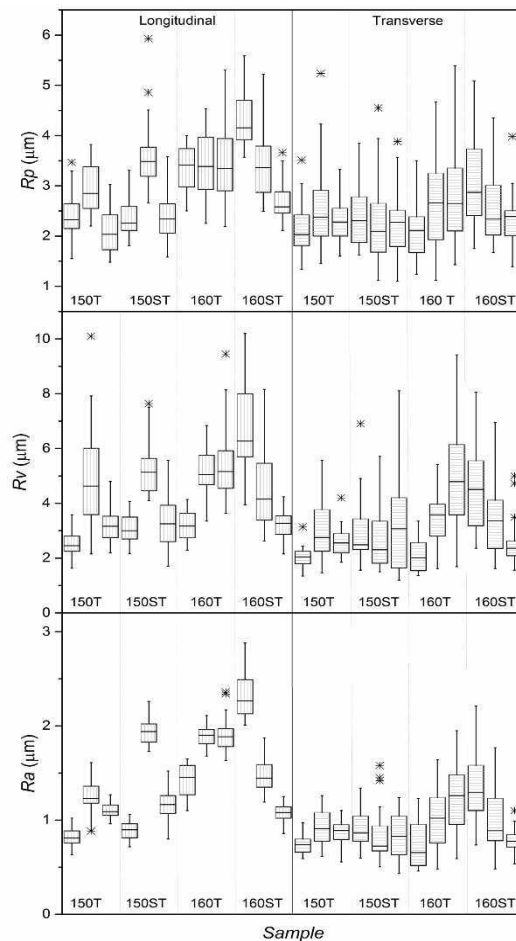
Fig. 4 *Box-Plot diagrams of Rp, Rv, and Ra for the samples molded at 150 °C and 160 °C and debound thermally (150T, 160T) and solvent/thermally (150ST, 160ST) and scanned in longitudinal and transverse directions*

An example of 3D data map obtained from the contactless surface scanning is depicted in Fig. 2. The data supplied is of the form $z = f(x, y)$, where z is the height of the profile, x stands for the position over the scanning direction, and y corresponds to the number of traces. Then,

First Interface Detection (FID) was selected as a measurement mode. The software takes into account the height of the first interference (i.e. the upper border of the transparent interference epresented by the first peak in the spectrum), Fig. 3.

Surface mapping data was evaluated from the fracture planes (meaning conversion into series of profiles), where 200 profiles in both *x*- and *y*-axes were obtained for each sample. Surface parameters Rp, Rv, and Ra were treated with Anderson-Darlin normality test ($\alpha = 0.95$) in accordance with ISO 4287. According to this test, the normality of the data was denied on the confidential level of 0.95 %. This means that the examined surfaces contain non-random inhomogeneities, which must be detected with a suitable statistical tool serving as a base for the relation of the surface properties to the processing conditions.

Primary statistical evidence might be Box-Plot diagrams of Rp, Rv, and Ra showing the considerable scatter of the measured data as shown on the example for surface samples injected at 150 and 160 °C, and then debound thermally or solvent/thermally, Fig. 4.

Thus, the next issue is an evaluation of differently processed samples (change of temperature during moulding) when the normality of the data is absent. Kruskal-Wallis statistical approach has been selected as it enables simple analysis of a data to scatter. A zero-hypothesis expects that the particular surface roughness parameters (Rp, Rv, Ra) have the same median values in the sample groups.

In the following, the Zero-hypothesis for Ra parameter of the samples moulded at two different temperatures and debound thermally (150T and 160 T) in the longitudinal direction (Fig. 5) is:

- $H_0: Median_{R_{a_l}}(Sample\ 150T\ number1) =$

  $Median_{R_{a_l}}(Sample\ 150T\ number2) =$

  $Median_{R_{a_l}}(Sample\ 150T\ number3) =$

  $Median_{R_{a_l}}(Sample\ 160T\ number1) =$

  $M_{R_{a_l}}(Sample\ 160T\ number2) =$

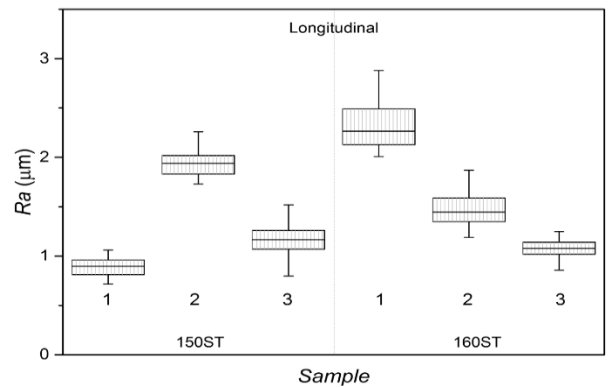 $M_{edianR_{a_l}}(Sample\ 160T\ number3)$

- $H_A: NON$

- $p = 0$
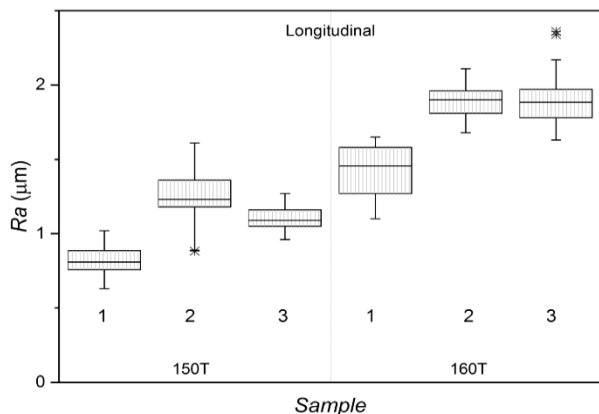
Fig. 5 *Box plots of temperature dependent thermally debound surfaces 150T and 160T with respect to the R_a parameter - longitudinal direction*

Zero hypothesis H_0 is denied on the confidential level 0.95 %, i.e. we suppose that the differences in the investigated surfaces are due to the changes in the processing conditions (temperature).

The same conclusion has been made for the samples moulded at two different temperatures and debound by a combined solvent/thermal route (150ST and 160ST) in the longitudinal direction (Fig. 6):

- $H_0: M_{R_{a_l}}(Sample\ 150ST\ number1) =$

  $M_{R_{a_l}}(Sample\ 150ST\ number2) =$

  $M_{R_{a_l}}(Sample\ 150ST\ number3) =$

  $M_{R_{a_l}}(Sample\ 160ST\ number1) =$

  $M_{R_{a_l}}(Sample\ 160ST\ number2) =$

  $M_{R_{a_l}}(Sample\ 160ST\ number3)$

- $H_A: NON$

- $p = 0$

Fig. 6 *Box plots of temperature-dependent thermal/solvent debound surfaces 150ST and 160ST with respect to the R_a parameter - longitudinal direction*

Similarly for both process conditions in transit use direction (Figure 7a, b):

- $H_0: M_{R_{a_t}}(Sample\ 150T\ number1) =$

  $M_{R_{a_t}}(Sample\ 150T\ number2) =$

  $M_{R_{a_t}}(Sample\ 150T\ number3) =$

  $M_{R_{a_t}}(Sample\ 160T\ number1) =$

  $M_{R_{a_t}}(Sample\ 160T\ number2) =$

  $M_{R_{a_t}}(Sample\ 160T\ number3)$

- $H_A: NON$

- $p = 0$

and

- $H_0: M_{R_{a_t}}(Sample\ 150ST\ number1) =$

  $M_{R_{a_t}}(Sample\ 150ST\ number2) =$

  $M_{R_{a_t}}(Sample\ 150ST\ number3) =$

  $M_{R_{a_t}}(Sample\ 160ST\ number1) =$

  $M_{R_{a_t}}(Sample\ 160ST\ number2) =$

  $M_{R_{a_t}}(Sample\ 160ST\ number3)$
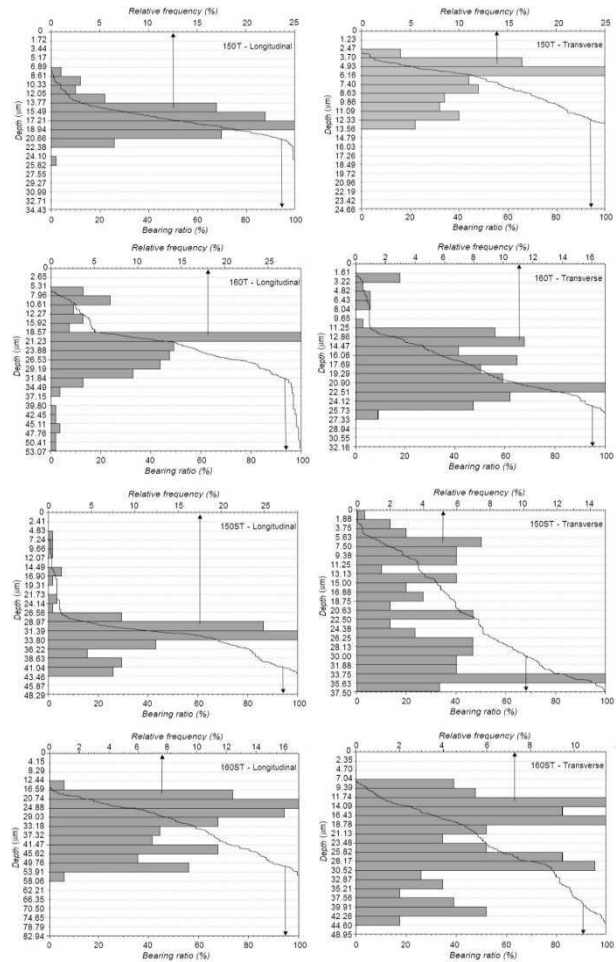
- $H_0 = NON$

- $p = 0$
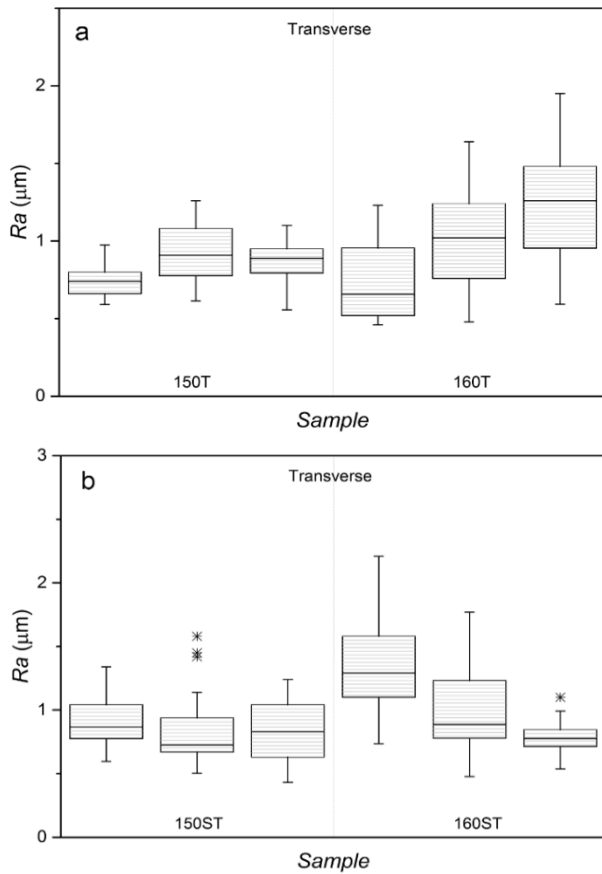
Fig. 7 *Box plots of temperature dependent thermally (a) and thermal/solvent (b) debound surfaces with respect to the Ra parameter - transverse direction*

Fig. 8 *Abbott-Firestone curves of cumulative probabilities of tested surfaces differing in temperature and debinding route*

Kruskal –Wallis method confirmed on the confidential level 0.95 % (i.e. 5 % error) that the medians of selected samples to search the effect of moulding temperature (150 °C or 160 °C), as well as the influence of debinding route, do not vary at random. Instead, they are dependent on the processing conditions. Thus, the surface properties might be related to the processing conditions, and based on this knowledge, the process can be optimised. Further, if the samples were produced differently, we may suppose that the changes in medians signify the change in a processing condition.

Taking into consideration the issues connected to the amplitude parameters of the surface roughness (Rp, Rv, Ra), it seems that the quantification of the surface roughness might improve if the cumulative probability of values in the selected range (1 mm) will be employed. It is called a material profile or Abbott-Firestone curve. The samples of the surfaces prepared at two different temperatures and debound thermally (150T, 160T), as well as those treated with a combined thermal/solvent debinding (150ST, 160ST), serve as examples for Abbott-Firestone evaluation, Fig. 8.

As can be seen from Figs. 4 - 7, the scatter values, which represent repeatability, show considerable uniformity in the individual quartiles of the presented graphs. Only the cases such as Fig. 7a, the box plot of parameter Ra for 160T shows a mild, and thus statistically insignificant, positive skewness. Statistically insignificant skewness can be observed also in the histograms in Figure 8.

Based on these curves of the cumulative probabilities of the parameters values in 1 mm length, it is much easier to detect the character of the surface resulting from the processing conditions during PIM, especially on demands of its flatness or pointedness. This method is also less time-consuming. The evaluation was provided on Rmr parameters according to ISO 4287 at 20 and 60 %.

From Fig. 5 it seemed that the surfaces obtained at lower moulding temperature (150 °C) are smoother in both longitudinal direction (x-axis) as well as transverse direction (y-axis). However, cumulative parameters (Abbott-Firestone curves) may intercept more than Ra, Rp and Rv amplitude parameters based on arithmetic. Abbott-Firestone curves include the characteristics of the profile shapes. This means that the method is suitable for the evaluation of the individual samples among each other, and simultaneously, the interception of the influence of the processing conditions. Figure 8 shows that the curves of the surfaces moulded at 150 °C decline much faster than those obtained at 160 °C. A steeper curve means low accumulation, and thus a sharp profile, which should be avoided whenever the smooth surface of the part is desired. In this respect, the final conclusion is that the higher (not lower) temperature of injection moulding results in the more suitable surface structure of the sintered item investigated.

4 Conclusion

Contactless scanning of the surfaces of aluminium oxide parts produced via powder injection moulding followed with the thorough statistical analysis has been carried out with the aim to investigate the influence of processing parameters - moulding temperature and debinding route – on the resulting sintered surface of these items. First, surface parameters Rp, Rv, and Ra obtained from the contactless scanning were treated with Anderson-Darlin normality test showing that the sintered ceramic surfaces contain not only accidental in homogeneities. Then, Kruskal-Wallis statistical approach has been employed for the interception of the influence of the processing conditions confirming that the particular surface roughness parameters (Rp, Rv, Ra) have the different median values in the sample groups.

Finally, Abbott-Firestone cumulative curves were found to be suitable for the evaluation of the individual samples among each other, and simultaneously, the interception of the influence of the processing conditions.

References

[1] KUČERA, V. & DALIBOR, V. (2018). Processing of Al-Si waste contaminated with iron by powder metallurgy, *Manufacturing Technology*, vol. 18, no. 1, pp. 61-65.

[2] HUBA, J., SANETRNIK, D., HNATKOVA, E., HAUSNEROVA, B. & DVORAK, Z. (2016). New application of powder injection molded product in medical field, *Manufacturing Technology*, vol. 16, no. 1, pp. 94-98.

[3] USAMA, M.A., JEFFREY, R.A. (2011). A review of micro-powder injection moulding as a micro-fabrication technique. *J. Micromech. Microeng.* 21, 1-22 (2011)

[4] TAY, B.Y., LIU, L., LOH, N.H., TOR, S.B., MURAKOSHI, Y., MAEDA, R. (2005). Surface roughness of microstructured component fabricated by µMIM. *Mater. Sci. Eng.* 396, 311–319 (2005)

[5] LIU, L., LOH, N.H., TAY, B.Y., TOR, S.B., MURAKOSHI, Y., MAEDA, R. (2007). Effects of thermal debinding on surface roughness in micro powder injection molding. *Mater. Lett.* 61, 809-812 (2007)

[6] SUPRIADI, S., BAEK, E.R., CHOI, C.J., LEE, B,T. (2007). Binder system for STS 316 nanopowder feedstocks in micrometal injection molding. *J. Mater. Process. Technol.* 187–188, 270–273 (2007)

[7] ROTA, A. (2002). New features in material issues for metallic micro components by MIM. *Proc. PM2TEC* pp 10/49–57 (2002)

[8] YIN, H., JIA, C., QU, X. (2008). Micro powder injection molding—large scale production technology for micro-sized components. *Sci. China Ser. E: Technol. Sci.* 51, 121–6 (2008)

[9] PIOTTER, V., FINNAH, G., ZEEP, B., RUPRECHT, R., HAUSSELT, J. (2007). Metal and ceramic micro components made by powder injection molding. *Mater. Sci. Forum.* 534–536, 373–376 (2007)

[10] GERMAN, R.M. (2009). Medical and dental applications for microminiature powder injection moulding (microPIM) - a roadmap for growth. *PIM Int.* 3, 21–29 (2009)

[11] LI, S.G., FU, G., READING, I., TOR, S.B., LOH, N.H., CHATURVEDI, P., YOON, S.F., YOUCEF-TOUMI, K. (2007). Dimensional variation in production of high-aspect-ratio micro-pillars array by micro powder injection molding. *Appl. Phys. A-Mater.* 89, 721–728 (2007)

[12] ŠČURY, J. & PASTIRČÁK, R. (2016). Effect of technological parameters on the heat transfer coefficient in alloy AlCu4Ti using squeeze casting technology, *Manufacturing Technology*, vol. 16, no. 3, pp. 622-626.

[13] HAUSNEROVA, B., SANETRNIK, D., PONIZIL, P. (2013). Surface structure analysis of injection molded highly filled polymer melts. *Polym. Comp.* 34, 1553-1558 (2013)

[14] ZRAK. A.. MEŠKO. J.. SLÁDEK. A.. VICEN. M. (2016). Evaluation of Properties from the Cutting Surface after Applying Laser Beam Technology Using Different Scales of Cutting Speed. In: *Manufacturing Technology*. Vol. 16. No. 6. pp. 1404 - 1408. UJEP. Czech Republic.

[15] BOTKO, F., HATALA, M., MITALOVA, Z., CEP, R., RIMAR, M., BERNAT, A. & VYBOSTEK, J. (2018). Qualitative evaluation of machined surface of aluminum alloy AlCu4Mg1 depend on feed rate, *Manufacturing Technology*, vol. 18, no. 2, pp. 201-207

[16] ŠLAPÁKOVÁ, M., KŘIVSKÁ, B., GRYDIN, O. & CIESLAR, M. (2018). The influence of casting methods on microstructure of Al-Mg-Sc-Zr alloy, *Manufacturing Technology*, vol. 18, no. 1, pp. 130-134.

[17] JINFENG ZHANG, CHAO FENG, YUNHUI MA, WEI TANG, SHUAI WANG, XIN ZHONG. (2017). Non-destructive analysis of surface integrity in turning and grinding operations (2017) *Manufacturing Technology*, 17/3, pp. 412-418.

LIST OF PUBLICATIONS

Journal articles:

SANETRNIK D., HAUSNEROVA B., PATA V., On-line Rheometry Investigation of Flow/Slip Behaviour of Powder Injection Molding Feedstocks, *Polymers*, 2019, 11, 432

HAUSNEROVA B., PATA V., SANETRNIK D., Surface Properties of Powder Injection Molded Parts Related to Molding Conditions, *Manufacturing Technology*, 2018, 18, 895-899

SANETRNIK D., HAUSNEROVA B., FILIP P., HNATKOVA E., Influence of capillary die geometry on wall slip of highly filled powder injection molding compounds, *Powder Technology*, 2018, 325, 615-619

LIN D., SANETRNIK D., CHO H., CHUNG S.T, KWON Y.S., KATE K.H., HAUSNEROVA B., ATRE S.V., PARK S.J., Rheological and thermal debinding properties of blended elemental Ti-6Al-4V powder injection molding feedstock, *Powder Technology*, 2017, 311, 357-363

HAUSNEROVA B., MUKUND B. N., SANETRNIK D., Rheological properties of gas and water atomized 17-4PH stainless steel MIM feedstocks: Effect of powder shape and size, *Powder Technology*, 2017, 312, 152-158

HNATKOVA E., SANETRNIK D., PATA V., HAUSNEROVA B., DVORAK Z., Mold Surface Analysis after Injection Molding of Highly Filled Polymeric Compounds, *Manufacturing Technology*, 2016, 16, 86-90

HUBA J., SANETRNIK D., HAUSNEROVA B., HNATKOVA E., DVORAK Z., New Application of Powder Injection Molding Product in Medical Field, *Manufacturing Technology*, 2016, 16, 94-98

HUBA J., SANETRNIK D., HNATKOVA E., HAUSNEROVA B., Mechanical Properties of New and Recycled PIM Feedstocks, *Applied Mechanics and Materials*, 2015, 732, 103-106, ISSN: 1662-7482

HAUSNEROVA B., SANETRNIK D., PONIZIL P., Surface structure analysis of injection molded highly filled polymer melts, *Polymer Composites*, 2013, 34, 1553–1558

SANETRNIK D., HAUSNEROVA B., Moldability of Highly Filled Polymers. *Chemické Listy, Special Issue*, 2013, 107, 81-82, ISSN: 1213-7103

HAUSNEROVA B., SANETRNIK D., PONIZIL P., Eliminating separation during powder injection molding, *Society of Plastics Engineers, Plastics Research Online*, 2013

Conference proceedings:

HNATKOVA E., SANETRNIK D., PATA V., HAUSNEROVA B., DVORAK Z., Mold Surface Analysis after Injection Molding of Highly Filled Polymeric Compounds, *ICTKI2016 Conference,* Litoměřice, 2016

HUBA J., SANETRNIK D., HAUSNEROVA B., HNATKOVA E., DVORAK Z., New Application of Powder Injection Molding Product in Medical Field, *ICTKI2016 Conference,* Litoměřice, 2016

HUBA J., SANETRNIK D., HAUSNEROVA B., HNATKOVA E., DVORAK Z., ZLINSKY V., New Design of Adenoid Curette Produced via Powder Injection Molding Technology, *8th International Conference on MATERIALS SCIENCE*, Rome, 2015

HNATKOVA E., SANETRNIK D., HAUSNEROVA B., Effects of SA surfactant on critical solid loading and flow properties of PIM feedstocks, *2nd International conference on rheology and modelling of materials*, Miskolc-Lillafured, 2015

HNATKOVA E., SANETRNIK D., HAUSNEROVA B., Effects of Molecular Weight on Entrance Pressure Drop in Highly Filled Systems, *2nd International conference on rheology and modelling of materials*, Miskolc-Lillafured, 2015

HAUSNEROVA B., SANETRNIK D., HNATKOVA E., Wall-slip as a phenomenon attending processing of highly powder particle filled polymer melts, *6th international Conference on Mechanics and Materials in Design*, Ponta Delgada Azores 2015

HAUSNEROVA B., SANETRNIK D., Critical Issues of Ceramic Injection Molding Feedstocks (Invited Lecture), *2015 EMN Ceramic Meeting*, Orlando 2015

HUBA J., SANETRNIK D., HNATKOVA E., HAUSNEROVA B., Mechanical properties of sintered PIM test specimens, *International Conference Plastko 2014,* Zlín, 2014

HAUSNEROVA B., SANETRNIK D., PARAVANOVA G., Slip of Highly Filled Powder Injection Molding Compounds: Effect of Flow Channel Roughness, *7th International conference Times of Polymers and Composites*, Ischia, 2014

HAUSNEROVA B., SANETRNIK D., Quantitative Analysis of Surface Properties Resulting from Powder-Binder Separation, *Euro PM 2013*, Gothenburg, 2013

CURRICULUM VITAE

Name: **Daniel Sanétrník**

Date of birth: 18th March 1988
Address: Tř. Spojenců 8851, Otrokovice 76502
Nationality: Czech
Contact: dsanetrnik@utb.cz

Education: 2012 – present
Tomas Bata University in Zlin, Faculty of Technology
Doctoral degree study in Process Engineering, Tools and Processes

2010 – 2012
Tomas Bata University in Zlín, Faculty of Technology
Master degree study in Chemistry and Materials Technology, Materials Engineering.

2007 – 2010
Tomas Bata University in Zlín, Faculty of Technology
Bachelor degree study in Chemistry and Materials Technology, Materials Engineering.

Work Experience: 10/2012 - present
Researcher at Centre of Polymer Systems, Tomas Bata University in Zlin, Zlin, Czech Republic

Training Abroad: 8.9. – 23.10. 2014
POSTECH Pohang University of Science and Technology, South Korea, Department of Mechanical Engineering

11.4. – 14.6. 2016
POSTECH Pohang University of Science and Technology, South Korea, Department of Mechanical Engineering

Projects: 2012 – present
TE01020216 Centre of advanced polymeric and composite materials, provider: TAČR
- Member of research team

2015 – present
LO1504 Centre of polymer systems plus, provider: MŠMT
- Member of research team

2013 – 2015
CZ.1.05./2.1.00/03.0111 Centre of polymer systems, provider: OP VaVpI
- Member of research team

2016
IGA/FT/2016/002 Research of polymer composite materials and their processing tools, provider: Internal Grant Agency of Tomas Bata University in Zlín
- Member of research team

2015
IGA/FT/2015/001 New Trends in the Field of Polymer Composite Materials and Tools for Their Processing, provider: Internal Grant Agency of Tomas Bata University in Zlín
- Member of research team

2014
IGA/FT/2014/003 Research of polymer composite materials and their processing tools, provider: Internal Grant Agency of Tomas Bata University in Zlín
- Member of research team

2013
IGA/FT/2013/022 Polymer composite materials and their processing, provider: Internal Grant Agency of Tomas Bata University in Zlín
- Member of research team

Daniel Sanétrník

Optimization of processing of powder injection molding feedstocks prone to phase separation

Optimalizace procesu vstřikování práškových materiálů vykazujících fázovou separaci

Doctoral Thesis

106